REPORT DOCUMENTATION PAGE

Form Approved OMB No. 0704-0188

1. AGENCY USE ONLY (Leave Blank)	2. REPORT DATE	3. REPORT TYPE AND DATES COVERED
	July 1997	Final (June 1, 1994 - May 31, 1997)

4. TITLE AND SUBTITLE
Unstable Fingered Flow in Soil-Oil-Water-Air Systems: Theoretical Predictions and Experimental Verification

5. FUNDING NUMBERS
F49620-94-1-0291

6. AUTHORS
Tammo Steenhuis, Jean-Yves Parlange, David DiCarlo, Alon Rimmer, Christophe Darnault, Tim Bauters, and Barnes Bierck

7. PERFORMING ORGANIZATION NAME(S) AND ADDRESS(ES)
Department of Agricultural and Biological Engineering
Riley-Robb Hall
Cornell University, Ithaca, NY 14853

8. PERFORMING ORGANIZATION REPORT NUMBER

9. SPONSORING / MONITORING AGENCY NAME(S) AND ADDRESS(ES)
US Air Force AFOSR/NA
110 Duncan Avenue, Suite B115
Bolling AFB, DC 20332-8080

10. SPONSORING / MONITORING AGENCY REPORT NUMBER

11. SUPPLEMENTARY NOTES

12a. DISTRIBUTION / AVAILABILITY STATEMENT
Approved for public release; distribution unlimited.

12b. DISTRIBUTION CODE

13. ABSTRACT *(Maximum 200 words)*

Contamination of soils, sediments, and groundwater with non-aqueous phase liquids (NAPLs) is the most widespread environmental problem. *In situ* remediation technologies are the only viable treatments. Cleanup procedures are often instituted and operated with limited knowledge of contaminant vapor and liquid mass transfer and transport. We have used this Air Force grant to improve and extend into three-phase systems two separate visualization techniques which can rapidly record fluid concentrations in our soil slabs: light transmission and attenuation of synchrotron radiation. The techniques are complementary, and both provide high temporal and spatial resolution of fluid concentrations. Using these improved techniques we have obtained data concerning the source and scope of oil and water flow important for *in situ* remediation. We found that preferential flow in two- and three-phase systems (also called fingering) can control the movement of water through oil-contaminated soils and, thus, affect many remediation techniques. From theoretical arguments and high-speed experiments, we have been able to determine properties such as the size and fluid content in the fingers. Early experiments suggest that surfactants break up the fingers, yielding a better water-oil mixture with positive effects for biological breakdown of oils.

14. SUBJECT TERMS			15. NUMBER OF PAGES
			16. PRICE CODE
17. SECURITY CLASSIFICATION OF REPORT	18. SECURITY CLASSIFICATION OF THIS PAGE	19. SECURITY CLASSIFICATION OF ABSTRACT	20. LIMITATION OF ABSTRACT
UNCLASSIFIED	UNCLASSIFIED	UNCLASSIFIED	UL

NSN 7540-01-280-5500

Standard Form 298 (Rev. 2-89)
Prescribed by ANSI Std. Z39-1
298-102

UNSTABLE FINGERED FLOW IN SOIL-OIL-WATER-AIR SYSTEMS

Tammo Steenhuis, Jean-Yves Parlange,
David DiCarlo, Alon Rimmer, Christophe Darnault, and Tim Bauters
Department of Agricultural and Biological Engineering
Cornell University, Ithaca, NY 14853

Barnes Bierck
1019 Highland Woods Road
Chapel Hill, NC 27514

Final Report
July 1997

Grant No. F49620-94-1-0291

BACKGROUND AND SIGNIFICANCE

Contamination of soils, sediments, and groundwater with non-aqueous phase liquids (NAPLs) is the most widespread environmental problem facing the Air Force. *In situ* remediation technologies are the only viable treatments that offer the potential of gaining control over the huge costs and extended time required to clean up contaminated Air Force sites. Cleanup procedures are often instituted and operated with limited knowledge of both the physical and chemical processes which may govern contaminant vapor and liquid mass transfer and transport. To be effective, complete hydronamic control of the subsurface at the remediation site is critical. One of the complicating factors in hydronamic control is the creation of preferential flow paths generated by chaotic disturbances in the flow field. These phenomena are not predicted well with current multiphase flow process models, especially when gravity plays a role (Rimmer et al., 1996), which dictates the use of very conservative and expensive risk-analysis criteria. On many occasions, this has rendered the use of *in situ* treatment remedies ineffective because of hydronamic bypassing of subsurface pollutants.

The complexity of preferential flow of water and non-aqueous phase liquids is largely unappreciated because few techniques permit accurate measurement of water and NAPL contents in rapidly changing flow fields. Until now, rapid measurements of fluid concentrations have been limited to two-phase systems (i.e., systems with two mobile fluids), and the first part of this work focussed on these NAPL and water systems. However, in most contamination sites, NAPLs, water, and air coexist within the soil matrix yielding a more complex three-phase system. For these systems, it is much more difficult to obtain accurate saturations, as two independent measurements are needed at each point. Previous measurement techniques have been limited to static or steady state flow conditions as the measurement times are long. This has severely limited the study of instabilities in three-phase systems.

We have used this Air Force grant to improve and extend into three-phase systems two separate visualization techniques which can rapidly record fluid concentrations in our soil slabs: light transmission and attenuation of synchrotron radiation. The techniques are complementary and both provide high temporal and spatial resolution of fluid concentrations, necessary as the properties of preferential flow can change on short time scales. Using these improved techniques we have obtained data concerning the source and scope of preferential flow in two- and three-phase systems.

The specific research performed during this grant is summarized as follows. During the first year of the grant, we began testing the theoretical predictions for two-phase flow by using both techniques. In the second year, we extended the study of two-phase flow to include surfactants and their effects on preferential flow. The light transmission technique has been made quantitative for two-phase oil and water systems and we have extended the technique to three-phase systems (oil, water, and air) (Darnault et al., in preparation). Attenuation of synchrotron radiation has been used to provide highly accurate and rapid concentrations within preferential two-phase flow. Importantly, rapid measurements of three-phase saturations have been achieved by using dual

energies from the synchrotron radiation. Two other related studies have been carried out. The first studied oil and water movement through wetted and non-wetted tubes to understand the basics of fluid entrapment. The second study consisted of the production of preferential flow as a function of the solid-liquid contact angle as in water repellant or NAPL coated soils.

THEORETICAL BACKGROUND

The theory leading to the instability of the interface between fluids in a porous medium has been the topic of continuous research in fields of chemical engineering, fluid mechanics, and petroleum engineering since the discovery of interfacial instability by Hill (1952). Hill showed that the downward displacement of fluid 1 into fluid 2 is unstable if

$$kg(\rho_1-\rho_2) - \theta_a v(\mu_1-\mu_2) > 0 \qquad (1)$$

Here ρ_1 and ρ_2 are the fluid densities, μ_1 and μ_2 are the viscosities, υ is the interfacial velocity, k is the intrinsic permeability of the media, θ_a is the porosity available for fluid transmission, and g is the gravitational acceleration. This instability condition is satisfied when water infiltrates into a sandy soil saturated with a light oil, thus producing preferential flow paths.

For the water-air system, previous work by Parlange and Hill (1976) calculated the finger size (d) for water infiltrating air dry soil which subsequent experiments found to be valid (Glass et al., 1989). Under this contract, we have broadened this analysis to include water infiltrating into oil saturated soil with the assumption that the oil pressure remains constant ahead of the finger (Chandler et al., 1997, see Appendix A for more detail). The resulting finger width is related to the air-water width by

$$\frac{d_{oil}}{d_{air}} = \frac{\dfrac{\sigma_{oil}}{\sigma_{air}}}{1 - \dfrac{\rho_o}{\rho_w} - \dfrac{v\,(\theta_{w_f} - \theta_{w_i})}{K_{w_f}}} \qquad (2)$$

where σ_{oil} and σ_{air} are the water-oil and water-air surface tensions, respectively, K_{wf} is the conductivity of the tip in the water finger, v is the velocity of the front if it would have remained flat, and θ_{wi} and θ_{wf} are the initial and final water contents in the finger, respectively.

EXPERIMENTS

The two high-speed data acquisition techniques - Light Transmission and Synchrotron X-Ray attenuation - each have their unique advantages. The light transmission technique involves the video recording of light and/or color transmission through a soil slab. The concentration of each fluid can be directly related to the transmitted intensity for the air-water system and hue (or color) for the NAPL-water system in which the water is colored blue (Chandler et al., 1997; Rimmer

et al., 1997, see Appendix B). Light transmission allows a spatial field of 250,000 points to be measured and, thus, provides measurements of the flow throughout the whole chamber. Synchrotron x-ray attenuation is based upon the same technique as gamma-ray attenuation, the more fluid in the radiation path, the more the radiation is absorbed (Liu et al., 1993). The advantage of a synchrotron source is that the large quantity of radiation (10,000 times greater than conventional sources) allows data to be taken at a much faster rate than from gamma-ray sources. X-ray attenuation measures fluid concentration at one position at any time, but at a much higher accuracy and with much greater soil choices than the light transmission technique.

In all of the experiments, a two-dimensional polycarbonate chamber (thickness =1 cm) was filled with sand and shaken to prevent settling during the fluid injection. Several ports were strategically located throughout the slab, in which high-speed tensiometers were placed to measure the pressures of the oil and water. The tensiometer readings were fed into a computer for direct comparison with fluid concentrations. For two-phase measurements, soils were saturated with Soltrol 220, a light non-toxic NAPL somewhat similar to kerosene and/or quadricyclane. Water was applied to the top surface, to simulate rain or water forcing on a contaminated soil. Fingering was found to occur and was studied as a function of soil sieve sizes, water application rates, and surfactant concentration.

Light Transmission

As both phases in the oil-water system are clear liquids, in our original experiment the visual contrast was enhanced by dying the water with 0.1 mg/l FD&C blue dye and the oil with 0.2 mg/l Sudan IV red dye (Aldrich Chemical Co.). Rainfall was simulated by dripping water uniformly across the top, and Figure 1 depicts time slices of the water infiltration. The measured width of the fingers, 5-8 cm, compare very favorably with the predicted width from the stability analysis. When surfactants are applied to the water, the fingers tend to break up and wander horizontally, and the water flow covers more of the chamber.

Recently, we have modified the video imaging technique so as to obtain quantitative fluid saturations. The modification consists of dyeing only the water phase and analyzing the color (or hue) content of the transmitted light. To test and calibrate this technique, a chamber with individual cells was built from the same materials and the same thickness as the experimental chambers. Figure 2 is a picture of the light transmission through such a chamber, with each cell packed with sand and different concentrations of oil, water, and air. Cells with more water appeared bluer to the eye, and cells with more oil appeared brighter to the eye. By trial and error with different dyes, it was determined that when a concentration of 0.025 mg/l FD&C blue dye is added to the water phase, the measured hue content of the transmitted light is proportional to the water content inside the porous media. This relationship is shown in Figure 3. The linearity of this relationship produces higher accuracy fluid concentrations than those obtained in water-air systems which use the intensity of the transmitted light. The visualization technique for oil and water has been accepted for publication (Darnault et al., 1997, see Appendix C).

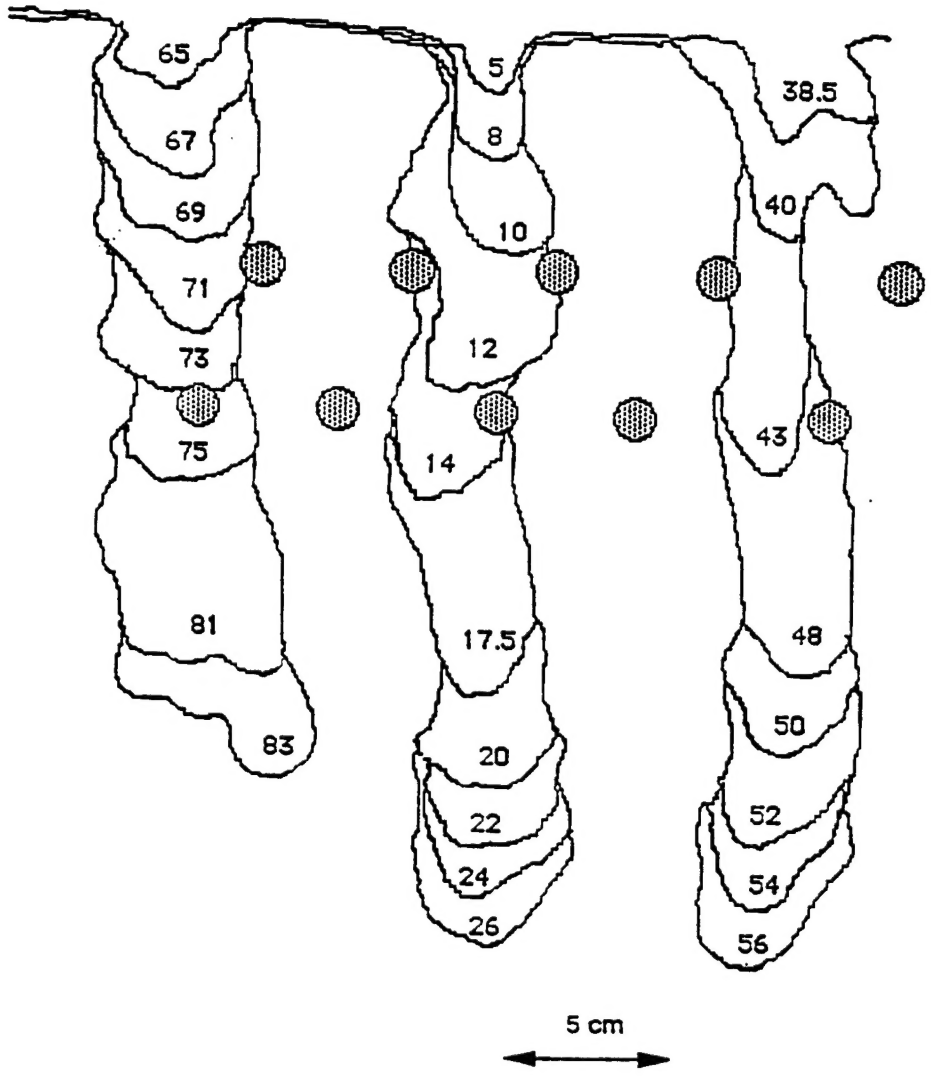

Figure 1: Water fingering in oil saturated soil. Each line represents the position of the water fingers at equal time intervals. The gray circles are the positions of the tensiometers (from Chandler et al., 1995, see Appendix A).

Using this light transmission apparatus, fluid concentrations within preferential flow paths were measured. Inside a water finger penetrating an oil saturated soil there exists two distinct regions. The lower part of the finger has a high concentration of water (0.25 cm^3/cm^3), effectively displacing most of the oil. But, behind this region the water concentration is lower (0.17 cm^3/cm^3), indicating that the oil is re-entering the finger. This behavior is similar to that observed in water and air systems. The lower water content behind the finger tip also inhibits further widening of the finger, leaving large portions of the oil unmoved. These results match those seen in the synchrotron work of the first year, but the light transmission technique allows for a study of the whole flow field, at least for homogenous soils.

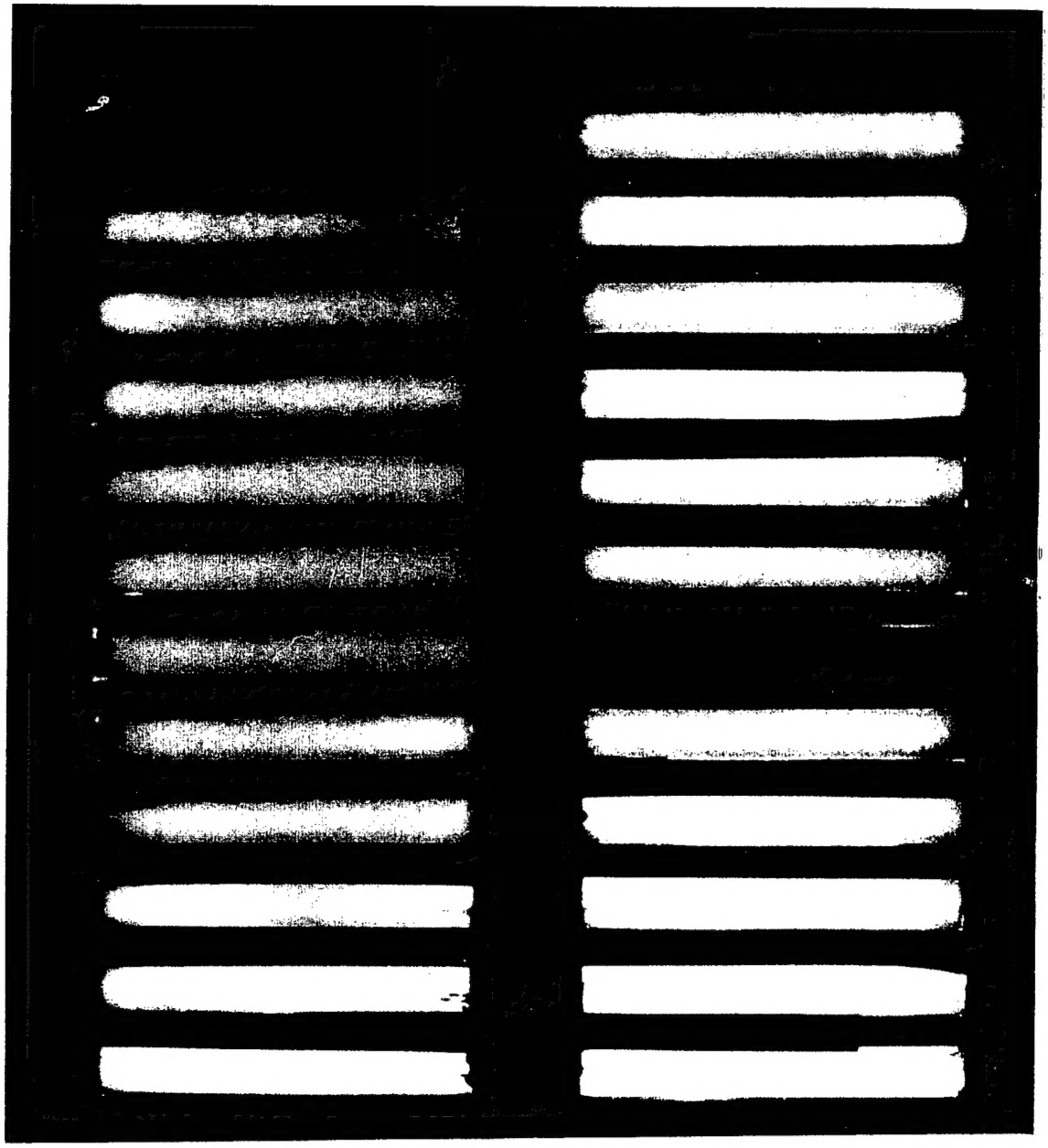

Figure 2: A picture of the calibration chamber, with cells filled with varying amounts of oil, water, and air. The transmitted intensity and hue can be related to the fluid contents inside each cell.

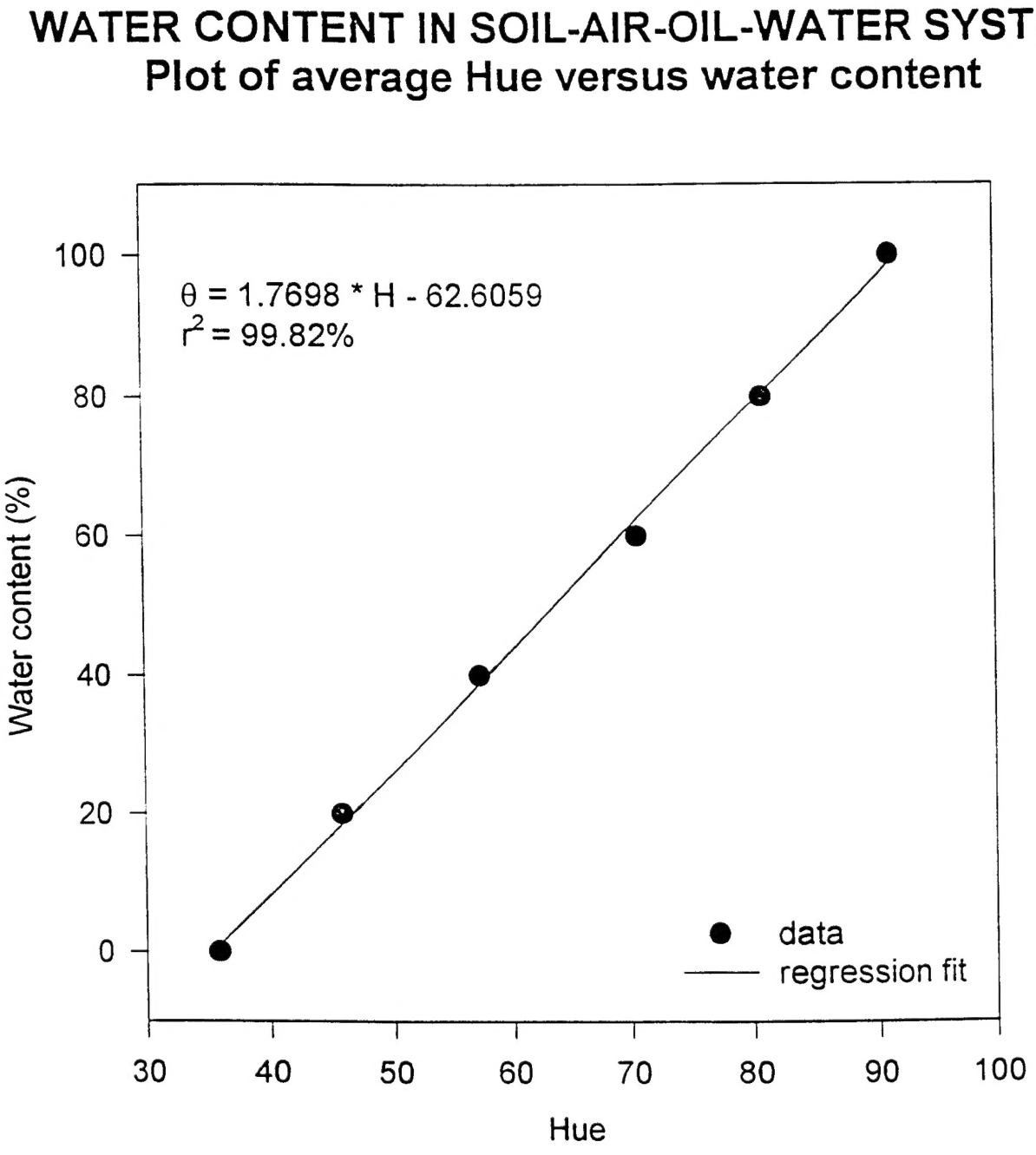

Figure 3: Relationship between the hue of the transmitted light and water content of the sand.

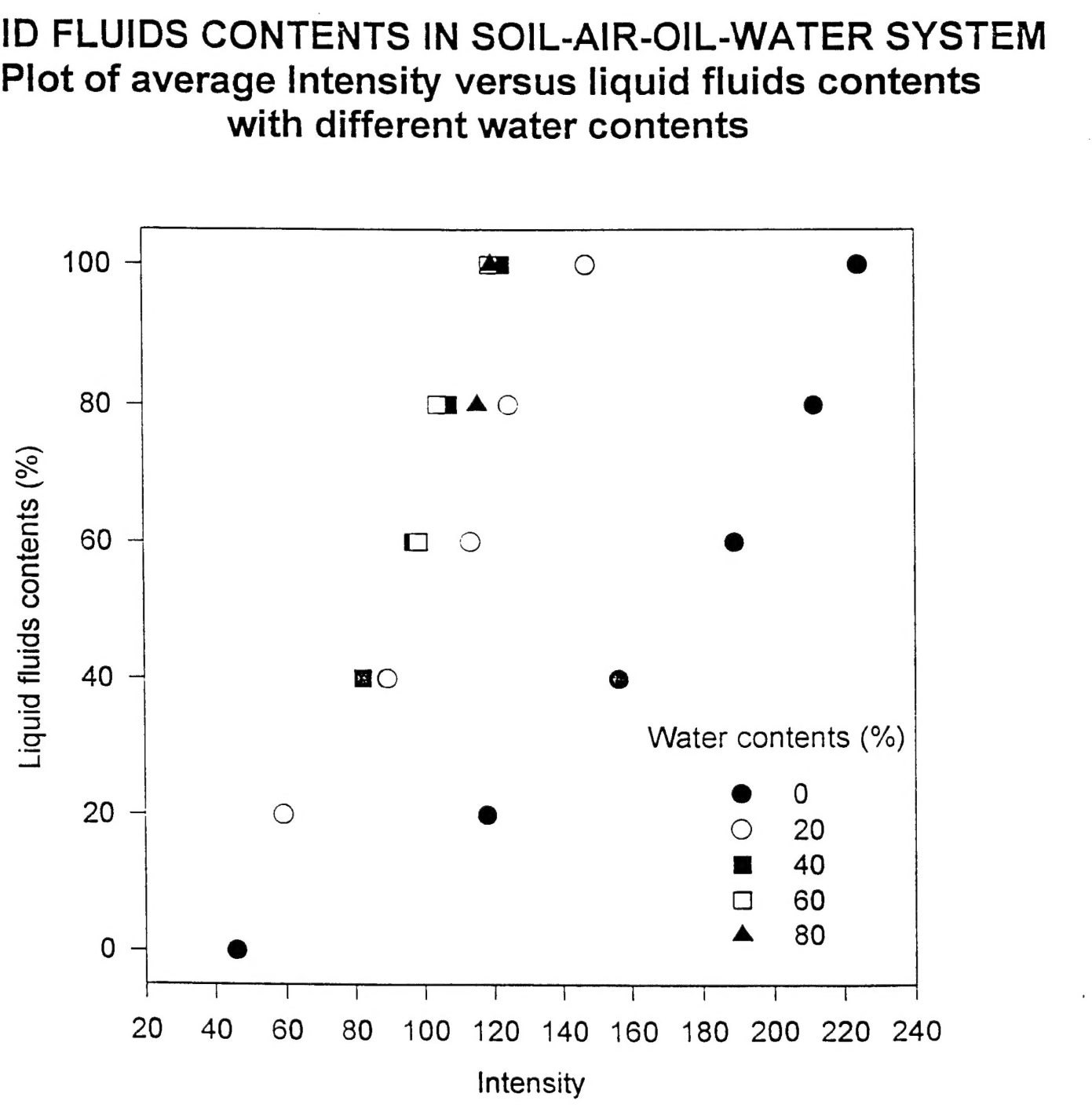

Figure 4: Relationship between the intensity of the transmitted light and the total fluid content of the sand. Different calibration curves are used depending on the hue of the transmitted light.

Recently, we extended light transmission to rapidly measure saturations in three-phase flow. When the output of the color camera is converted into hue, saturation, and intensity, we find that, as before, the hue is related only to the water content, and for known water content the intensity is related to the total fluid content. Figure 4 shows how the intensity depends on the total fluid content for different water contents. The curves are identical except at low water contents where the intensity is much greater for a given fluid content. Still, there exists a one-to-one correspondence between fluid content and intensity once the water content is known from the measured hue. Thus, we can convert the measured color and intensity at every pixel of the camera into oil, water, and air contents inside our sand filled chamber. This is the first technique that can rapidly measure three-phase concentrations over a whole flow field. More details are provided in Appendix D (DiCarlo et al., 1996).

Synchrotron X-ray Attenuation

During the first year of funding, we used synchrotron x-ray attenuation to measure concentrations of fluids to a volumetric accuracy of 0.01 on a time scale of one second. The source of the radiation was the F-2 beam line at the Cornell High Energy Synchrotron Source (CHESS). Further details of the apparatus are described in the first progress report.

In each experiment, water was applied at a single point in the top at varying fluxes (0.5 to 70.0 cm^3/min). A finger began to form within 10 cm of the top, which methodically moved down the chamber. Measurements of the oil and water pressure at points within the finger were obtained versus time. Water concentrations were measured approximately 30 cm from the top of the chamber as functions of time and horizontal position within the finger. Figure 5 shows an oil-water hysteresis curve obtained by measuring the water content and pressure through an infiltration and re-infiltration cycle. Hysteresis curves are an important parameter which controls the persistence of fingered flow, and can be used to predict the success of different cleanup strategies.

For important three-phase saturations, we have developed a technique where the harmonics of synchrotron radiation produce the necessary intense dual energy x-ray beam. The water and oil phases were doped such that each phase was sensitive to each energy photon. This beam passed through our sample chamber and incident and transmitted x-rays were measured using scintillation detectors which provided the necessary energy resolution. The chamber was placed on a new movable platform which had a range of 50 x 30 cm. A schematic of the beam line is shown in Figure 6. Using this technique, we were able to obtain three-phase saturations with an accuracy of .02 volumetric over time scales as small as 5 seconds.

Our initial three-phase studies consisted of oil infiltrating into dry and partially water saturated soil. The chamber was filled with water from below to a height in the chamber of 40 cm, and subsequently drained until the water fringe was at a height of 12 cm. Thus, initially the soil slab had three distinct regions, 12 cm of water saturated sand at the bottom, followed by 28 cm of partially water saturated sand, and finally 15 cm of air dry sand on top. Oil was applied through a point source at the top of the chamber at a rate of 4 ml/min. A finger formed which moved quickly

through the dry sand, and slowly through the partially wet sand, before finally hitting the water table and spreading laterally. The experiment was run with varying sieve size sands, and the fluid contents were measured as the finger passed through the dry and partially water saturated sands.

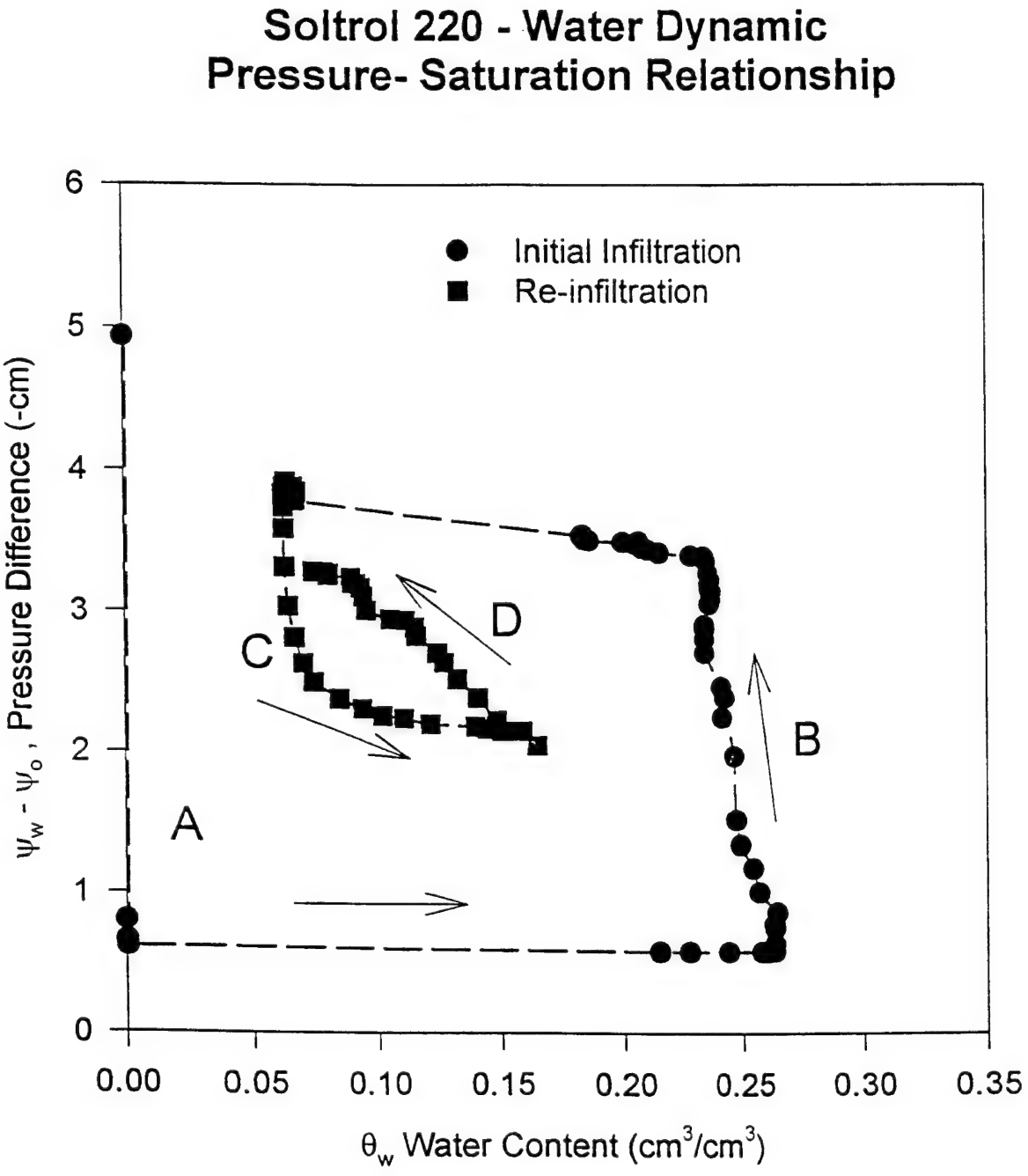

Figure 5: Hysteresis of the primary and secondary wetting and drying curves in an oil and water system measured with synchrotron x-rays.

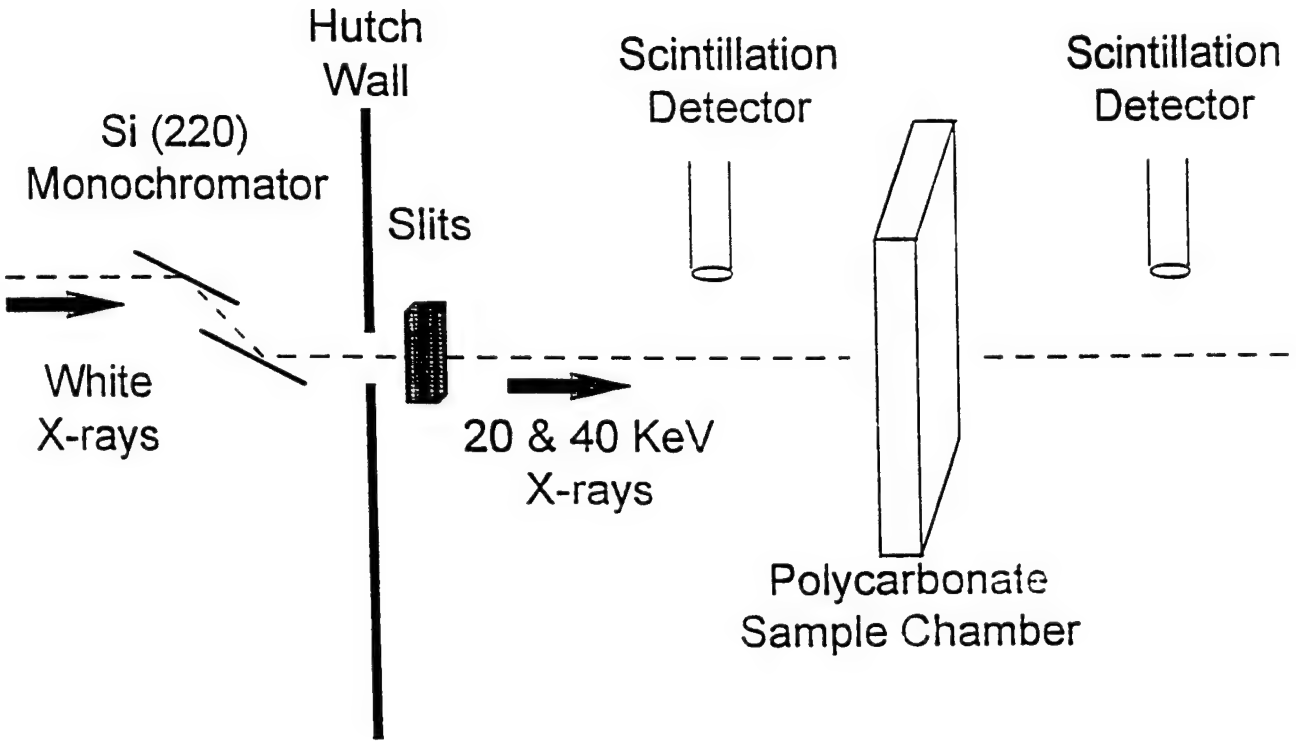

Figure 6: A schematic of the experimental setup at the F-2 hutch of CHESS. The monochromator transforms the white x-ray beam into a multiple energy beam. Scintillation detectors measure the intensity of both energy x-rays by detecting air scattering from the main beam. The sample chamber is mounted on a movable platform allowing measurements from many different positions within the chamber.

Figure 7 shows the measured fluid saturations as the oil finger penetrated the partially water saturated 30/40 sand, one of many data sets. Data were accumulated over 3 second intervals, and the error bars are the expected variance due to the count times in the detector. As the oil penetrated the sand, it drove out the water.

Other Experiments

In a separate experiment (Rimmer et al., 1996, see Appendix E), we compared how the theory of wetting and nonwetting liquid motion in tubes was related to the size of ganglia in a porous medium. It appeared that the size of the entrapped ganglia, when gravity alone is the cause of the motion, was closely related to the tube size in which the wetting-nonwetting fluid configuration was stable.

In studies of preferential flow, the contact angle is important. A special case is wetting and nonwetting soils, in which the finger width depends highly on the degree of water repellency.

Identical soils were treated with OTS (octadecyltrichlorasilane Fisher Scientific), to varying degrees of repellency and, thus, contact angle. When the soil had a positive water entry pressure, fingering took place, bypassing most of the matrix. The results are presented in Appendix F (Bauters et al., 1997).

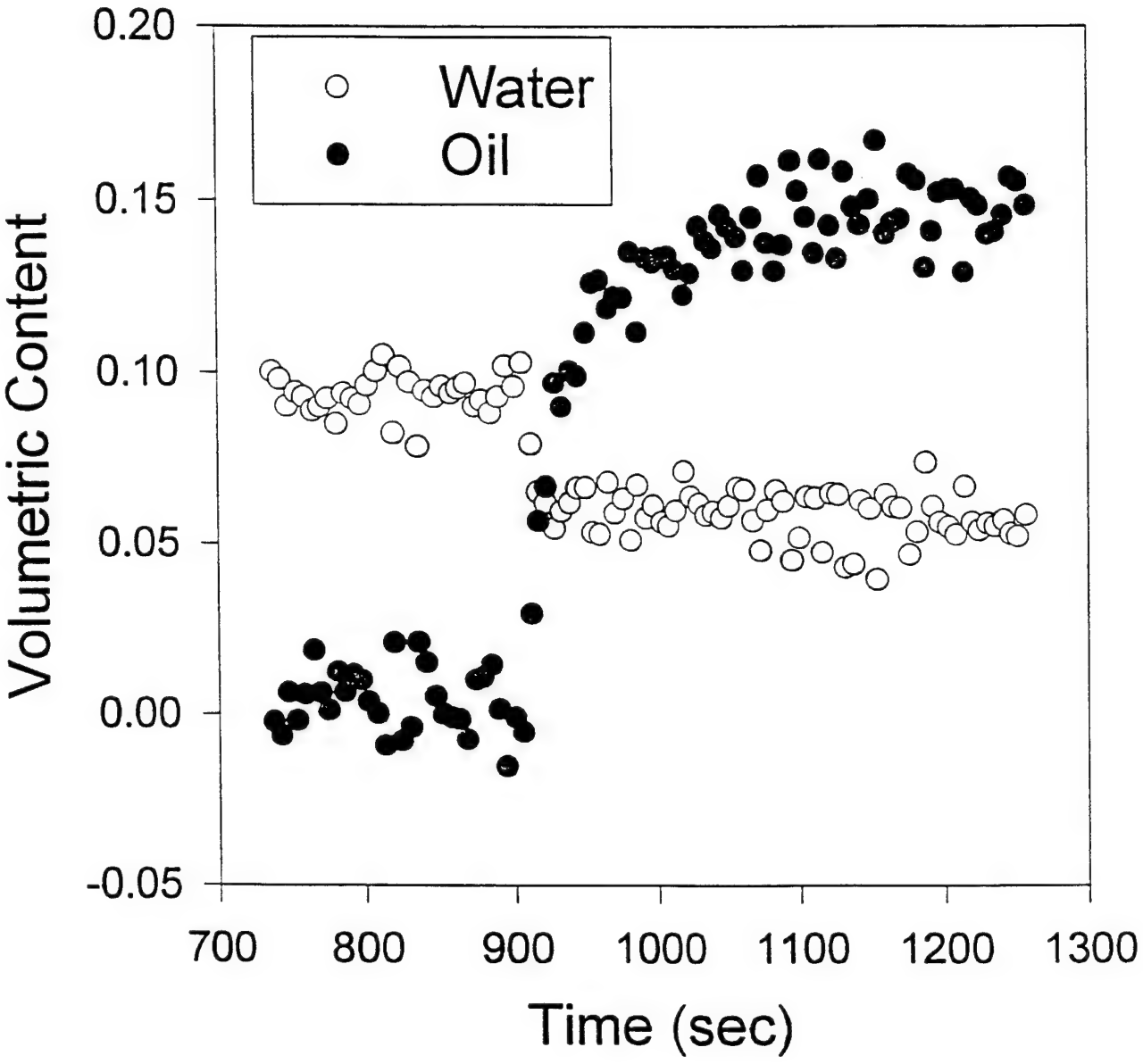

Figure 7: Water and oil contents versus time as the oil finger passes through partially water saturated 30/40 sand. The oil content does not reach saturation and water content is driven lower by the invading oil.

Initial experiments have shown that the addition of surfactants caused the water density in the finger to be less uniform, and the infiltrating water covered much more of the experimental chamber, albeit with smaller fingers. We have repeated these experiments with four different surfactants, using synchrotron x-rays. We found that if we used Eq. (2), the finger width was slightly over predicted, because the theory assumes that the energy loss in oil is negligible flowing around the tip, while in reality there is some resistance. The results are presented in Appendix G (DiCarlo et al., 1997). (Note that, in this research, we examined fingering under gravity with two fluids of about equal viscosity. In contrast, viscous fingering is caused by the difference in viscosity of the two fluids.) The advantage of these studies was that we were able to investigate the effect of contact angle without the complication influences of changing the properties of the oil in the system.

In conclusion, for certain soils, fingering can control the movement of water through oil-contaminated soils and, thus, affect many remediation techniques. From theoretical arguments and high speed experiments, we have been able to determine properties such as the size and water content in the water fingers. Early experiments suggest that surfactants break up the fingers, yielding a better water-oil mixture with positive effects for biological breakdown of oils.

REFERENCES

Bauters, T.W.J., D.A. DiCarlo, T.S. Steenhuis, and J.-Y. Parlange. 1997. Preferential Flow in Water Repellent Soils. Submitted to Soil Science Society of America Journal.

Chandler, D., Z. Cohen, J.-Y. Parlange, and T. Steenhuis. 1997. Unstable Fingered Flow of Water into Light Oil. Submitted to Water Resources Research.

Darnault, C.J.G., J.A. Throop, A. Rimmer, D.A. DiCarlo, T.S. Steenhuis, and J.-Y. Parlange. 1997. Visualization by Light Transmission of Oil and Water Contents in Transient Two-Phase Flow Fields. Journal of Contaminant Hydrology. (Accepted)

DiCarlo, D.A., T.W.J. Bauters, T.S. Steenhuis, J.-Y. Parlange, and B.R. Bierck. 1996. High Speed Measurements of Three-Phase Flow Using Synchrotron X-Rays. Water Resources Research 33(4):569-576.

DiCarlo, D.A., T.W.J. Bauters, C.J.G. Darnault, E. Wong, B.R. Bierck, T.S. Steenhuis, and J.-Y. Parlange. 1997. Surfactant Induced Changes in Gravity Fingering of Water Through a Light Oil. Submitted to Water Resources Research.

Glass, R.J., T.S. Steenhuis, and J.-Y. Parlange. 1989. Mechanism for Finger Persistence in Homogeneous, Unsaturated, Porous Media: Theory and Verification. Soil Science 148(1):60-70.

Hill, S. 1952. Channeling in Packed Soil Columns. Chemical Engr. Science 1:247-253.

Liu, Y., B.R. Bierck, J.S. Selker, T.S. Steenhuis, and J.-Y. Parlange. 1993. High Intensity X-Ray and Tensiometer Measurements in Rapidly Changing Preferential Flow Fields. Soil Science Society of America Journal 57:1188-1192.

Parlange, J.-Y and D.E. Hill. 1976. Theoretical Analysis of Wetting Front Instability in Soils. Soil Science 122:236-239.

Rimmer, A., J.-Y. Parlange, T.S. Steenhuis, D.A. DiCarlo, C. Darnault, and W. Condit. 1996. Wetting and Nonwetting Fluid Displacements in Porous Media. Trans. Porous Media 25:205-215.

Rimmer, A., D.A. DiCarlo, T.S. Steenhuis, J.-Y. Parlange, and B.R. Bierck. 1997. Rapid Fluid Content Measurement Method in an Oil-Water-Sand System Using Synchrotron X-Rays. J. Contaminant Hydrology. (Accepted)

ACKNOWLEDGMENTS/DISCLAIMER

This work was sponsored (in part) by the U.S. Air Force Office of Scientific Research, under Grant/Contract Number F49620-94-1-0291. The views and conclusions contained herein are those of the authors and should not be interpreted as necessarily representing the official policies or endorsements of the U.S. Air Force Office of Scientific Research or the U.S. Government.

PUBLICATIONS

Bauters, T.W.J., D.A. DiCarlo, T.S. Steenhuis, and J.-Y. Parlange. 1997. Preferential Flow in Water Repellent Soils. Submitted to Soil Science Society of America Journal.

Chandler, D.G., Z. Cohen, E. Wong, D.A. DiCarlo, T.S. Steenhuis, and J.-Y. Parlange. 1997. Unstable Fingered Flow of Water into a Light Oil. Resubmitted to Water Resources Research.

Darnault, C.J.G., J.A. Throop, A. Rimmer, D.A. DiCarlo, T.S. Steenhuis, and J.-Y. Parlange. 1997. Visualization by Light Transmission of Oil and Water Contents in Transient Two-Phase Flow Fields. Journal of Contaminant Hydrology. (Accepted)

DiCarlo, D.A., T.W.J. Bauters, T.S. Steenhuis, J.-Y. Parlange, and B.R. Bierck. 1996. High Speed Measurements of Three-Phase Flow Using Synchrotron X-Rays. Water Resources Research 33(4):569-576.

DiCarlo, D.A., T.W.J. Bauters, C. Darnault, T.S. Steenhuis, and J.-Y. Parlange. 1997. Surfactant Induced Changes in Gravity Fingering of Water Through a Light Oil. Submitted to Water Resources Research.

Rimmer, A., J.-Y. Parlange, T.S. Steenhuis, D.A. DiCarlo, C. Darnault, and W. Condit. 1996. Wetting and Nonwetting Fluid Displacements in Porous Media. Trans. Porous Media 25:205-215.

Rimmer, A., DA. DiCarlo, T.S. Steenhuis, J.-Y. Parlange, and B.R. Bierck. 1997. Rapid Fluid Content Measurement Method in an Oil-Water-Sand System Using Synchrotron X-Rays. Journal of Contaminant Hydrology. (Accepted)

PRESENTATIONS

"Fingers in Oil-Water Systems". American Geophysical Union Fall Meeting. December 11-15, 1995. San Francisco, CA. (Oral Presentation)

"Vapor-Transport Driven Growth of Finger Flow Patterns". European Geophysical Society XXI Assembly. May 6-10, 1996. The Hague, Netherlands. (Oral Presentation)

"Preferential Flow Paths in Water Repellant Soils: A Laboratory Study". European Geophysical Society XXI Assembly. May 6-10, 1996. The Hague, Netherlands. (Oral Presentation)

"Measurements of Three-Phase Flow Using High Intensity Synchrotron X-Rays". American Geophysical Union Spring Meeting. May 20-24, 1996. Baltimore, MD. (Poster Presentation)

"Estimating of Transport Parameters in Unsaturated Soil with Synchrotron Radiation and Fast Responding Tensiometers". European Geophysical Society XXII Assembly. April 21-25, 1997. Vienna, Austria. (Oral Presentation)

"Effect of Soil Water Repellency in Flow and Transport". European Geophysical Society XXII Assembly. April 21-25, 1997. Vienna, Austria. (Oral Presentation)

"Three-Phase Flow and Other Possible Fluid Measurements Using Synchrotron X-Rays". American Geophysical Union. May 27-30, 1997. Baltimore, MD. (Poster Presentation)

APPENDIX A

UNSTABLE FINGERED FLOW OF WATER INTO A LIGHT OIL

**D.G. Chandler, Z. Cohen, E. Wong,
D.A. DiCarlo, T.S. Steenhuis,
and J.-Y. Parlange**

Re-submitted to Water Resources Research

UNSTABLE FINGERED FLOW OF WATER INTO A LIGHT OIL

David G. Chandler, Zachary Cohen, Eva Wong,

David A. DiCarlo, Tammo S. Steenhuis*, and J.-Yves Parlange[1]

ABSTRACT

The fingered flow theory for air-water systems was extended to predict the width of water fingers in oil-water systems, assuming that the pressure in the oil phase remains constant. It is shown that the scaled diameters of oil-water fingers can be found from the diameters of air-water fingers using the ratio of the surface tension and the difference between the densities of the oil and water. Finger diameters measured for water infiltrating into light oil were in agreement with finger diameters scaled from measurements of air-water fingers.

*Corresponding Author.

[1]Department of Agricultural and Biological Engineering, Cornell University, Ithaca, NY 14853.

INTRODUCTION

Interest in subsurface transport mechanisms responsible for anomalies from conventional models of convective-dispersive flow has increased with concern over groundwater contamination by pesticides and non-aqueous phase liquids. One particularly important mechanism is fingered flow due to instabilities. Studies of unstable flow of water through unsaturated porous media and fingering of two liquids in Hele-Shaw cells have led to various descriptions of these phenomena, both physical and theoretical (Saffman and Taylor, 1958). Chuoke et al. (1959) extended the Hele-Shaw result to soils using an undefined "effective" surface tension.

Parlange and Hill (1976) accounted for the capillarity of the media by treating the wetting front as diffuse, rather than discontinuous, in their theory of wetting front instability. The moisture content and capillary pressure of the fingered flow resulting from such an instability have been well described for air-water systems in terms of the initial moisture content and grain size distribution of the media (Glass et al., 1989a,b; Baker and Hillel, 1990; Liu et al., 1993; Selker et al., 1992b,c). Glass et al. (1991) apparently following the approach of Parlange and Hill developed general equations for finger diameters in immiscible fluids, but subsequently Glass and Nicholl (1996) found these equations did not predict the observed finger behavior in oil-water systems. However, Glass et al. (1991) assumed inadvertently that the front was discontinuous. In this paper we again use the diffuse front behavior of Parlange and Hill (1976) but assume that the oil provides little resistance to the movement of the water finger (in agreement with the conditions of our experiment). We show that minimum finger diameters for

oil-water systems are thus obtained by taking into account the oil phase density and the oil-water surface tension. We also demonstrate that viscosity is not a factor in determining the minimum finger size.

BACKGROUND

This theory of unstable displacement of a light oil by water in porous media follows the approach used to describe wetting front instability of water in homogeneous soils by Parlange and Hill (1976). The purpose of the theory is to estimate the stabilizing effect of surface tension (see Appendix) and requires an analysis of the transition from oil-phase predominance to water-phase predominance across the front. The earlier approach of Glass et al. (1991) in which the transition takes place explicitly across a discontinuous front is inconsistent with the physical process of stabilization introduced by the matric potential (surface tension effect).

To formulate analytically an equation for the finger diameter in an oil-water system, we make use of our experimental observations that the oil pressure, p_o, within the chamber remains static (no flow) when an unstable water-oil front moves downward, indicating that the oil has no difficulty escaping ahead of the front as the instability initially develops. This assumption is crucial to the present formulation. Only when the finger penetrates deeply into the chamber does the oil pressure around the finger tip influence finger propagation and the present theory break down. Defining Z as the vertical coordinate with the origin and at the free oil surface then,

$$\frac{p_o}{\rho_o g} - Z = 0 \qquad (1)$$

where

ρ_o = density of oil

p_o = oil pressure

Z = vertical coordinate

g = acceleration of gravity

and the o subscript indicates the oil phase.

The hydraulic potential in the water phase, ϕ_w, is defined in terms of water head as:

$$\phi_w = \frac{p_w}{\rho_w g} - Z; \quad Z \le \overline{Z}_f + z_f \qquad (2)$$

When the oil pressure is static, Eq. (2) can be rewritten by subtracting $p_o/\rho_w g - Z\rho_o/\rho_w$, (which here according to Eq. (1) is zero because of the choice of the reference point for the gravity potential) as:

$$\phi_w = \psi_w - Z\left(1 - \frac{\rho_o}{\rho_w}\right); \quad Z \le \overline{Z}_f + z_f \qquad (3)$$

where

p_w = pressure in the water phase (units of energy per unit volume of water)

ρ_w = density of water

ψ_w = matric potential, defined as $(p_w - p_o)/\rho_w g$

$\overline{Z}_f + z_f$ = location of the perturbed water-oil front

$\overline{Z}_f$ = average position of the water-oil front

and the w subscript indicates the water phase.

A water-oil front is defined as the boundary between the oil and the water where the water content is equal to θ_{w_f} (Figure 1). The average position of the front is $Z = \overline{Z}_f$. To simplify the notation we introduce a new Lagrangian coordinate, z, with its origin at the average position of the front, thus, $z = Z - \overline{Z}_f$.

To find the most unstable wavelength, the front at time t, is perturbed as (Saffman and Taylor, 1958; Parlange and Hill, 1976):

$$z_f = ae^{i\lambda x+\omega t} \tag{4}$$

For two-dimensional gravity driven flow, the distance z_f is measured vertically down from the average position of the front, $z = 0$, in the direction of the gravity, along the x axis (Figure 1); λ is the wave number, ω is the growth rate (Glass et al., 1990). At the front there must be a critical pressure difference before fingering can be initiated. Hillel (1987) referred to this pressure difference as the "water entry" potential, h_{we}. In the oil-water system, h_{we} can be expressed as:

$$h_{we} = \frac{p_{w_f} - p_{o_f}}{\rho_w g} \tag{5}$$

where

p_{o_f} = oil pressure at the front

p_{w_f} = water pressure at the front

and the f subscript refers to properties measured at the front. By definition h_{we} is equal to the matric potential ψ_w at the front, ψ_{wf}. As we will see later the exact value of h_{we} is not important for calculation of the finger width because it is being offset by other constants.

The relationship between the Darcy velocity of the water, v, in the z direction and the velocity of the curved front at the onset of the instability, u, is (Saffman and Taylor, 1958; Parlange and Hill, 1976):

$$v = u + \frac{\partial z_f}{\partial t} \tag{6}$$

Noting that the Darcy velocities are proportional to the hydraulic potential gradient, we can find, by combining Eqs. (4) and (6), that at the front:

$$- \frac{K_{w_f}}{\theta_{w_f} - \theta_{w_i}} \frac{\partial \phi_w}{\partial Z} = u + \frac{\partial z_f}{\partial t} \tag{7}$$

where

K_{w_f} = the hydraulic conductivity of the water entry pressure, which is usually assumed to be the saturated hydraulic conductivity

θ_{w_f} = water content at and behind the front

θ_{w_i} = initial water content, which could be equal to zero

Following Parlange and Hill (1976) we expect the velocity of the curved front and the velocity of the front, $\overline{v}$, if it had remained flat, to be related as:

$$u = \bar{v} - \alpha_{oil}\frac{\partial^2 z_f}{\partial^2 x} \tag{8}$$

with the correction term proportional to the curvature of the front and α_{oil} given by:

$$\alpha_{oil} = \alpha_{air}\frac{\sigma_{oil}}{\sigma_{air}}. \tag{9}$$

It is this calculation, given in the Appendix, which takes into account the diffuse nature of the flow. The subscript "oil" refers to the oil-water system and the subscript "air" to the water-air system. Equation (9) assumes that the contact angle of the air-water and oil-water systems are the same. If this is not the case, the surface tensions should be multiplied by the contact angle. Here, we make the assumption that the contact angles are small enough for their cosines to be practically equal to one. However, this assumption is not fundamental for the theory that is presented.

Combining Eqs. (4), (7), and (8) and differentiating z_f with respect to time and x we find at the front that:

$$-\frac{K_{w_f}}{\theta_{w_f}-\theta_{w_i}}\frac{\partial \phi_w}{\partial Z} = \bar{v} + a\left(\omega + \alpha_{oil}\lambda^2\right)e^{i\lambda x + \omega t} \tag{10}$$

Note that the hydraulic potential, ϕ_w, **behind** and **up to** the front (Figure 1) satisfies Laplace's equation because in that region the moisture content is constant and equal to θ_{w_f},

$$\nabla^2 \phi_w = 0 \tag{11}$$

A general solution of Eq. (11) where ϕ_w is differentiated with respect to x and Z and that satisfies Eq. (10) at the front so that the perturbation decays as $Z \rightarrow -\infty$ is:

$$\phi_w = -\frac{\theta_{w_f} - \theta_{w_i}}{K_{w_f}}\left[\bar{v}\left(Z - \overline{Z}_f\right) + a\left(\frac{\omega}{\lambda} + \alpha_{oil}\lambda\right)e^{i\lambda x + \omega t + \lambda(Z - \overline{Z}_f)}\right] + h_{we} + \overline{Z}_f\left(1 - \frac{\rho_o}{\rho_w}\right) \qquad (12)$$

where $[h_{we}-_f(1-\rho_o/\rho_w)]$ is the integration constant such that at the front the matric potential equals the water entry potential (Eq. (5)). Equation (12) may be rewritten as:

$$-\frac{K_{w_f}}{\theta_{w_f} - \theta_{w_i}}\left[\frac{p_w - p_o}{\rho_w g} - \frac{\rho_w - \rho_o}{\rho_w}z - h_{we}\right] = \bar{v}z + z_f\left(\frac{\omega}{\lambda} + \alpha_{oil}\lambda\right)e^{\lambda z + i\lambda x + wt} \qquad (13)$$

Evaluating Eq. (13) at the front where $z = z_f$ and noting that for $z_f << 1$ the exponential λz becomes 1, we find that:

$$\frac{\rho_w - \rho_o}{\theta_f - \theta_i} = \bar{v}\frac{\rho_w}{K_{w_f}} + \frac{\rho_w}{K_{w_f}}\left(\frac{\omega}{\lambda} + \alpha_{oil}\lambda\right) \qquad (14)$$

The most unstable wave number (in the oil-water system), λ_{oil}, is obtained from Eq. (14) by calculating $d\omega/d\lambda$ and setting it equal to zero, i.e., $\omega/\lambda_{oil} = \alpha_{oil}\lambda_{oil}$. Equation (14) can then be rewritten for the most unstable wave number as:

$$\frac{\rho_w - \rho_o}{\theta_{w_f} - \theta_{i_f}} = \bar{v}\frac{\rho_w}{K_{s_f}} + 2\alpha_{oil}\lambda_{oil}\frac{\rho_w}{K_{s_f}} \qquad (15)$$

In order to compare the fingers in the oil-water system with air-water fingers, we take as reference the λ_{air} for the air-water system which, when $v \rightarrow 0$ (Parlange and Hill, 1976), is given by:

$$2\alpha_{air}\lambda_{air} = \frac{K_{w_f}}{\theta_{w_f} - \theta_{w_i}} \tag{16}$$

where α_{air} for the air-water system is defined for the same fluid contents as in the oil-water system:

$$\alpha_{air} = \frac{S_{air}^2}{2\left(\theta_{w_f} - \theta_{w_i}\right)^2} \tag{17}$$

Finally, since the finger width, d, is inversely proportional to λ, $d \approx \pi/\lambda$ (Parlange and Hill, 1976, Figure 1), Eqs. (15) and (16) give the ratio and finger diameters in the oil-water system, d_{oil}, and in the air-water system, d_{air}, as:

$$\frac{d_{oil}}{d_{air}} = \frac{\frac{\sigma_{oil}}{\sigma_{air}}}{1 - \frac{\rho_o}{\rho_w} - \frac{\bar{v}\left(\theta_{w_f} - \theta_{w_i}\right)}{K_{w_f}}} \tag{18}$$

If the assumption of oil moving freely from the wetting front away is incorrect, we expect the finger to be wider than predicted. Thus, Eq. (18) predicts the narrowest finger expected to be observed in the oil-water system. Finally, if the term with $\bar{v}$ is negligible (which it will be for our case), Eq. (18) differs from the result of Glass et al. (1991) by a term $(1+\mu_o/\mu_w)$ which appears in the denominator (see their Eq. (17)).

MATERIALS AND METHODS

Two sets of experiments were performed with oil-water systems. The first set was performed with 20-30 sand in a relatively large chamber and gave initial estimates of finger diameter. To confirm that these experiments were not an artifact, a second set of experiments were performed at a later date with 12-20 sand in which the methods by which the water was added and the oil was removed were changed. Moreover, the oil pressure was measured to test the assumption in the model of static pressure in the displaced phase.

In experimental set I a glass walled chamber with interior dimensions of 80 cm by 50 cm by 1 cm was used (Figure 2). For each trial, the chamber was loaded with white silica sand which had been sorted between standard #20 and #30 sieves, cleaned in the manner of Glass et al. (1989a) to remove organic contaminants and air dried. Following vibrational packing (Selker, 1992a), vacuum degassed oil (Soltrol 220, Philips Petroleum Co.) was introduced slowly from the bottom of the chamber until it ponded above the sand surface. Degassed, distilled water was applied to the oil-saturated slab by two techniques: At a rate of 0.2 $ml/cm^2/min$, using a cam-driven oscillating dripper and 2.0 ml/min via a stationary dripper located near the center of the chamber above the oil surface. Overflow drains at both sides of the chamber and an underdrain manifold were arranged to maintain the oil-free surface at 1 cm above the sand.

In experimental set II a chamber was used with interior dimensions of 55 cm by 33 cm by 1 cm. The chamber was filled and saturated with oil in a manner similar to experimental set I. From

five ports at the bottom of the chamber the oil was pumped at a rate of 2 ml/min into a stoppered Ehrlenmeyer flask with water. The water which was forced out of the flask was applied to the top of the chamber 0.5 cm below the oil surface via a small glass tube. In this case no free water surface formed on top of the sand and fingers started immediately. Pressures in the oil phase were measured at 11, 19, and 36 cm below the oil-free surface with 1 cm diameter, fast responding tensiometers mounted flush with the chamber wall (Rimmer et al., 1996). Of the 20 experiments which were performed, we reported finger diameters from the six experiments for which the chamber loading technique was adequately uniform and oil pressure could be measured consistently.

Finger dimensions were determined by coloring the water with 50 mg/l FD&C blue dye #1 and the oil with 0.2 mg/l Sudan IV red dye (Aldrich Chemical Co.). Traces were made from video images (experimental set I) or directly with transparent sheets on the chamber wall (experimental set II). Finger diameters were measured when the finger tip did not change any more in time (experimental set I) or was near or at the bottom of the chamber (experimental set II).

RESULTS

Two types of results were obtained: Finger diameters for experimental sets I & II and the oil pressure for experimental set II.

Examples of finger traces for trials from each of the experimental sets in which the flow rate was near 2 cm^3min^{-1} are shown in Figures 3 and 4. Finger widths for both experimental sets are shown in Figures 5 and 6 for flow rates comparable to air-water experiments which we have performed previously. In general, the average finger diameter was nearly constant for the first 15 cm and started to increase gradually below that depth. For experimental set II the increase in finger width was even more notable near the bottom of the chamber. In experimental set I the fingers did not reach the bottom of the chamber. Instead, new fingers formed when the fingers were near 30 cm depth. The finger width for experimental set I with the 20-30 sand was 4.8 cm with a standard deviation of 1 cm. For experimental set II, the width was initially 4.7 cm, also with a standard deviation of 1 cm and then below 30 cm increased to a width of 8.6 cm with a standard deviation of 3 cm.

An example of the oil pressure measured in experimental set II for tensiometers at 11, 19, and 36 cm below the oil-free surface is given in Figure 7. The pressure in each of the tensiometers remained nearly constant once the sand slab had been saturated with oil. A slight pressure increase was found at all tensiometers throughout the course of the experiment, reflecting displacement of oil by water during the course of the experiment. More importantly the oil pressure difference between the tensiometers was constant, regardless of the finger having passed by the tensiometers.

DISCUSSION

Fingers grew at constant but small velocities for each experiment. However, in contrast to fingers observed in similar experiments in the air-water system (Selker et al., 1992b,c) finger velocities (although internally constant) were more variable for different application rates and chamber regions. For stationary water application rates of 2 ml/min, finger velocities ranged from 0.019 to 0.022 cm/sec. For linear water application of 0.2 ml/min/cm^2, the average finger velocities were lower, varying between 0.005 and 0.009 cm/sec. In all cases the influence of the term with $\overline{v}$ in Eq. (18) was negligible.

A critical assumption in the development of the unstable flow theory for the oil-water system is that the oil pressure remains static throughout the experiment. This assumption is validated by the static difference in oil pressure between any two tensiometers (Figure 7), e.g.: The pressure difference between tensiometers 3 and 4 remained static at approximately 13.6 cm, which is equivalent to the difference in oil head between them, 17 cm, multiplied by the density of Soltrol, 0.80 g/cm^3. Taking into account the specific weight of oil and a distance of 2.5 cm between them, show that the pressure is static. Hence the static oil pressure assumed in the model was valid.

The predicted finger diameter for the oil-water system is based on the physical constants and the velocities of the fingers in each system, assuming that the diameter and velocity of an individual finger are constant. The physical constants required for scaling fingers between systems (Eq.

(18)) are the fluid densities and interfacial tensions for each of the two fluids within the porous medium, the hydraulic conductivity of the sand and the porosity of the media. Water and Soltrol-220, have densities of 1.00 and 0.80 $g \cdot cm^{-3}$, respectively, at 20° C (Cary et al., 1989). The water-air interfacial tension is 73 $g \cdot sec^{-2}$, however, interfacial tension is neither well defined nor constant over time (Schroth et al., 1995). Schroth et al. (1996) found the Soltrol-water interfacial tension between 40 and 46 $g \cdot sec^{-2}$. Cary et al. (1989) also reported a surface tension for Soltrol and water of 45 $g \cdot sec^{-2}$. We repeatedly measured the interfacial tension for the Soltrol and water used by us (with and without the dyes) to be 32 to 33 $g \cdot sec^{-2}$ with a Fisher Scientific Model 21 ring tensiometer. The hydraulic conductivities for the 12-20 and 20-30 sand were 30 cm/min (Schroth et al., 1996) and 20 cm/min, respectively. The porosities are 0.36 cm^3/cm^3 (Selker et al., 1992a; Liu et al., 1993). Additional parameters required for calculating finger diameter by Glass et al. (1991) are the viscosities of water and Soltrol which are 0.01 and 0.047 $g \cdot sec\text{-}1 \cdot cm^{-1}$, respectively (Cary et al., 1989).

The finger diameters for the top 15 cm of our experiments as well as others (Selker et al., 1992; Liu et al., 1994; Darnault et al., 1996; Hendrickx and Yao, 1996; DiCarlo et al., 1997; Rimmer et al., 1996) are shown in Table 1. The difference in finger widths between experimental sets where point source water application and those where uniform linear water applications were used, is remarkably robust. Taking all finger diameters into account we find the average oil-water finger width in the 12-20 sands to be 2.9 times that of air-water fingers. For the 20-30 sand it is 2.3 times greater.

To calculate the theoretical scaling for finger diameters in air-water and oil-water systems, we neglect the velocity term because the finger velocity is much less than the saturated conductivity of the media. We will calculate the scaling factor for Eq. (18) and compare this with the scaling of Glass et al. (1991) and Chuoke et al. (1959). The scaling calculated for Glass et al. (1991) is larger by a factor of $(1+\mu_o/\mu_w)$ over that in Eq. (18). Chuoke et al.'s (1959) scaling (as formulated by Glass et al., 1991) is similar to Eq. (18) but to the power 0.5. Because of the uncertainty of the Soltrol-water interfacial tension, the calculated scaling factors are shown in Figure 8 for the full range of the aforementioned interfacial tensions. Also plotted are the observed ranges of scaling between the oil-water and air water fingers of Table 1. Whereas that Eq. (18) predicts the scaling in minimum finger diameters quite well, the scaling proposed by Glass et al. (1991) overpredicts and that of Chuoke et al. (1959) slightly underpredicts finger width for oil-water systems.

In both experimental sets the finger width increased below 15 cm (Figures 5 and 6). In earlier experiments with air-water systems (Glass et al., 1989a, 1990; Selker et al., 1992a,b; Liu et al., 1993, 1994) this widening at the bottom was not observed. There are several explanations possible for the widening. First, the nature of the flow field produced in the oil-water system differed from that in the air-water system. A second less likely explanation (because the theory takes this into account) is the difference in pressure profile: The air pressure remains atmospheric while in the oil the pressure increases with depth. One would expect a continuous increase with depth for the oil-water fingers which was not the case. A final explanation for variability in finger width in the oil-water system is that the greater density of the displaced fluid

in the oil-water system as compared to the air-water system reduces the driving force and renders the finger width more sensitive to anisotropy in the sand slab. Currently, we are investigating the density differences in the chambers with x-rays at the Cornell High Energy Synchrotron Source.

CONCLUSIONS

Unstable wetting front theory was developed for oil-water systems. The theory is different from air-water systems (where the air pressure remains atmospheric) in that the pressure in the oil is increasing with depth. Nevertheless, if the oil pressure does not change as the finger approaches, then the oil has no difficulty escaping ahead of the wetting front. According to the presented theory, the minimum finger widths in oil-water systems may be scaled to air-water fingers using the densities and interfacial tensions of the fluids, whereas fluid viscosities need not be considered for scaling widths of gravity driven fingers. Experiments showed that fingers in oil-water systems are consistent with the theoretical assumptions of constant finger velocity and width made for fingers in air-water systems. Moreover, the finger diameter observations agreed well with the theoretically predicted behavior. However oil-water fingers are apparently more sensitive to packing heterogeneities in the porous media than are air-water fingers. The increase of pressure head with depth in the oil-water system may also contribute to variations in finger dimensions. A more complex theoretical model is required to describe this case. Hence, further research is needed to describe the forces associated with flow of oil and the effect on fingered flow.

APPENDIX

To find α_{oil}, we introduce water in oil-saturated soil at a constant rate, Q, per unit length of a vertical line source. Then, for any distance, r, from the line source assuming that oil moves freely ahead of the front:

$$Q = -2\pi r K_w \frac{\partial \psi_w}{\partial r} \tag{A1}$$

Integration of Eq. (A1) yields:

$$\frac{Q}{2\pi} \ln \frac{r_i}{r_f} = \int_{\theta_{w_i}}^{\theta_{w_f}} K_w \frac{dh}{d\theta} d\theta \tag{A2}$$

since r_i (where $\theta = \theta_{w_i}$, Figure 6) and r_f (where $\theta = \theta_{w_f}$) do not differ by much. Equation (A2) can be rewritten by expanding the logarithmic term and neglecting higher order terms:

$$r_i = r_s + \frac{r_s 2\pi}{Q} \int_{\theta_{w_i}}^{\theta_{w_f}} K_w \frac{d\psi_w}{d\theta} d\theta \tag{A3}$$

From conservation of mass:

$$\pi \left(\theta_{w_f} - \theta_{w_i}\right) r_f^2 \approx Qt \tag{A4}$$

Then, following Parlange and Hill (1976) we obtain (differentiating Eq. (A3) with time):

$$u = \bar{v} - \alpha_{oil} r_f \tag{A5}$$

where $u = dr_f/dt$ is the velocity of the curved front and $\bar{v} \approx dr_i/dt$ or the velocity in the absence of surface tension effects:

$$\alpha_{oil} = \int_{\theta_{w_i}}^{\theta_{w_f}} K_w \frac{\frac{d\psi_w}{d\theta}}{\theta_{w_f} - \theta_{w_i}} d\theta \qquad \text{(A6)}$$

assuming the contact angles are the same then ψ_w for the oil-water and the air-water system scales as $\sigma_{oil}/\sigma_{air}$, we can write Eq. (A6) as:

$$\alpha_{oil} = \frac{S_{air}^2 \frac{\sigma_{oil}}{\sigma_{air}}}{2\left(\theta_{w_f} - \theta_{w_i}\right)} \qquad \text{(A7)}$$

where S_{air} is the sorptivity in the air-water system. Equation (8) is identical to Eq. (A5), replacing r_f by the curvature of the front.

REFERENCES

Baker, R. S., and D. Hillel, Laboratory tests of fingering during infiltration into a layered soil, *Soil Sci. Soc. Am. J.*, *54*, 20-30, 1990.

Cary, J. W., C. S. Simmons, and J. F. McBride, Predicting oil infiltration and redistribution in unsaturated soils, *Soil Sci. Soc. Am. J.*, *53*, 335-342, 1989.

Chuoke, R. L., P. van Meurs, and C. van der Poel, The instability of slow immiscible, viscous liquid-liquid displacements in porous media, *Trans. Am. Inst. Min. Eng.*, *216*, 188-194, 1959.

Darnault, C.J.G., J.A. Throop, A. Rimmer, D.A. DiCarlo, T.S. Steenhuis, and J.-Y. Parlange. 1996. Visualization by Light Transmission of Oil and Water Contents in Transient Flow Fields. Submitted to *Journal of Contaminant Hydrology*. 26 pp.

DiCarlo, D.A., T.W.J. Bauters, C. Darnault, T.S. Steenhuis, and J.-Y. Parlange. Vapor-Driven Growth of Preferential Flow Paths. (In preparation.)

Glass, R. J., T. S. Steenhuis, and J.-Y. Parlange, Wetting front instability. 2. Experimental determination of relationships between system parameters and two-dimensional unstable flow field behavior in initially dry porous media, *Water Resources Res.*, *25*, 1195-1207, 1989a.

Glass, R. J., J.-Y. Parlange, and T. S. Steenhuis, Mechanism for finger persistence in homogeneous, unsaturated, porous media: Theory and verification, *Soil Sci.*, *148*, 60-70, 1989b.

Glass, R. J., S. Cann, J. King, N. Bailey, J.-Y. Parlange, and T. S. Steenhuis, Wetting front instability in unsaturated porous media: A three-dimensional study in initially dry sand, *Trans. Porous Media J.*, *5*, 247-268, 1990.

Glass, R. J., J.-Y. Parlange, and T. S. Steenhuis, Immiscible displacement in porous media: Stability analysis of three-dimensional, axisymmetric disturbances with application to gravity-driven wetting front instability, *Water Resources Res.*, *27*, 1947-1956, 1991.

Glass, R. J. and M. J. Nicholl, Physics of gravity fingering of immiscible fluids within a porous media, An overview of current understanding and selected complicating factors, *Geoderma*, *70*, 133-164, 1996.

Hendrickx, J.M.H. and T-M. Yao. 1996. Prediction of Wetting Front Stability in Dry Field Soils Using Soil and Precipitation Data. In: Fingered Flow in Unsaturated Soil: From Nature to Model, T.S. Steenhuis, C.J. Ritsema, and L.W. Dekker, Editors. Special Issue of *Geoderma* 265-280.

Hillel, D. E., Unstable flows in layered soils: A review, *Hydrol. Proc.*, *1*, 143-147, 1987.

Liu, Y., B. R. Bierck, J. S. Selker, T. S. Steenhuis, and J.-Y. Parlange, High-intensity x-ray and tensiometer measurements in rapidly changing preferential flow fields, *Soil Sci. Soc. Am. J.*, *57*, 1188-1192, 1993.

Liu, Y., T. S. Steenhuis, and J.-Y. Parlange, Closed form solution for finger width in sandy soils at different water contents, *Water Resources Res.*, *30*, 949-952, 1994.

Parlange, J.-Y., and D. E. Hill, Theoretical analysis of wetting front instability in soils, *Soil Sci.*, *122*, 236-239, 1976.

Rimmer, A., D. DiCarlo, T. S. Steenhuis, B. Bierck, D. Durnford, and J.-Y. Parlange, Rapid fluid content measurement method in an oil-water-sand system using synchrotron x-rays, Submitted to *J. Cont. Hydrol.*, 1996.

Saffman, P. G., and G. Taylor, The penetration of a fluid into a porous medium or Hele-Shaw cell containing a more viscous liquid, *Proc. R. Soc. London, Ser. A*, *245*, 312-331, 1958.

Schroth, M. H., J. D. Istok, S. J. Ahearn, and J. S. Selker, Geometry and position of light nonaqueous-phase liquid lenses in water-wetted porous media, *J. Cont. Hydrol.*, *19*, 269-287, 1995.

Schroth, M. H, S. J. Ahearn, J. S. Selker, and J.D. Istok, Characterization of Miller-similar silica sands for laboratory hydrologic studies, *Soil Sci. Soc. Am. J.*, *60*, 1331-1339, 1996.

Selker, J. S., T. S. Steenhuis, and J.-Y. Parlange, Wetting front instability in homogenous sandy soils under continuous infiltration, *Soil Sci. Soc. Am. J.*, *56*, 1346-1350, 1992a.

Selker, J. S., P. Leclerq, J.-Y. Parlange, and T. S. Steenhuis, Fingered flow in two dimensions. Part 1: Measurement of matric potential, *Water Resources Res.*, *28*, 2513-2521, 1992b.

Selker, J. S., J.-Y. Parlange, and T. S. Steenhuis. Fingered flow in two dimensions. Part 2: Predicting finger moisture profile, *Water Resources Res.*, *28*, 2523-2528, 1992c.

Table 1. Summary of observed two-dimensional finger widths for oil-water and air-water fluid pairs in 12-20 and 20-30 sand.

Sand type:	12-20		20-30	
Fluids (initial-invading):	oil-water	air-water	oil-water	air-water
FINGER DIAMETER (cm)				
This study	4.7 (1.0)[1]	---	4.8 (1.0)	---
Rimmer et al. (1996)	---	---	4.6	---
Darnault et al. (1996)	5.3	---	---	---
DiCarlo et al. (1997)	---	1.7 (0.2)	---	2.3 (0.3)
Hendrickx & Yao (1996)[2]	---	1.6	---	2.6
Liu et al. (1994)	---	---	---	2.25
Selker et al. (1992a)	---	---	---	1.7
OBSERVED SCALING BETWEEN FLUID PAIRS		2.8		2.1

[1] The number in parentheses is the standard deviation when known.

[2] Three-dimensional finger width converted to a two-dimensional width by multiplying by $\pi/4.8$.

LIST OF FIGURES

Figure 8: Calculated and observed scaling of finger diameters in air-water and oil-water systems.

Figure 9: Water-oil front for a vertical line source.

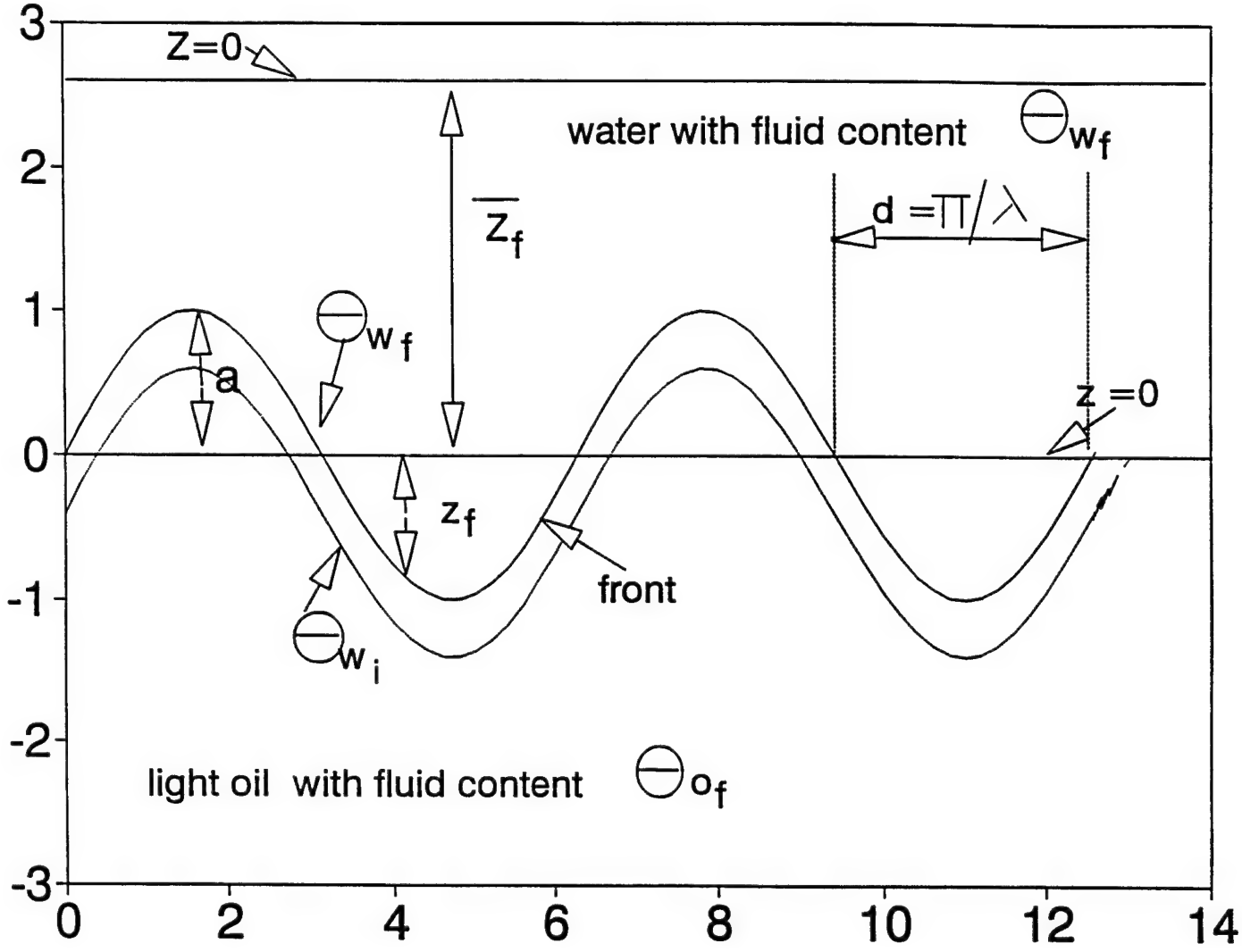
Z=0
water with fluid content
$\ominus_{w_f}$
$\overline{z_f}$
d =π/λ
$\ominus_{w_f}$
a
z =0
z_f
front
$\ominus_{w_i}$
light oil with fluid content
$\ominus_{o_f}$
3
2
1
0
-1
-2
-3
0
2
4
6
8
10
12
14

Fig 1

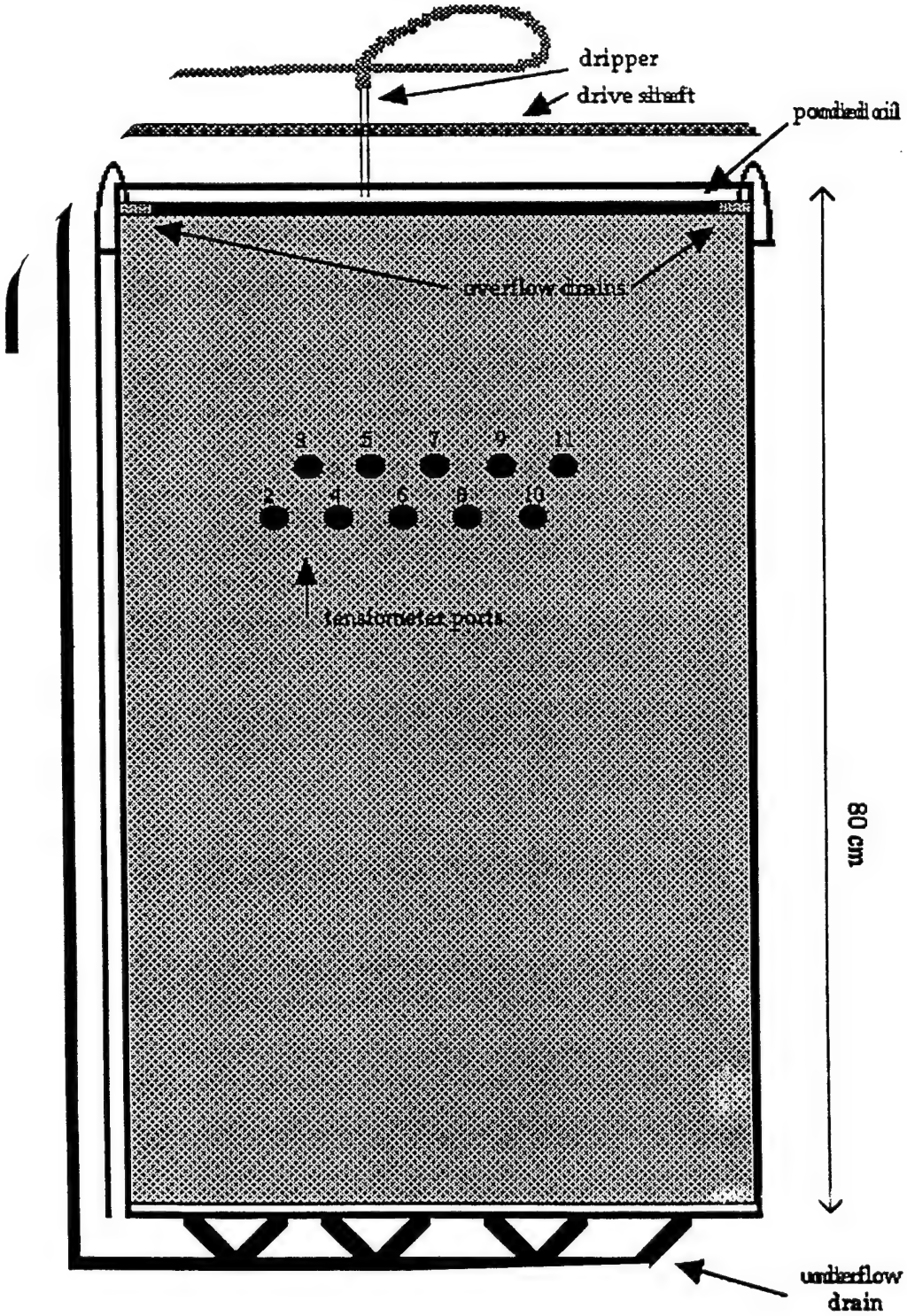
dripper
drive shaft
overflow drains
3
5
7
9
11
2
4
6
8
10
tensiometer ports
80 cm
underflow
drain

Fig 2

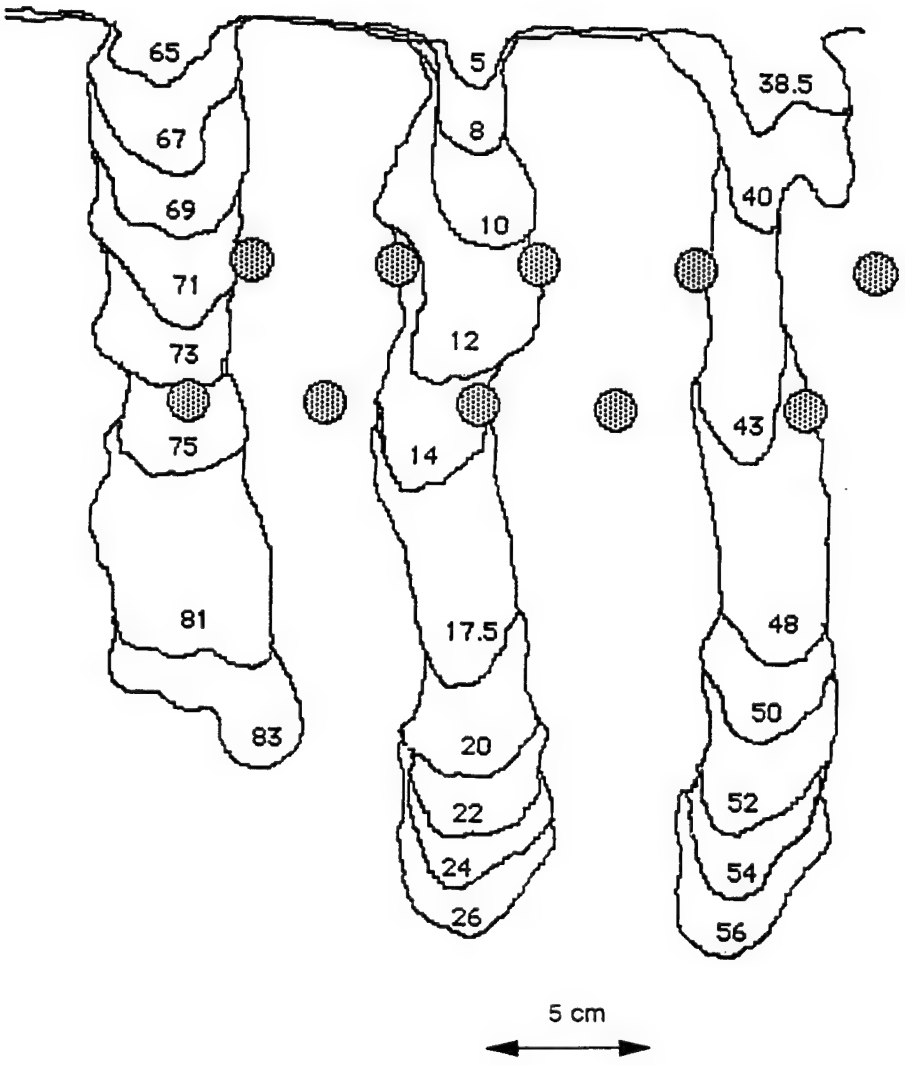
65
67
69
71
73
75
81
83
5
8
10
12
14
17.5
20
22
24
26
38.5
40
43
48
50
52
54
56
5 cm

Fig 3

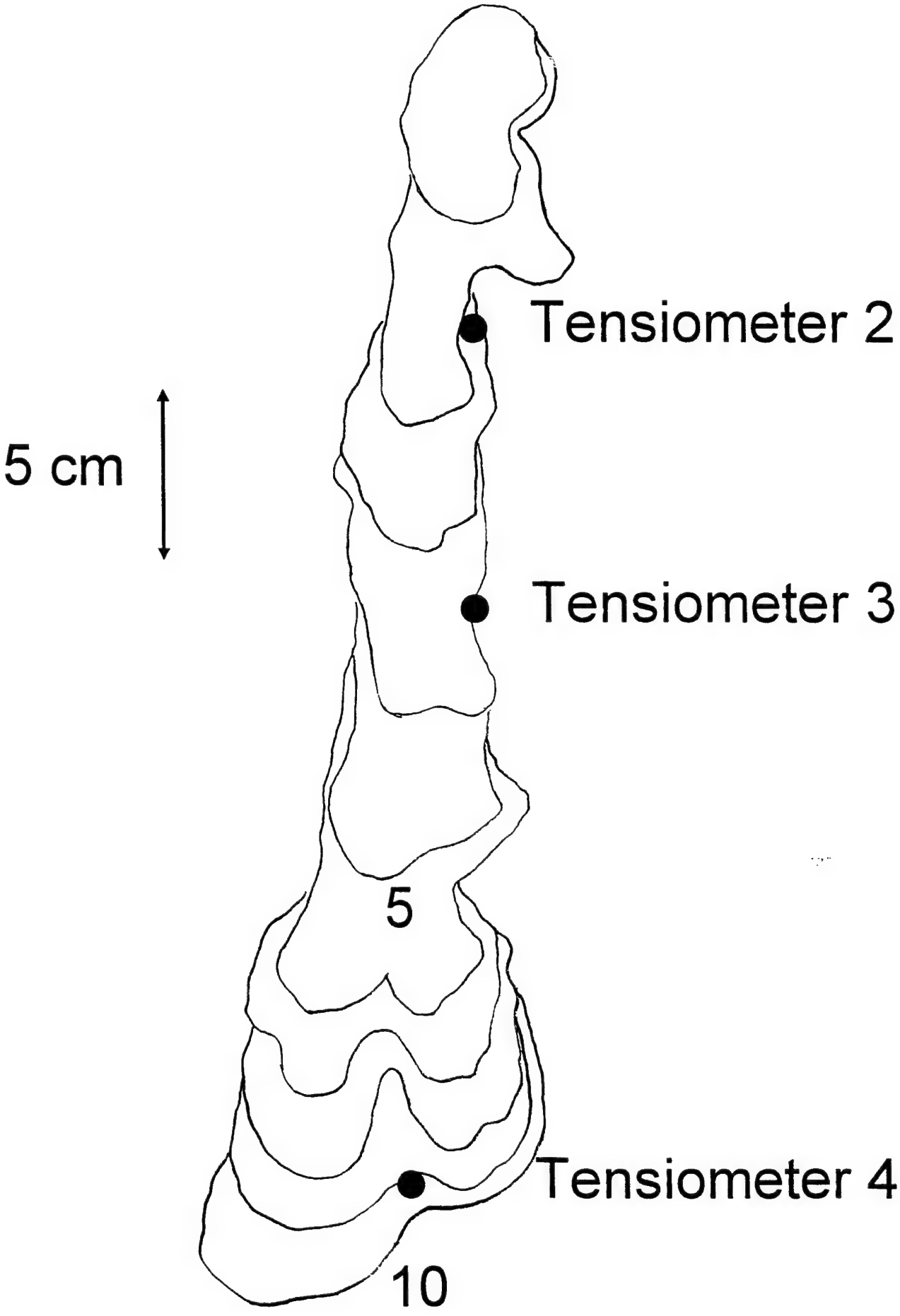

Fig 4

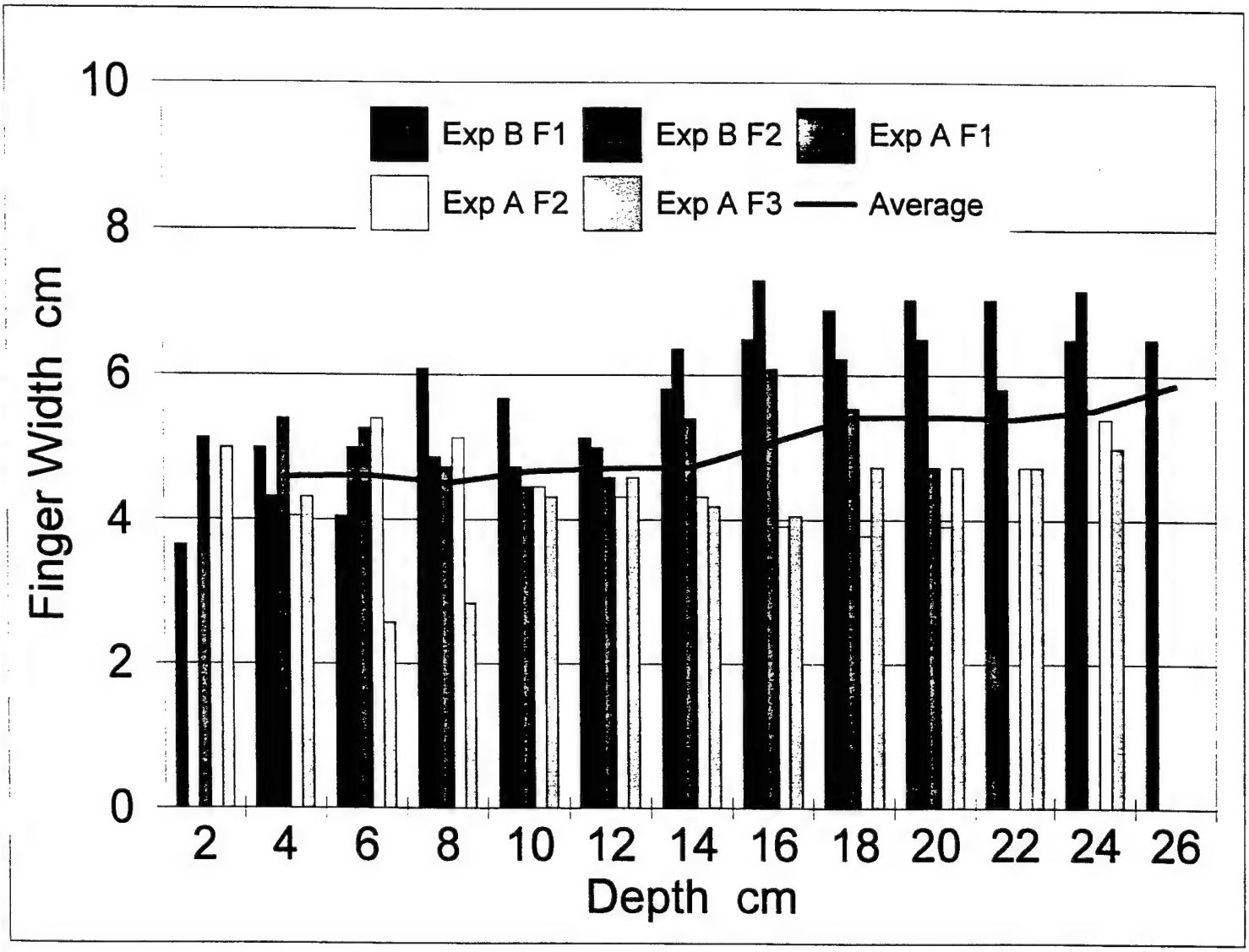
10
8
6
4
2
0
Finger Width cm
Exp B F1
Exp B F2
Exp A F1
Exp A F2
Exp A F3
Average
2
4
6
8
10
12
14
16
18
20
22
24
26
Depth cm

Fig 5

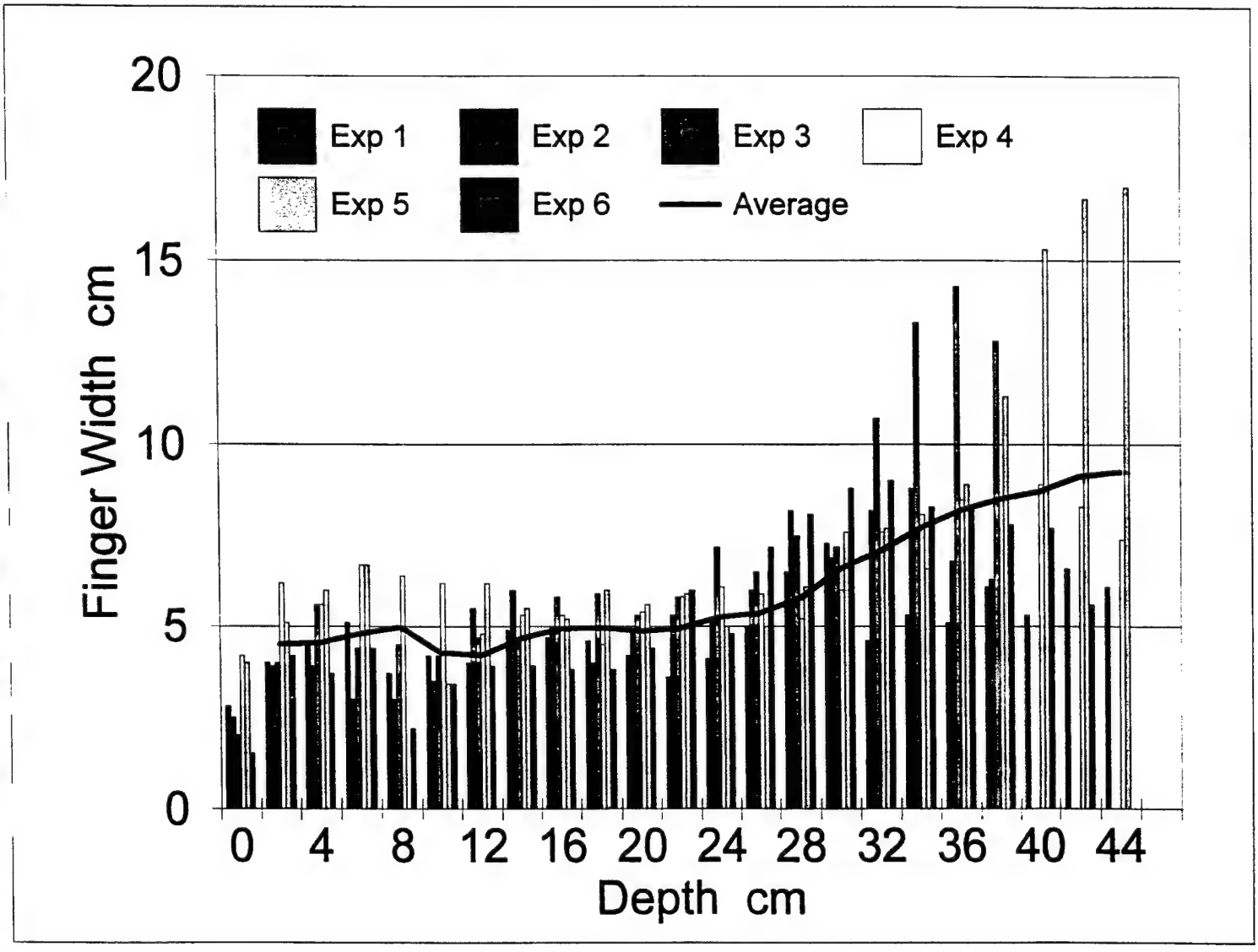
20
15
10
5
0
Finger Width cm
Exp 1
Exp 2
Exp 3
Exp 4
Exp 5
Exp 6
Average
0
4
8
12
16
20
24
28
32
36
40
44
Depth cm

Fig 6

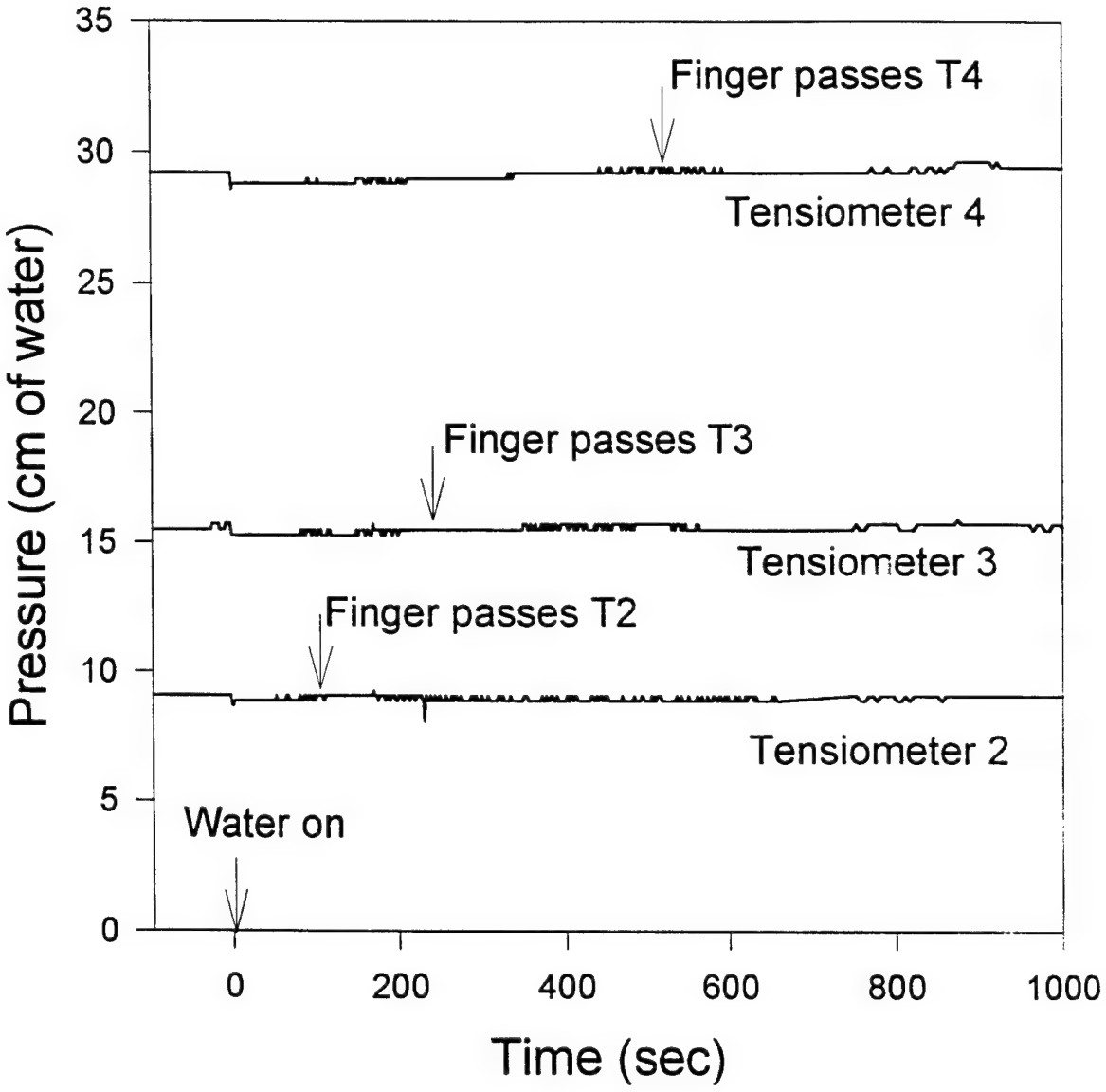
Oil Pressures
Pressure (cm of water)
35
30
25
20
15
10
5
0
Finger passes T4
Tensiometer 4
Finger passes T3
Tensiometer 3
Finger passes T2
Tensiometer 2
Water on
0
200
400
600
800
1000
Time (sec)

Fig 7

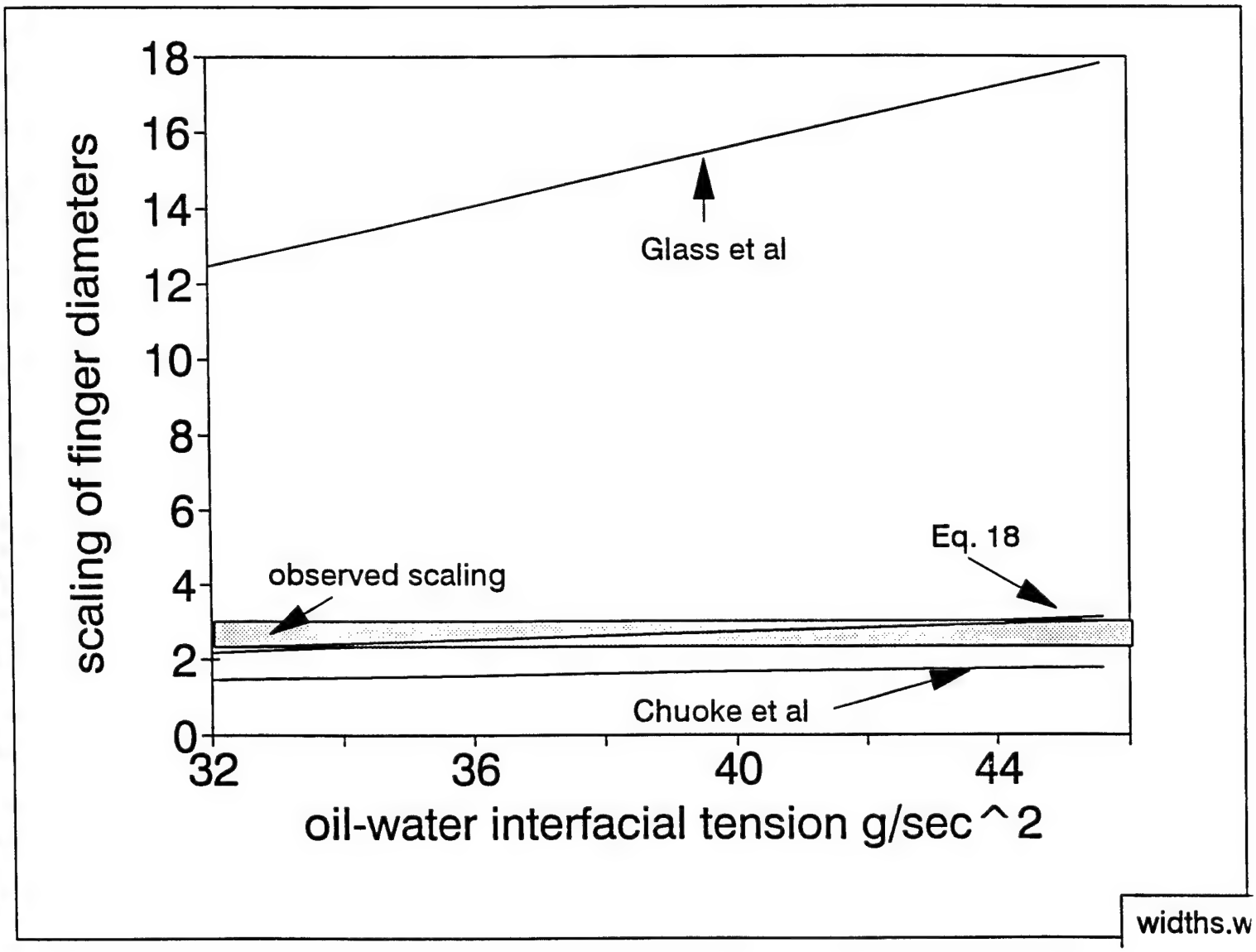
scaling of finger diameters
18
16
14
12
10
8
6
4
2
0
32
36
40
44
oil-water interfacial tension g/sec ^ 2
Glass et al
Eq. 18
observed scaling
Chuoke et al
widths.w

Fig 8

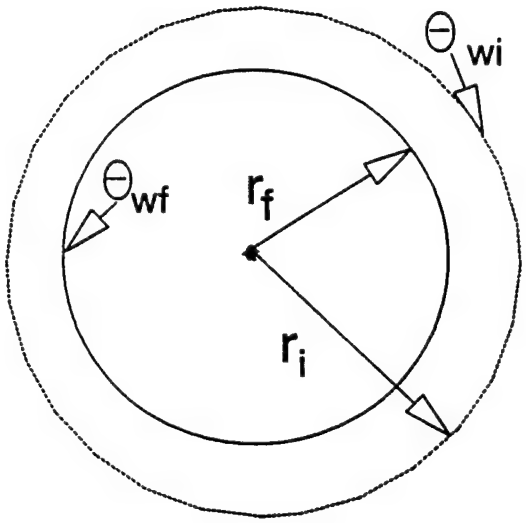

Fig 7

APPENDIX B

RAPID FLUID CONTENT MEASUREMENT METHOD IN AN OIL-WATER-SAND SYSTEM USING SYNCHROTRON X-RAYS

A. Rimmer, D.A. DiCarlo, T.S. Steenhuis,
B.R. Bierck, D. Durnford, and J.-Y. Parlange

Journal of Contaminant Hydrology (Accepted)

RAPID FLUID CONTENT MEASUREMENT METHOD IN AN OIL-WATER-SAND SYSTEM USING SYNCHROTRON X-RAYS

Alon Rimmer[1], David A. DiCarlo[1], Tammo S. Steenhuis[1]*,

Barnes Bierck[1], Deanna Durnford[2], and J.-Yves Parlange[1]

[1]Department of Agricultural and Biological Engineering, Cornell University, Ithaca, NY 14853.

[2]Department of Chemical and Bioresource Engineering, Colorado State University, Ft. Collins, CO 80523.

*Corresponding author.

ABSTRACT

The complexity of simultaneous flow of water and non-aqueous phase liquids is largely unappreciated because few techniques permit accurate quantitative measurement of water and oil contents in rapidly changing flow fields. High intensity x-rays were used at the Cornell High Energy Synchrotron Source (CHESS) to obtain rapid, accurate, and non-destructive quantitative measurements of the changing fluid contents in a porous media during infiltration events. Concomitant temporal pressure measurements were obtained for each liquid phase using rapid responding tensiometers. The system was used for measuring temporal volumetric fluid content changes during a water finger infiltration into sand saturated with a NAPL (Soltrol-220) in a two-dimensional soil slab. The fluid content distribution of a finger in the oil-water system was found to be similar to air-water systems. The hysteretic constitutive relationship between pressure and the content was developed from the data. The relationship was used to explain why the finger did not widen behind the tip, and why, upon re-infiltration, water followed the previously established path. These findings are relevant for cleanup of oil contaminated sites because it aids in the understanding of hydrologic control which is an essential component of cost-effective in situ remediation.

INTRODUCTION

Groundwater contaminants are introduced at or near the soil surface via spills, leakage from fuel tanks, or overfilling of tanks. Many of these contaminants are organic compounds of low water solubility, existing as separate liquid phases in soil pore spaces (Dane et al., 1992). The problem is severe. For example, the volume of contaminants at 130 Department of Energy (DOE) facilities alone exceeds 2,500 billion liters (Department of Energy, 1995; Wilkins et al., 1995). The anticipated life-cycle cleanup costs are expected to be greater than 300 billion dollars and will take at least 100 years using existing technologies.

In situ remediation technologies are the only viable approaches with potential for controlling the huge costs and extended times required to clean up these sites. However, cleanup procedures are often instituted and operated with limited knowledge of both the physical and chemical processes governing contaminant transport (Wilkens et al., 1995). To be effective complete hydrologic control of the subsurface at the remediation site is critical. Hydrologic control at NAPL contaminated sites can be improved by accurately measuring water and oil contents in rapidly changing flow fields (Mercer and Cohen, 1990).

Early observations of oil and water flow were made in Hele-Shaw flow cells by Saffman and Taylor (1958) and Chuoke et al. (1959). Currently, most real-time, non-intrusive measurements of oil and water contents in porous media are made using gamma- and x-ray attenuation techniques. For example, a dual energy gamma radiation method was described by Hopmans

and Dane (1986), and was applied to study saturation changes during monotonic liquid drainage (Lenhard et al., 1988; Dane et al., 1992). The x-ray absorption (film-based radiography) technique described by Tidwell and Glass (1994) can be used to obtain full field oil and water contents. However, the conventional x- and gamma-ray methods are limited by the relatively low intensity of Am 241, Cs 137, and x-ray tube sources, which do not permit accurate monitoring of flow phenomena occurring in porous media on temporal scales of seconds.

Other methods for determining oil and water fluid contents and that permit measurement of rapidly changing flow fields is the full-field visualization techniques, described by Van Geel and Sykes (1994) and Darnault et al. (1996) which involve dying the fluids and analyzing the visual information with computer graphics techniques. Van Geel and Sykes (1994) dyed the oil red, and analyzed the reflected light. This determined the fluid contents near the glass wall which may not represent that of the chamber. Darnault et al. (1996) colored the water with 0.005% blue dye and recorded the transmitted light from a bank of high frequency fluorescent lights behind the slab chamber. The color (or hue) of the images was related to moisture content values. However, scattering near the edges made it more difficult to see sharp boundaries. Moreover, the sands need to be translucent (Tidwell and Glass, 1994). While light transmission techniques allow monitoring of many array points in a relatively large two-dimensional section of a soil slab, x-ray attenuation permits more accurate water content measurements in a small section of any soil type.

A final destructive method for visualizing oil and water contents is by using oils that solidify. After solidification, the columns are sectioned and the distribution of oil studied (Conrad et al., 1992; Powers et al., 1992).

The objective of this paper is to present a method using synchrotron x-rays that allows rapid quantitative, and precise measurements of fluid contents in oil-water systems. Synchrotron radiation can be up to 10,000 times as intense than conventional x-ray sources, which decreases errors and counting times. Synchrotron beam lines are rapidly increasing and are available to the general scientific community.

To illustrate the application of the synchrotron x-ray technique, we experimented with fingered flow through a soil initially saturated with a light oil (Soltrol 220). Soltrol has negligible water solubility, very low volatility at room temperatures, as well as a low health hazard. We measured fluid contents and pressures in both phases using phase sensitive tensiometers. This study is relevant because fingered flow generated by chaotic disturbances in a flow field is one of the factors complicating hydrologic control during in situ cleanup, and can render the use of in situ treatment remedies ineffective because of hydrodynamic bypassing of subsurface pollutants. With the result of the synchrotron experiments, the forming and persistence of these bypass flow paths are explained. It is shown that because of hysteresis in the constitutive relationships, these paths are in equilibrium with the surrounding oil fluid. Finally, the synchrotron and other measurements are used to scale the finger diameter. By taking soil and fluid properties into account we calculate the dimensions of the bypass flow paths.

BACKGROUND

Unstable Flow Phenomena

Instabilities involving two immiscible fluids (known as bypass flow) have been observed in the oil industry for some time (Craft and Hawkins, 1959). General stability criteria for two liquids have been given by Saffman and Taylor (1958) and Chuoke et al. (1959) and specific criteria for air-water systems in soil by Parlange and Hill (1976), Raats (1973), Philip (1975), and Hillel and Baker (1988). In general, the flow will be unstable if the pressure difference between the two liquids is greatest where the fluid has intruded the farthest. This condition can be met when a less viscous fluid intrudes into a more viscous fluid, and/or when a denser fluid intrudes with gravity into a less dense fluid.

Diameters of fingers in air-water systems were calculated by Parlange and Hill (1976), Glass et al. (1989a,b), and Liu et al. (1994a). The equation derived from Parlange and Hill (1976) and by Liu et al. (1994a) is the simplest and applies to well sorted sands (i.e., those with narrow particle size distributions) where the slope of the wetting branch of the soil characteristic curve, $dh_{a/w}/d\theta_w$, is straight over the portion that $K(\theta)$ is decreases rapidly with moisture content and is written as by Liu et al. (1994a) as:

$$d_{a/w} \approx \frac{2\,\kappa\,\theta_f \left(\frac{dh_{a/w}}{d\theta_w}\right)}{\eta + 1.5} \qquad (1)$$

where κ is equal to π for two-dimensional fingers and 4.8 for three-dimensional fingers (Glass et al., 1990) and θ_f is the moisture content at the finger tip. η may be found as (Brooks and Corey, 1964):

$$\eta = \frac{2}{\lambda} + 3 \tag{2}$$

where λ is a positive index related to the pore size distribution of soil with values ranging from 2 to 7 resulting in η values between 3.3 and 4.

Based on Hele-Shaw type of experiments, finger width for two-phase immiscible liquid systems was given by Chuoke et al. (1959) who assumed that a relationship analogous to the Laplace-Young relationship exists between the macroscopic frontal curvature and the pressure jump across the front as (Glass et al., 1991b):

$$d_{o/w} = \kappa\left[\frac{3\sigma^*}{g(\rho_w - \rho_o)\left(1 - \frac{q}{K_{w_f}}\right)}\right]^{0.5} \tag{3}$$

A difficulty with Eq. (5) is the "effective" surface tension σ^* which has not been defined, although Homsy (1987) associated it with a modified capillary number. g is the gravity, ρ_w is specific weight of water, ρ_o is specific weight of oil, q is flux, and K_{wf} is the conductivity in the finger.

Chandler et al. (1996) assumed little resistance to moving of the oil and related finger widths for air-water systems, $d_{a/w}$ and oil-water systems $d_{o/w}$ as:

$$\frac{d_{o/w}}{d_{a/w}} = \frac{\frac{\sigma_{o/w}}{\sigma_{a/w}}}{1 - \frac{\rho_o}{\rho_w} - \frac{q}{K_{w_f}}} \tag{4}$$

where the σ's are the surface tension for fluid pairs. Combining Eqs. (1) and (4) and noting that the term with the velocity q/K_{wf} is usually small compared to the other term $(1-\rho_o/\rho_w)$, and the matric potential between fluid pairs scale as the surface tension (Parker and Lenhard, 1987), we find that:

$$d_{o/w} = \frac{2\,\kappa\,\theta_f \frac{dh_{o/w}}{d\theta_w}}{\left(1 - \frac{\rho_o}{\rho_w}\right)(\eta + 1.5)} \tag{5}$$

where the $dh_{o/w}/d\theta_w$ is the slope of the wetting part of the oil-water characteristic curve. For very low infiltration rates, the slope may change (Yao and Hendrickx, 1996) and the more complete equations of Parlange and Hill (1976) need to be used.

SCALING OF FINGER DIAMETER

Equation (3), assuming that σ^* scales like the surface tension, and Eq. (5) predict different finger scaling behavior with fluid density, fluid interfacial tension, and the coarseness of the porous media. In the following analysis we will compare widths of slow moving fingers and, thus, minimize the effects of the flux dependency. Noting that matric potential scales as the inverse

of the microscopic length (Miller and Miller, 1956) we can also write the finger scaling in the form:

$$d = d^* c \left[\frac{D_{50}^*}{D_{50}} \frac{G^*}{G} \frac{\sigma_{nw/w}}{\sigma_{nw/w}^*} \right]^b \tag{6}$$

where the superscript * is the "reference soil with reference fluids", $G = (1-\rho_{nw}/\rho_w)$ and accounts for different fluid densities, and D_{50} is mean particle diameter. The subscript w is for wetting and subscript nw for nonwetting. The coefficient, b, equals 1 for scaling according to Eq. (4) and b is 0.5 using Eq. (3) of Chuoke et al. (1959). The factor c is a correction factor for difference in moisture content in the finger tip and type of chamber used (2 or 3 dimensional). By introducing scaling factors for the particle size, f_D, for gravity, f_G, and surface tension, f_σ, Eq. (6) can be rewritten as:

$$d = c \left[f_D f_g f_\sigma \right]^b d^* \tag{7}$$

where

$$f_D = \frac{D_{50}^*}{D_{50}} \tag{8}$$

$$f_G = \frac{G^*}{G} \tag{9}$$

$$f_\sigma = \frac{\sigma_{nw/w}}{\sigma_{nw/w}^*} \tag{10}$$

$$c = c_\theta c_\kappa$$
$$c_\theta = \frac{\theta_f}{\theta_f^*} \qquad (11)$$
$$c_\kappa = \frac{\kappa}{\kappa^*}$$

In Eq. (11) the κ is the coefficient introduced by Glass et al. (1990), for 2-d ($\kappa=\pi$) and for 3-d ($\kappa=4.8$). The correction for moisture content in the finger tip, c_θ is based on fluid content measurements. The effect of the moisture content on the finger is not specified in Chuoke's Eq. (3). The correction factor tends to be small and, therefore, the high precision is not necessary.

Oil and Water Content Measurement Using Synchrotron X-Rays

Bierck et al. (1988) described a method using synchrotron radiation to monitor consolidation of clays under seepage stress. The high intensity of synchrotron radiation permitted acquisition of transmitted x-ray intensities through relatively thick regions (on the scale of centimeters) during short time intervals (in a second or less). This method was adapted as described by Liu et al. (1993) to measure water content changes during rapid water finger movement through sand.

In a two-fluid system, here oil and water, the water content can be directly related to the attenuation of the x-rays, $\ln(I/I_0)$, where I and I_0 are the transmitted and incident radiation intensities, respectively. Straightforward calculations (Liu et al., 1993; Lenhard et al., 1988) yield the water content in terms of the measured x-ray attenuation, as:

$$\theta_w = \frac{\ln\left(\frac{I}{I_0}\right) - \ln\left(\frac{I_{sat}}{I_0}\right)}{(\alpha_o - \alpha_w)x} . \qquad (12)$$

Here θ_w is the volumetric water content (cm^3/cm^3), I_{sat} is the transmitted intensity through the initially oil-saturated porous media, x is the thickness of the chamber (cm), and α_w and α_o are the attenuation coefficients (cm^{-1}) for the water and oil. The volumetric oil content θ_o is given by:

$$\theta_o = n - \theta_w , \qquad (13)$$

where n is the total pore volume.

MATERIALS AND METHODS

Experiments were carried out at the F-2 beam line of the Cornell High Energy Synchrotron Source (CHESS), which provides an intense, high energy x-ray beam (Batterman and Ashcroft, 1979). Using a Si(311) monochromator, the beam's energy was tuned to 33.2 KeV. This energy level was chosen because it was slightly above the iodine absorption edge and increased the contrast between oil and water doped with 30 g/l of potassium iodine. Subsequently, the beam passed through a set of slits, a sealed Xe ionization chamber, the sample chamber, and another sealed Xe ionization chamber. Ionization chambers produce a current directly proportional to the x-ray intensity that passes through them. The slits defined a beam cross-section of 0.1 cm high and 0.6 cm wide. For each ion chamber, the current was converted into a frequency, and acquired by a computer which automatically recorded the relative incident and

transmitted radiation. The sample chamber was mounted on a computer controlled translation stage, allowing monitoring of fluid content changes at different positions within the chamber.

The soil slab, illustrated in Figure 1, was a chamber 54 cm high, 23 cm wide, and 0.95 cm thick with 0.95 cm polycarbonate walls, equipped with four water and four oil tensiometer ports. The chamber was positioned vertically such that the x-rays struck (and, thus, monitored the fluid contents) 2 cm below the lower oil tensiometers and 30 cm below the top of the chamber. This initial position is indicated by a dotted line in Figure 1.

Two types of sieved silica sand were used to pack the chamber; either "20/30 sand" or "12/20 sand" with grain diameters between 0.59-0.85 mm and 0.85-1.5 mm, respectively. Soltrol 220, a mixture of alkanes C13 through C17 (Phillips 66 Company), provided the oil phase for the experiments. Distilled water doped with potassium iodine at 30 g/L, and colored blue with FD&C Blue #1, provided the aqueous phase. The potassium iodine increased the x-ray attenuation of the aqueous phase, and the blue food coloring allowed a visual inspection of water position.

Oil and water specific tensiometers were developed by modifying high-speed tensiometers (Selker et al., 1992a) to measure oil (ψ_o) and water (ψ_w) pressures. The matric potential is the difference of the oil and water pressure measurements. The interiors of the oil tensiometers were filled with oil and a hydrophobic plastic (hydrophilic glass) porous plate provided the connection to the soil. The water tensiometers used a porous glass plate with relatively large

pores. The oil tensiometers and their connections are illustrated in Figure 2. A three-way valve connected pressure transducers to either a tensiometer or the atmosphere, enabling readings of reference pressures during experiments. Each transducer output was amplified, converted into a frequency, and captured by a data acquisition system. Calibration of the readings into centimeters of water was achieved by recording the transducer output under a sequence of measured water column heights. During the experiments, the pressure data was recorded simultaneously with the x-ray intensity measurements.

EXPERIMENTAL PROCEDURE

Initially the constants in Eqs. (12) and (13) (x, η, α_w, and α_o), were measured. The thickness of the chamber, x, was determined using a dial caliper, and the porosity was calculated from the volume of oil required to saturate a given volume of the packed soil slab.

The attenuation constants α_w and α_o were determined using the method described by Lenhard et al. (1988). A polycarbonate standard cell with five sequential, 0.5 cm thick compartments was employed. X-ray attenuation was measured for the (empty) standard cell after each compartment was sequentially filled with either water or oil. A linear regression of the attenuations yielded the attenuation constants for the two fluids. This procedure was repeated several times throughout the experimental period to verify the stability of the standards and the beam.

Six separate finger experiments were conducted using two sieved sand types (12/20 and 20/30; the numbers refer to the sieve numbers) and three water infiltration rates (Table 1). As we were interested in testing both the changing fluid contents versus time within the finger, and the fluid contents in a horizontal cross section of the finger, x-ray attenuation measurements were collected in two different fashions. The first consisted of measuring the attenuation at one particular position versus time, the second consisted of measuring the attenuation versus the horizontal position of the chamber. In a typical experiment, most of the time was spent observing fluid changes within the finger boundaries, with periodic checks of how the finger cross section had changed. The tensiometer data was taken at all times.

Using a peristaltic pump, the sand was saturated from the bottom with oil. Once the chamber was filled with oil, water was infiltrated through a point source at the top of the chamber. A closed drainage system, described below, maintained a relatively constant oil level and pressure even as the water displaced the oil. A nalgene tube connected the bottom of the chamber to the side of an oil filled drainage bottle (Figure 1). Another tube connected the top of the drainage bottle to a T-fitting set at the height of the chamber oil level. As water displaced the oil, the excess oil drained through the bottom of the chamber and out through the T-fitting, keeping the oil level constant. The experiment ended when water displaced all the oil in the collecting bottle, thus filling the exit tube with water and raising the oil pressure.

The applied water initially spread both horizontally and vertically while at the top of the chamber, but soon a water finger formed and moved slowly down the chamber. In the coarse

12/20 sand the finger moved straight down, while in the finer 20/30 sand its path tended to meander slightly sideways. During re-infiltration episodes the water followed its previous path down through the chamber.

Relative pressure measurements in the synchrotron were found to have an accuracy of 0.1 cm of water, but absolute pressures were found to be much less accurate (approximately 5 cm of water). In order to improve the overall accuracy, the experiments were repeated without using the x-ray technique under the same conditions to determine absolute pressures in the fingers. These experiments showed identical relative pressure changes, but also provided absolute pressures accurate to 1.0 cm of water. Thus, pressure data taken simultaneously with the x-ray data was offset to match the absolute pressures obtained from the concomitant experiments. In these experiments we also measured size and shape of the fingers.

RESULTS AND DISCUSSION

The observations of the distribution of the fluid contents and pressure in the fingers is shown first because it allows us to illustrate the utility of the synchrotron x-rays for documenting the relatively fast moving unstable flows. Then we will show how these measurements can be used to obtain the hysteretic constitutive relationships that explain why fingers are persistent and how fingers scale for Miller and Miller similar soils.

Observations

Table 1 shows the diameter and moisture content in the finger tips for the six synchrotron experiments. The porosity of the sand was 0.36. The oil and water contents in the tip of the fingers for the 12/20 sand obtained with the synchrotron experiment compared well with those obtained with the light transmission technique of Darnault et al. (1996). To our knowledge there are no other measurements available for comparison purposes of fluid contents in rapidly moving oil-water fingers.

Although in each of the six synchrotron experiments accurate measurements of the oil and water contents in the finger were obtained, both sets of tensiometers were contacted by the water finger in only one of the experiments (#5). The 12/20 sand was used and the water infiltration and (re-infiltration) rate was 2.3 ml min^{-1}. A finger, 3-4 cm in width, formed and moved down the chamber, contacting the center sets of tensiometers. Figure 3 shows the temporal changes in water content and capillary potential (ψ_w - ψ_o) during the first infiltration. The passage of the finger can be seen in the time delays between the response of the top and center tensiometers. Also, the water content readings were obtained about 50 sec later than the center tensiometer reading. The pressures and water content exhibit behavior typical of fingers and unstable flow as observed in water-air systems by Selker et al. (1992b); the water content rises abruptly, levels off temporarily, and then drops to a constant value when the finger hits the bottom of the chamber at around 1000 sec. When the water was turned off at approximately 1500 sec, the water content underwent another abrupt drop as the water drains to the bottom and is replaced

by oil. The tensiometer readings also show the typical behavior of unstable flow in which the matric potential decreases behind the front. Also, after the water is turned off the matric potential drops even further.

Figure 4 shows the temporal changes in water content during a re-infiltration episode. In contrast to the initial infiltration, neither the water content nor the pressure difference decreased until the water was turned off. The flow within the original finger boundaries does not show the characteristic drop of pressure behind the finger tip and has characteristics similar to a "standard" wetting front (i.e., when water infiltrates in a soil with a horizontal wetting front) in which the matric potential increases at the front and then remains relatively constant behind the wetting front. Also, the time delays between the tensiometer and water readings is much less than was observed in the initial infiltration (Figure 3), showing a much quicker passage of the pulse. All re-infiltration episodes exhibited identical behavior although they are not reported here.

Figure 5 shows the horizontal profile at selected times during the infiltration and re-infiltration cycles. The profile extends from about the middle of the finger to outside of the finger, depicting the wide variation of water contents at the same height. The measured horizontal boundary of the finger is about 8-10 mm wide, but the actual boundary is likely much smaller than this, as much of the measured width is due to the fact that the x-ray beam was 6 mm wide. In addition, the boundary (and, thus, the width of the finger) did not change measurably during

re-infiltration episodes. Note that this follows the air-water finger observations in which during re-infiltration the finger width remains the same and the moisture content is lower.

Persistence

Most theory of unstable flow has been focussed on the instability itself. Persistence of fingers over time especially in oil-water systems has received only little attention as noted by Glass and Nicholl (1996). In air-water systems the hysteretic nature of the constitutive relationship has been crucial to understanding the finger persistence (Glass et al., 1989c; Liu et al., 1994b). We will show here that for oil-water systems the hysteresis plays much the same role.

The synchrotron data presented above allows us to construct for oil-water systems the constitutive relationship between the fluid pressure difference and water content. Taking into account the travel time between pressure and fluid content measurement location, the data in Figures 3 and 4 are replotted to give the primary and secondary wetting loops in Figure 6. In this figure, the letter "A" refers to the primary wetting branch beginning at A1 (oil saturated soil) via A2 (finger front starts affecting the readings) to A3 (just behind the finger tip front). Shortly after the finger tip passes the tensiometers, the pressure starts decreasing at B1 which is the starting point of the primary drying branch, "B". Between points B1 and B2, the matric potential decreases further while the finger remains at the high moisture content. This represents the wetted water bulb similar to the air-water systems (Selker et al., 1992b). Then while the finger tip is moving farther down, both moisture content and matric potential are decreasing until point

B3 where the water is turned off. At point B4 no water is draining out of the chamber anymore. Branches "C" and "D" are the wetting and drying curves during re-infiltration. Both water content and matric potential are lower in the finger tip during re-infiltration than the initial infiltration resulting in secondary wetting and drying branches within the primary loops. All the re-infiltrations followed the second smaller hysteresis loop (only one is shown here).

The data in Figure 6 make it possible to understand why the finger during the initial infiltration into the oil saturated soil does expand only in the lowest portion of the tip and why the finger during re-infiltration does not go outside its confines set during the initial experiments. Sideways movement of the finger is governed by the sorptivity. Only when the sorptivity is zero the finger will not expand sideways. The sorptivity, S, can be defined as (Parlange, 1975; Brutsaert, 1976):

$$S^2 = 2\sqrt{\theta_f}\int_{\psi_{out}}^{\psi_f}\sqrt{\theta_w}\,K_w(\psi)\,d\psi \qquad (14)$$

where the conductivity, $K_w(\psi)$ and the moisture content, θ_w, are functions of matric potential on the wetting branch. The integration constants are ψ_f which is the matric potential inside the finger and ψ_{out} is potential outside the finger. Although the conductivity function is not known it is obvious that the K_w is zero when the water content is zero. Consequently, if the moisture content of the wetting curve between the integration constants is zero, we can safely assume that the sorptivity is zero too.

To examine whether the finger is expanding it is necessary to investigate the relationships of fluid contents in and outside the finger. Earlier we found that the water content matric potential relationship for the soil outside the finger is on the primary wetting loop (indicated by "A") and the soil inside the finger is on curve "B" during the initial infiltration experiment or curves "C" or "D" for each of the re-infiltration experiments (Figure 6).

The matric potential decreases with increasing distance above the finger tip. When the matric potential, ψ_f, decreases below the matric potential of point A2 (-0.75 cm in Figure 6), the moisture content between ψ_f and ψ_{out} is zero and, hence, the sorptivity calculated in Eq. (8) becomes zero. Accordingly, anywhere in the finger with a matric potential less than -0.75 cm, the finger will not expand. Only in the region near the finger front the finger is expanding.

During re-infiltration the matric potential inside the finger varies from -2 to -4 cm. At these tensions the water contents on the primary wetting curve remain zero. Thus, the conductivity and sorptivity are also zero, and the finger cannot cross the original boundary of the earlier established finger. We can now also understand why the finger has a stable-like wetting front inside the "old" (i.e., previously formed) finger. Within the "old" finger the infiltration and sideways movement are governed by the secondary hysteresis loops, with a finite sorptivity value at all pressures behind the finger tip.

These findings are important because it shows that knowledge concerning the constitutive relationships are required for hydrodynamic control in remediation sites with immiscible liquids.

It also shows that when models do not include these hysteretic constitutive relationships, no realistic planning of cleanup procedures can be achieved. The difficulty is, however, that the hysteretic constitutive relations for oil-water systems are generally not known. We will investigate next if Miller and Miller (1956) scaling can be used to obtain the hysteretic constitutive relations as well as the finger diameter.

Scaling of Fingers

Before we compare the observed and predicted width by scaling we will justify the scaling parameters used.

Glass et al. (1991a), Parlange et al. (1990), and Schroth et al. (1996) found that the sands in Table 2 are Miller and Miller scale similar and can be scaled according to Eq. (8) with the mean particle sizes given in Table 2.

The scaling factor for interfacial tension, f_σ, is somewhat uncertain due to unknown contact angle (Chandler et al., 1996) and the change of interfacial tension of oil and water in time (Schroth et al., 1995). Here we derive the scaling for interfacial tension, f_σ, by matching the soil characteristic curves of oil-water and air-water systems. This has the advantage that $\sigma_{o/w}$ includes the unknown contact angle. Schroth et al. (1996) found f_σ, values between 1.6 and 1.8 by matching drainage curves in oil-water and air-water systems for different sand sizes. In Figure 7, we compared the scaled 12/20 air-water drainage curve of Schroth et al. (1996) using

f_σ = 1.76 and the soil oil-water characteristic curve (Figure 5). The scaled soil characteristic air-water curve for 20/30 sand (Liu et al., 1994a) is also depicted. All three drainage curves are close and certainly within the experimental error of the tensiometers. The slight difference in slope between Schroth et al. (1996) and both Liu et al. (1994a) and ours is likely caused by the calculation procedure followed by Schroth et al. (1996) to correct for the difference in moisture content within the tempi cell. The wetting curves of Liu et al. (1994a) and ours are also very close. The slight offset between the two curves is either caused by the oil-water curve not going all the way to saturation or slight differences in reading the absolute pressures. A value of f_σ = 1.76 or an interfacial tension of 41 $g \cdot sec^{-2}$ for oil-water and 72 $g \cdot sec^{-2}$ for air-water will be used here.

The scaling factor for 2-d and 3-d fingers, f_Π, for air-water systems is equal to $4.8/\pi$ (Glass et al., 1990). It is the same for oil-water systems. The scaling factor, f_G, is either equal to 1 or 0.2 depending on the reference fluid.

Table 2 gives the finger diameters for a number of experiments reported in the literature. For 2-d fingers the average finger width was taken. For 3-d column experiments by Yao and Hendrickx (1996) coalescence of fingers is a problem in measuring the diameter and because most fingers were small (see their Figure 6). The minimum finger diameter was more appropriate and is reported in Table 2.

Using the above scaling factors and the 20/30 sand oil-water as the reference soil and liquid with an average diameter of 6 cm, the finger diameters for the other experiment in Table 2 were calculated with Eq. (7) for $b = 1$ and $b = 0.5$. The predicted scaled finger diameters are compared with the observed finger diameters in Figure 8. Note that not all moisture contents in the tips were measured and some were estimated based on similar experiments. In general, there was a satisfactory agreement between the scaled finger size and the observed value. A value of $b = 1$ gives a slightly better estimate than $b = 0.5$.

CONCLUSIONS

Unstable flow experiments were carried out in slab chambers with Soltrol and water. High-intensity synchrotron radiation coupled with pressure measurements was an effective method of studying flow instabilities in oil-saturated porous media.

Hysteresis in the constitutive relations was the governing mechanism for the temporal persistence of fingered flow. Hysteresis provided the soil with a memory of previously formed finger paths.

The results show that fingered flow into an oil saturated porous media has similar properties to fingered flow into dry porous media, but with different length scales, pressure heads, and fluid contents. Scaling of unstable flow paths might overcome some of the difficulties of measuring the constitutive relations in oil-water systems for different soil.

These results will ultimately be incorporated in theories of preferential flow and lead to better hydrological control of in situ remediation in which immiscible fluids are a problem.

ACKNOWLEDGEMENTS

We gratefully thank Christophe Darnault, John Phillips, and Edward Zhang for their experimental assistance. This work was sponsored (in part) by the Air Force Office of Scientific Research, under grant/contract number F49620-94-1-0291. Also, the knowledgeable help of the CHESS staff is greatly appreciated.

REFERENCES

Batterman, B.W. and N.W. Ashcroft. 1979. CHESS: The New Synchrotron Radiation Facility at Cornell. Science 206:157-161.

Bierck, B.R., S. Wells, and R.I. Dick. 1988. Compressible Cake Filtration: Monitoring Cake Formation and Shrinkage Using X-Rays from a Synchrotron Source. J. Water Poll. Cont. Fed. 60:645-650.

Brooks, R.H. and A.T. Corey. 1964. Hydraulic Properties of Porous Media. Hydrology Paper 3. Colorado State University, Fort Collins, CO. 27 pp.

Brutsaert, W.H. 1976. The Concise Formulation of Diffuse Sorption in a Dry Soil. Water Resources Res. 12:1118-1124.

Chandler, D.G., Z. Cohen, E.Y. Wong, D.A. DiCarlo, T.S. Steenhuis, and J.-Y. Parlange. 1996. Unstable Fingered Flow of Water into a Light Oil. Submitted to Water Resources Res.

Chuoke, R.L., P. van Meurs, and C. van der Poel. 1959. The Instability of Slow, Immiscible Viscous, Liquid-Liquid Displacement in Permeable Media. Petrol. Trans. AIME 216:188-194.

Conrad, S.H., J.L. Wilson, W.R. Mason, and W.L. Peplinski. 1992. Visualization of Residual Organic Liquid Trapped in Aquifers. Water Resources Res. 28:467-478.

Craft, B.C. and M.F. Hawkins. 1959. Applied Petroleum Reservoir Engineering. Chemical Engineering Series. Prentice Hall, Englewood Cliffs, NJ.

Dane, J.H., M. Oostrom, and B.C. Missildine. 1992. An Improved Method for the Determination of Capillary Pressure-Saturation Curves Involving TCE, Water and Air. J. Cont. Hydr. 11:69-81.

Darnault, C.J.G., J.A. Throop, A. Rimmer, D.A. DiCarlo, T.S. Steenhuis, and J.-Y. Parlange. 1996. Visualization by Light Transmission of Oil and Water Contents in Transient Flow Fields. Submitted to J. Cont. Hydr.

Department of Energy. 1995. Closing the Circle on Splitting the Atom: The Environmental Legacy of Nuclear Weapons Production in the United States and What DOE is Doing About It. U.S. Department of Energy, Office of Strategic Planning and Analysis, Washington, DC.

DiCarlo, D., T.W.J. Bauters, C. Montemagno, T.S. Steenhuis, J.-Y. Parlange, C.J. Ritsema, and L.W. Dekker. 1996. Vapor-Transport Driven Growth of Finger Flow Patterns. (Abstract.) 21st General Assembly of the European Geophysical Society Abstract Book. The Hague, Netherlands, May 6-10, 1996. p. C319.

Glass, R.J., J.-Y. Parlange, and T.S. Steenhuis. 1989a. Wetting Front Instability. 1. Theoretical Discussion and Dimensional Analysis. Water Resources Res. 25(6):1187-1194.

Glass, R.J., T.S. Steenhuis, and J.-Y. Parlange. 1989b. Wetting Front Instability. 2. Experimental Determination of Relationships Between System Parameters and Two-Dimensional Unstable Flow Field Behavior in Initially Dry Porous Media. Water Resources Res. 25(6):1195-1207.

Glass, R.J., T.S. Steenhuis, and J.-Y. Parlange. 1989c. Mechanism for Finger Persistence in Homogeneous, Unsaturated, Porous Media: Theory and Verification. Soil Sci. 148(1):60-70.

Glass, R.J., S. Cann, J. King, N. Bailey, J.-Y. Parlange, and T.S. Steenhuis. 1990. Wetting Front Instability in Unsaturated Porous Media: A Three-Dimensional Study in Initially Dry Sand. Transport in Porous Media Journal 5:247-268.

Glass, R.J., L. Orear, W.C. Ginn, J.-Y. Parlange, and T.S. Steenhuis. 1991a. Miller Scaling of Finger Properties. American Geophysical Union-Soil Science Society of America Characterization of Transport Phenomena in the Vadose Zone Workshop. Tucson, AZ. April 2-5, 1991.

Glass, R.J., J.-Y. Parlange, and T.S. Steenhuis. 1991b. Immiscible Displacement in Porous Media: Stability Analysis of Three-Dimensional, Axisymmetric Disturbances with Application to Gravity-Driven Wetting Front Instability. Water Resources Res. 27(8):1947-1956.

Glass, R.J. and M.J. Nicholl. 1996. Physics of Gravity Fingering of Immiscible Fluids Within a Porous Media. An Overview of Current Understanding and Selected Complicating Factors. Geoderma 70:133-164.

Hillel, D. and R.S. Baker. 1988. A Descriptive Theory of Fingering During Infiltration into Layered Soils. Soil Sci. 146(1):51-56.

Homsy, G.M. 1987. Viscous Fingering in a Porous Media. Annu. Rev. Fluid Mech. 19:271-311.

Hopmans, J.W. and J.H. Dane. 1986. Calibration of a Dual-Energy Gamma Radiation System for Multiple Point Measurements in a Soil. Water Resources Res. 7:1009-1114.

Lenhard, R.J., J.H. Dane, J.C. Parker, and J.J. Kaluarchchi. 1988. Measurement and Simulation of One-Dimensional Transient Three-Phase Flow for Monotonic Liquid Drainage. Water Resources Res. 24(6):853-863.

Lenormand, R. 1985. Différents mécansimes de déplacements visqueux et capillaires en milieu poreux: Diagramme de phase. C.R. Acad. Sc. Paris t. 301 Série II (5):247-250.

Liu, Y., B.R. Bierck, J.S. Selker, T.S. Steenhuis, and J.-Y. Parlange. 1993. High Intensity X-Rays and Tensiometer Measurements in Rapidly Changing Preferential Flow Fields. Soil Sci. Soc. Am. J. 57:1188-1192.

Liu, Y., T.S. Steenhuis, and J.-Y. Parlange. 1994a. Closed Form Solution for Finger Width in Sandy Soils at Different Water Contents. Water Resources Res. 30(4):949-952.

Liu, Y., T.S. Steenhuis, and J.-Y. Parlange. 1994b. Formation and Persistence of Fingered Flow Fields in Coarse Grained Soils Under Different Moisture Contents. J. Hydr. 159:187-195.

Mercer, J.W. and R.M. Cohen. 1990. A Review of Immiscible Fluids in the Subsurface: Properties, Models Characterization and Remediation. J. Cont. Hydr. 6:107-163.

Miller, E.E. and R.D. Miller. 1956. Physical Theory for Capillary Flow Phenomena. J. Applied Phys. 27:324-332.

Parker, J.C. and R.J. Lenhard. 1987. A Model for Hysteretic Constitutive Relations Governing Multi-Phase Flow. 1. Saturation-Pressure Relations. Water Resources Res. 23:2187-2196.

Parlange, J.-Y. 1975. On Solving the Flow Equation in Unsaturated Soils by Optimization: Horizontal Infiltration. Soil Sci. Soc Am. J. 39:415-417.

Parlange, J.-Y. and D.E. Hill. 1976. Theoretical Analysis of Wetting Front Instability in Soils. Soil Sci. 122:236-239.

Parlange, J.-Y., R.J. Glass, and T.S. Steenhuis. 1990. Application of Scaling to the Analysis of Unstable Flow Phenomena. Chapter 5, In: Scaling in Soil Physics: Principles and Applications, D. Hillel and D.E. Elrick, Editors. Soil Sci. Soc. Am. Special Pub. No. 25. pp. 53-57.

Philip, J.R. 1975. Stability Analysis of Infiltration. Soil Sci. Soc. Am. Proc. 39:1042-1049.

Powers, S.E., L.M. Abriola, and W.J. Weber. 1992. An Experimental Investigation of Non-Aqueous Phase Liquid Dissolution in Saturated Sub-Surface Systems. Steady State Mass Transfer Rates. Water Resources Res. 28:2691-2705.

Raats, P.A.C. 1973. Unstable Wetting Fronts in Uniform and Non-Uniform Soils. Soil Sci. Soc. Am. Proc. 39:1042-1049.

Saffman, P.G. and G.F.R.S. Taylor. 1958. The Penetration of a Fluid into a Porous Medium or Hele Shaw Cell Containing a More Viscous Liquid. Proc. R. Soc. London Ser A. 246:312-331.

Schroth, M.H., J.D. Istok, S.J. Ahearn, and J.S. Selker. 1995. Geometry and Position of Light Nonaqueous-Phase Liquid Lenses in Water-Wetted Porous Media. J. Cont. Hydr. 19:269-287.

Schroth, M.H, S.J. Ahearn, J.S. Selker, and J.D. Istok. 1996. Characterization of Miller-Similar Silica Sands for Laboratory Hydrologic Studies. Soil Sci. Soc. Am. J. 60:1331-1339.

Selker, J.S., P. Leclerq, J.-Y. Parlange, and T.S. Steenhuis. 1992a. Fingered Flow in Two Dimensions. Part 1. Measurement of Matric Potential. Water Resources Res. 28(9):2513-2521.

Selker, J.S., P. Leclerq, J.-Y. Parlange, and T.S. Steenhuis. 1992b. Fingered Flow in Two Dimensions. Part 2. Predicting Finger Moisture Profile. Water Resources Res. 28(9):2523-2528.

Selker, J.S., T.S. Steenhuis, and J.-Y. Parlange. 1992c. Wetting Front Instability in Homogeneous Sand Soils Under Continuous Infiltration. Soil Sci. Soc. Am. J. 56(5):1346-1350.

Tidwell, V.C. and R.J. Glass. 1994. X-Ray and Visible Light Transmission for Laboratory Measurements of Two-Dimensional Saturation Fields in Thin-Slab Systems. Water Resources Res. 30:2873-2882.

Van Geel, P.J. and J.F. Sykes. 1994. Laboratory and Model Simulations of a LNAPL Spill in a Variably-Saturated Sand. 1. Laboratory Experiment and Analysis Technique. J. Cont. Hydr. 17:1-25.

Wilkins, M.D., L.M. Abriola, and K.D. Pennel. 1995. An Experimental Investigation of Rate-Limited Nonaqueous Phase Liquid Volatilization in Unsaturated Porous Media: Steady State Mass Transfer. Water Resources Res. 31:2159-2172.

Yao, T-M. and J.M.H. Hendrickx. 1996. Stability of Wetting Fronts in Dry Homogeneous Soils under Low Infiltration Rates. Soil Sci. Soc. Am. J. 60:20-28.

Table 1: Synchrotron experiments.

Experiment	Initial Applic.	Rate cm^3/min	Finger Width cm	Moisture Content in Tip
I	20/30	1.0	4-7	0.27
II	20/30	2.3	3.5-7	missed
III	20/30	3.8	5-9	0.30
IV	12/20	1.0	2-4	0.30
V	12/20	2.3	2.5-4	0.27
VI	12/20	3.8	2-4	0.20

Table 2: Overview of finger experiments and parameters needed for scaling.

Experiment	Type	Interfacial Tension g/sec^2	D_{50} mm	Density Resident Fluid $g \cdot cm_{-3}$	Water Content Finger Tip $cm^3 \cdot cm_{-3}$	Observed Finger Diameter cm
This study	I	41	0.77	0.8	0.27	5.5
	II	41	0.77	0.8	0.27	5.2
	III	41	0.77	0.8	0.3	7
	IV	41	1.1	0.8	0.3	3
	V	41	1.1	0.8	0.27	3.25
	VI	41	1.1	0.8	0.2	3
Yao and Hendrickx, 1996						
	perlite	72	1.1	0	0.35	3
	perlite	72	0.77	0	0.35	4
	perlite	72	0.53	0	0.35	6
	perlite	72	0.34	0	0.35	10
	sand	72	1.1	0	0.35	2.5
	sand	72	0.77	0	0.35	4
	sand	72	0.53	0	0.35	6.5
Chandler et al., 1996						
		41	1.1	0.8	0.3	4.7
		41	0.77	0.8	0.3	4.8
Selker et al., 1992c						
		72	0.77	0	0.35	1.8
		72	0.53	0	0.35	3.3
Liu et al., 1994b						
		72	0.77	0	0.35	2.3
DiCarlo et al., 1996						
		72	1.1	0	0.35	1.7
		72	0.77	0	0.35	2.3

FIGURE CAPTIONS

Figure 1: Front and side view of the experimental chamber. There was one set of top tensiometers and three sets of middle tensiometers. Water contents were measured at the scanning elevation, directly below the middle tensiometers. The bottle and the outflow tube were used to keep the oil pressure constant during water infiltration.

Figure 2: Close-up view of an oil tensiometer inserted into the chamber. Water tensiometers were completely filled with water and used a ceramic porous plate.

Figure 3: Water content and pressure measurements as the initial finger moved down the chamber through oil-saturated 12/20 sand. Both water content and pressure rose abruptly at the front of the finger, and fell behind the finger tip, indicative of unstable flow. The water was turned on at $t = 0$ sec. When the water was turned off at $t = 1500$ sec, both readings dropped again.

Figure 4: Water content and pressure measurements during a re-infiltration of the finger. No drops in content or pressure are observed while the water is on, indicating that the re-infiltration is now in a stable flow pattern.

Figure 5: Horizontal profile of the water content within the finger. There is no increase in finger size for re-infiltration events.

Figure 6: Pressure-water content relationship from the finger in the 12/20 sand. A and B are the initial wetting and drying curves, and C and D are the secondary wetting and drying curves.

Figure 7: Observed (obs) and scaled (sc'd) oil-water characteristic curves for Soltrol 220 and water (o/w). The scaled curves were derived from Schroth et al. (1996) and Liu et al. (1994a).

Figure 8: Comparison of scaled finger diameter (Eqs. (7-11)) according to theory originally developed by Parlange and Hill (1976) (b = 1) and Chuoke et al. (1959) (b = 0.5).

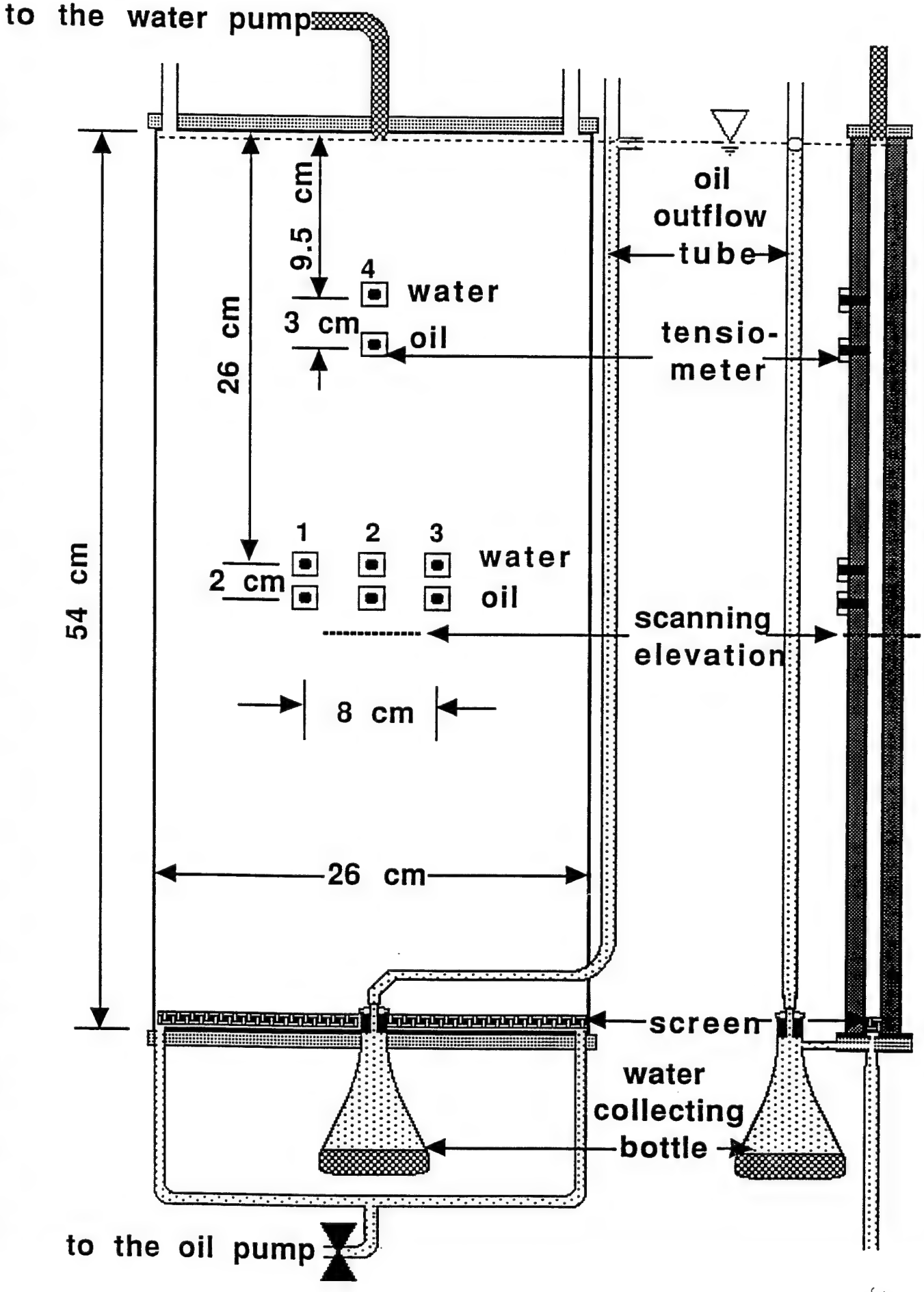
to the water pump
9.5 cm
4
water
3 cm
oil
26 cm
54 cm
oil
outflow
tube
tensio-
meter
1
2
3
water
2 cm
oil
scanning
elevation
8 cm
26 cm
screen
water
collecting
bottle
to the oil pump

Fig. 1

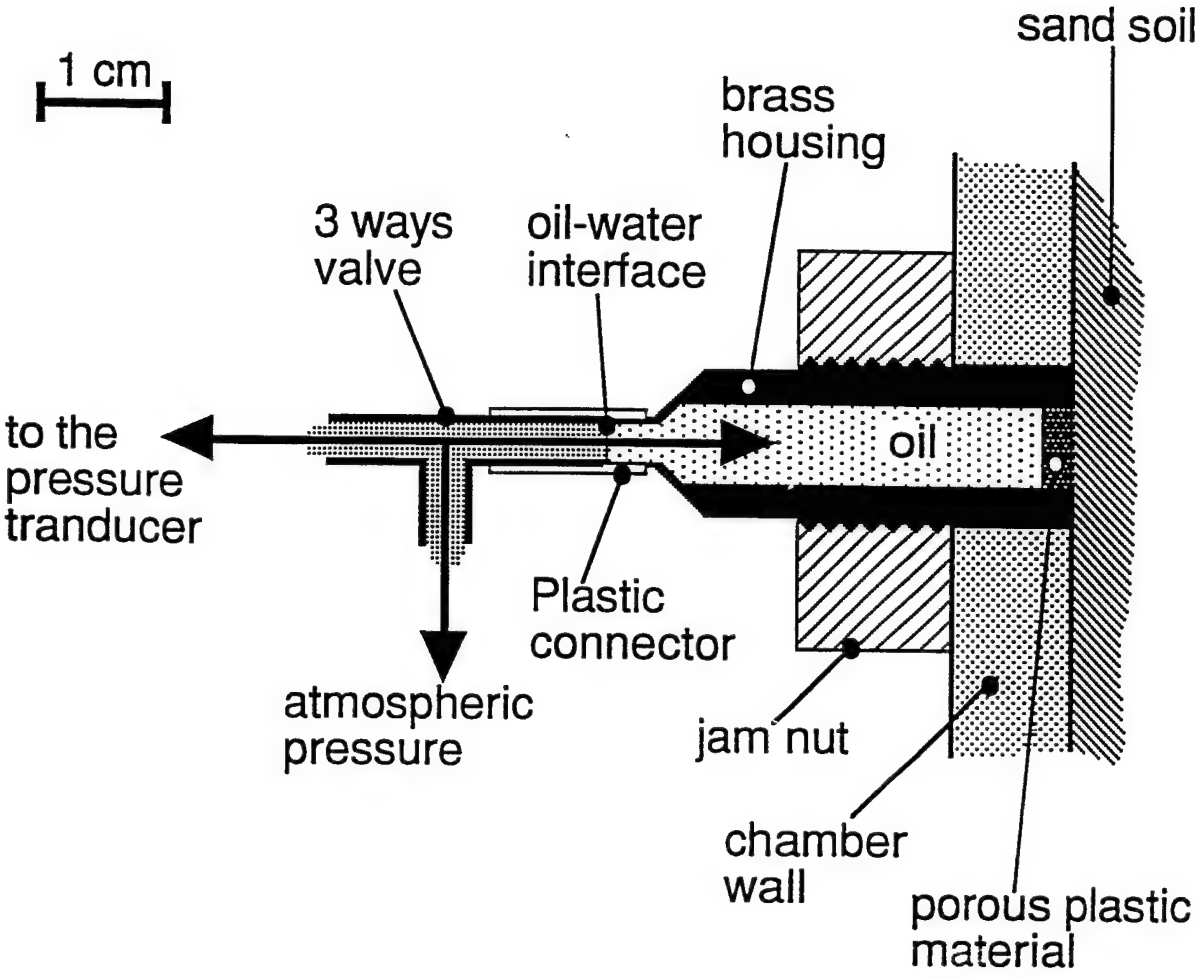
1 cm
sand soil
brass
housing
3 ways
valve
oil-water
interface
to the
pressure
tranducer
oil
Plastic
connector
atmospheric
pressure
jam nut
chamber
wall
porous plastic
material

Fig. 2

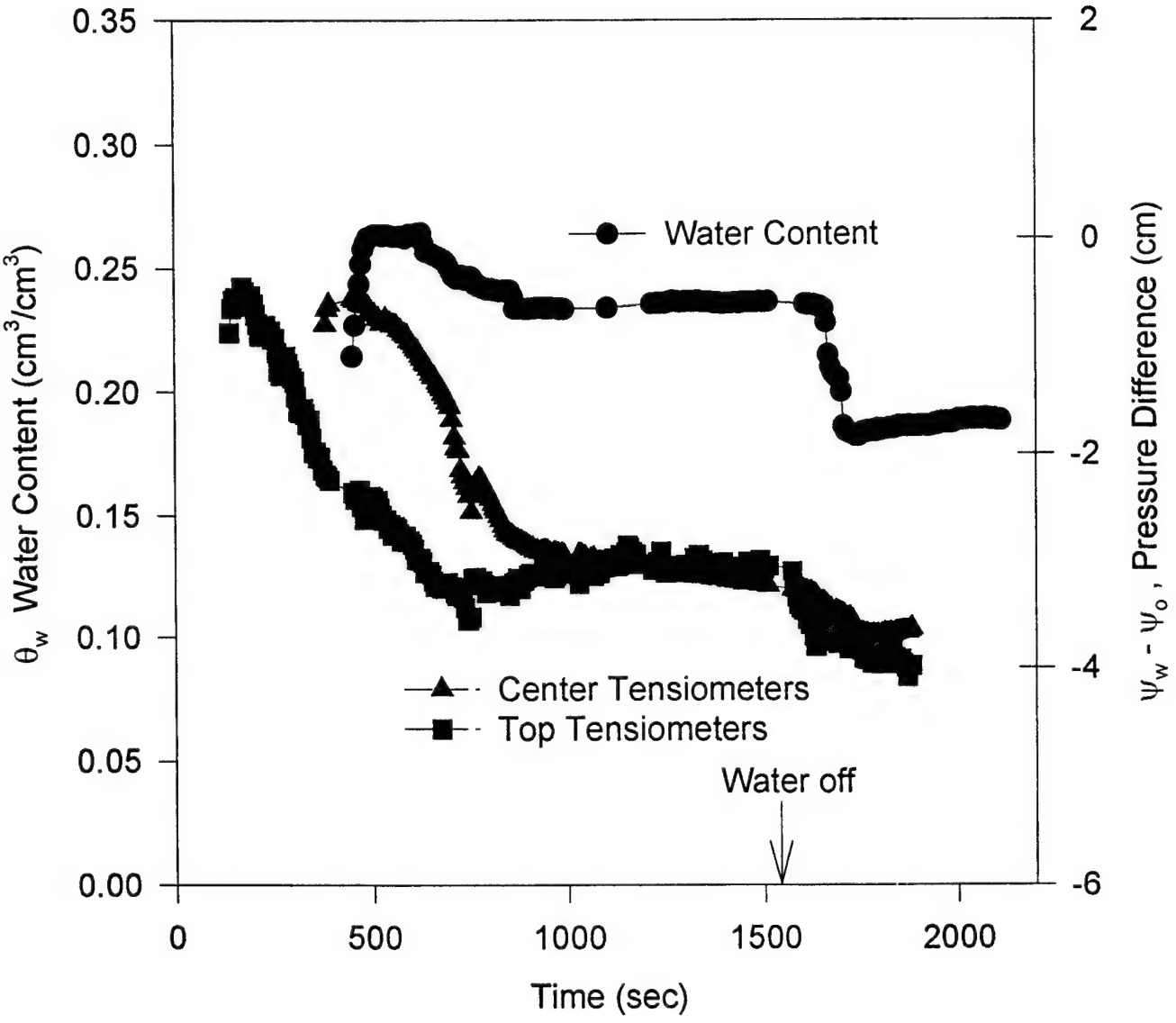
Initial Infiltration
0.35
0.30
0.25
0.20
0.15
0.10
0.05
0.00
2
0
-2
-4
-6
0
500
1000
1500
2000
Time (sec)
θw Water Content (cm3/cm3)
ψw - ψo , Pressure Difference (cm)
Water Content
Center Tensiometers
Top Tensiometers
Water off

Fig. 2

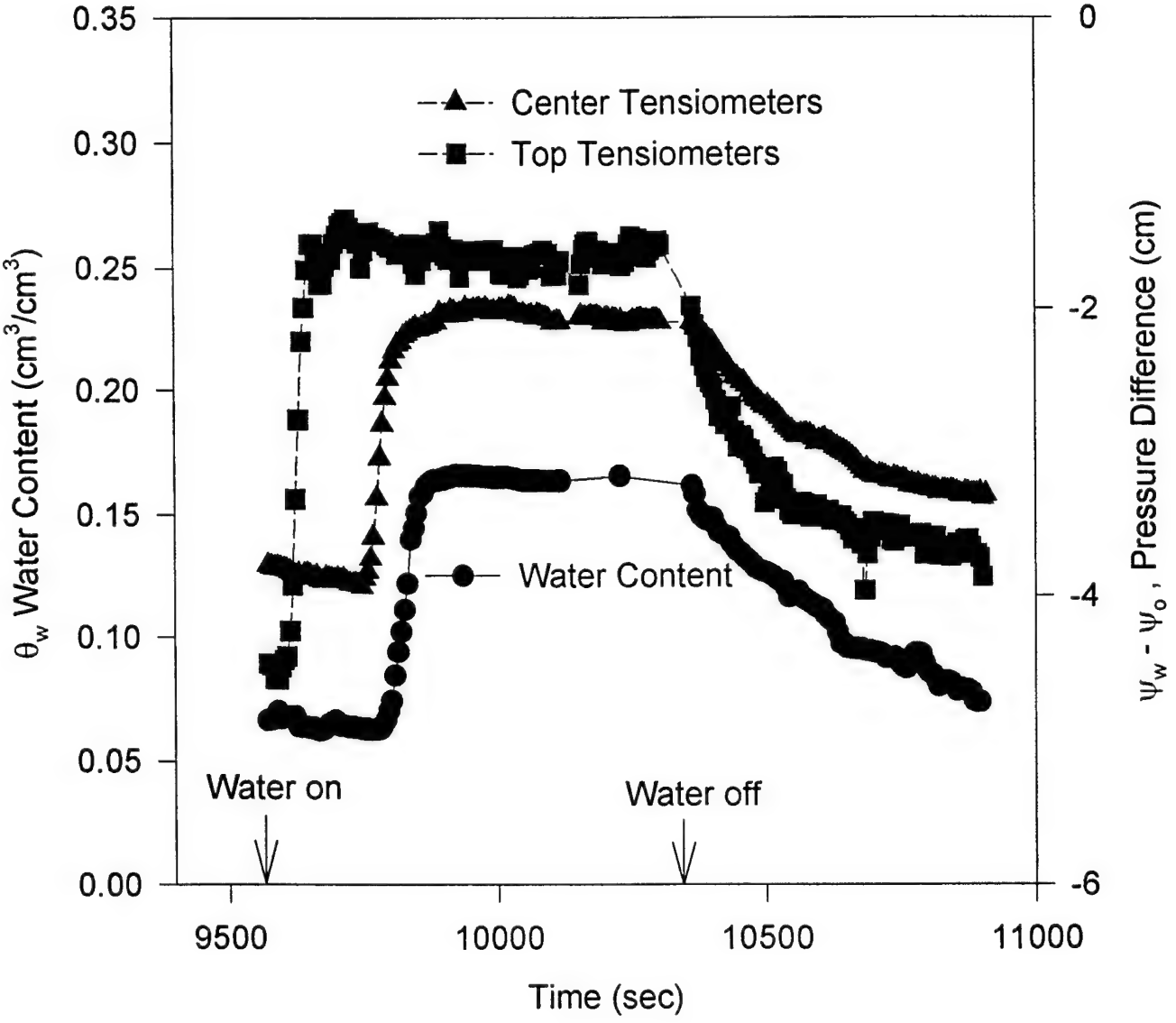
Re-Infiltration
0.35
0.30
0.25
0.20
0.15
0.10
0.05
0.00
0
-2
-4
-6
9500
10000
10500
11000
Time (sec)
θ_w Water Content (cm^3/cm^3)
$\psi_w - \psi_o$, Pressure Difference (cm)
Center Tensiometers
Top Tensiometers
Water Content
Water on
Water off

Fig. 4

Horizontal Finger Profile

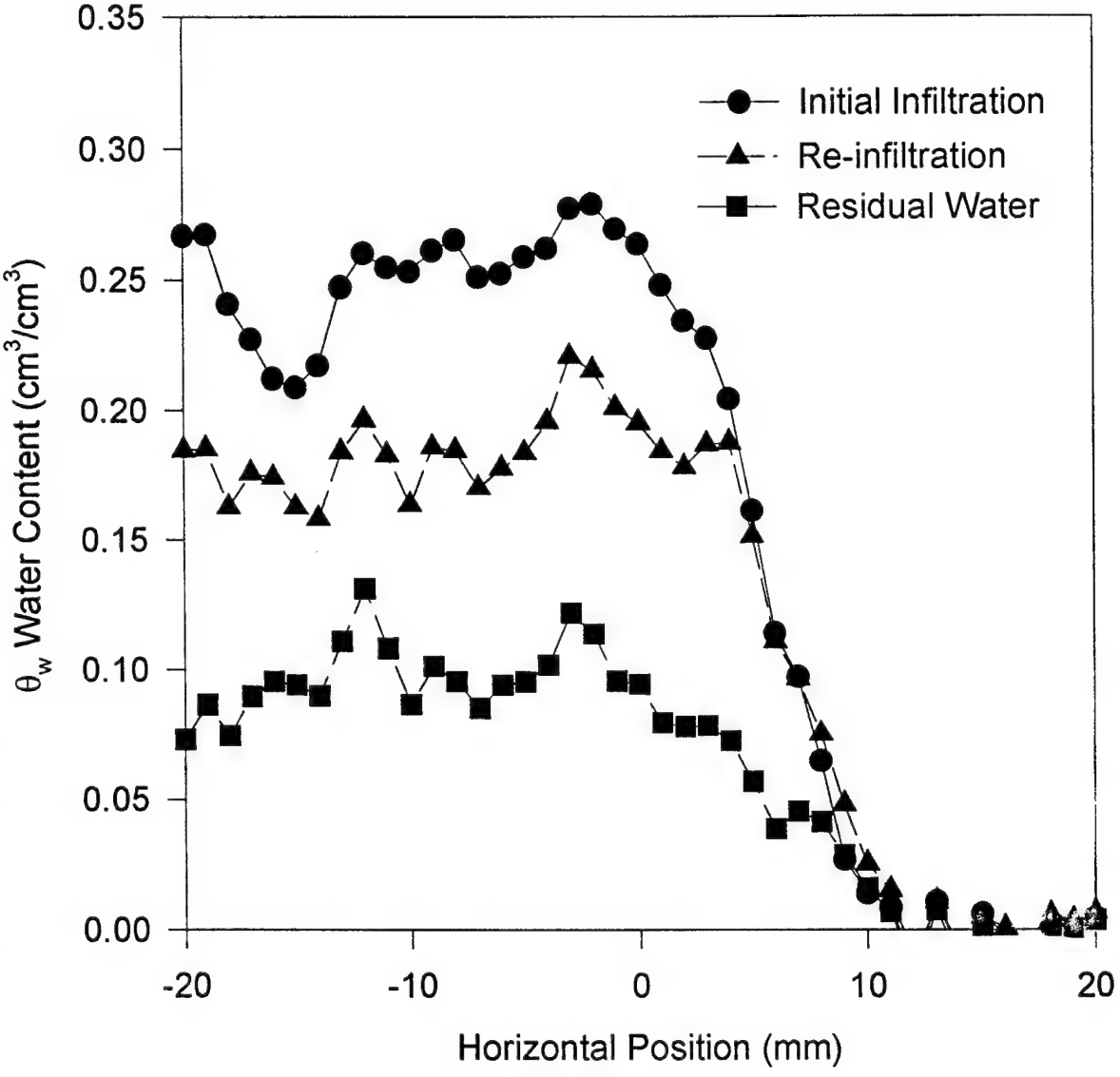

Fig. 5

Soltrol 220 - Water Dynamic Pressure- Saturation Relationship

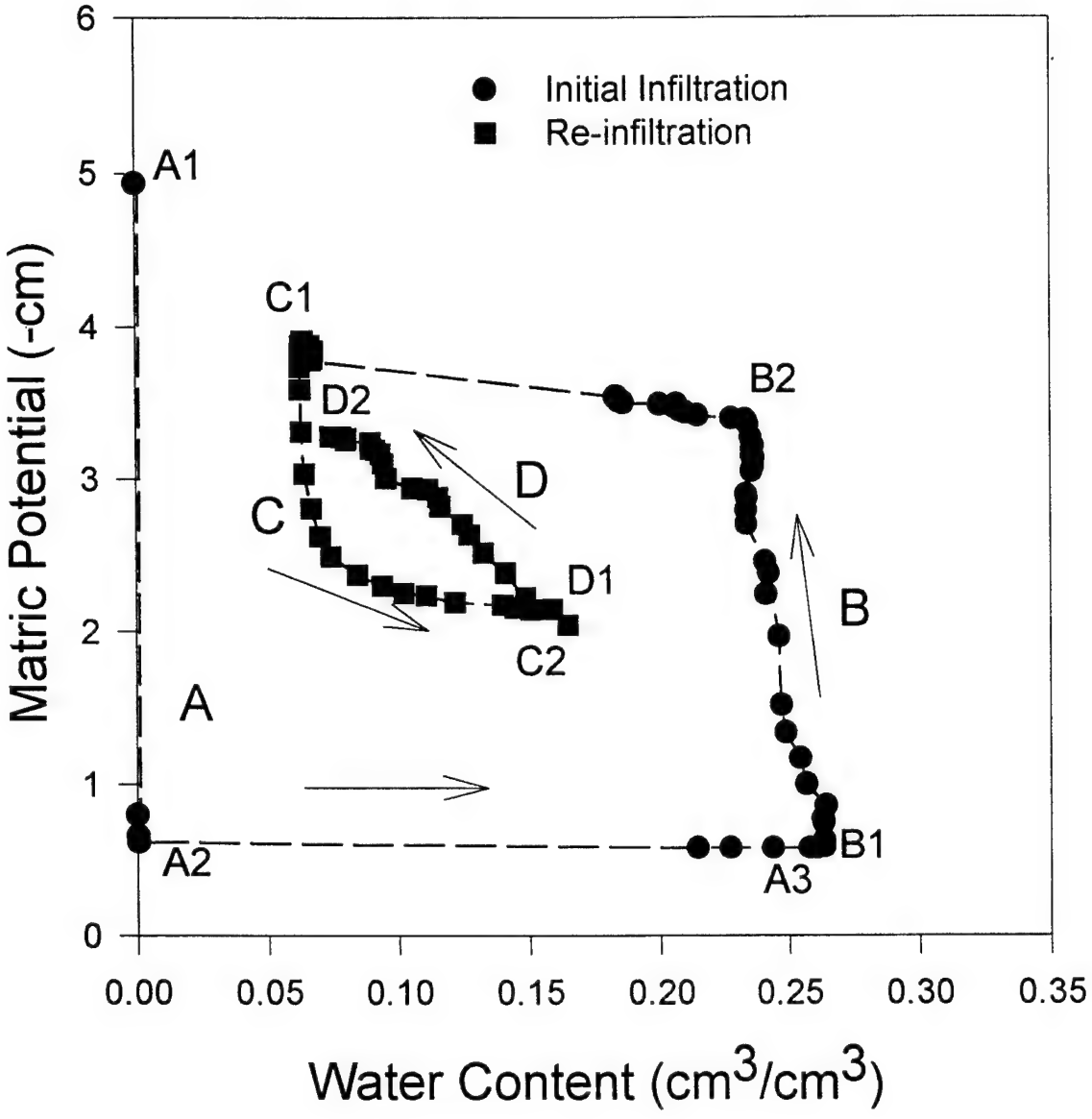

Fig. 6

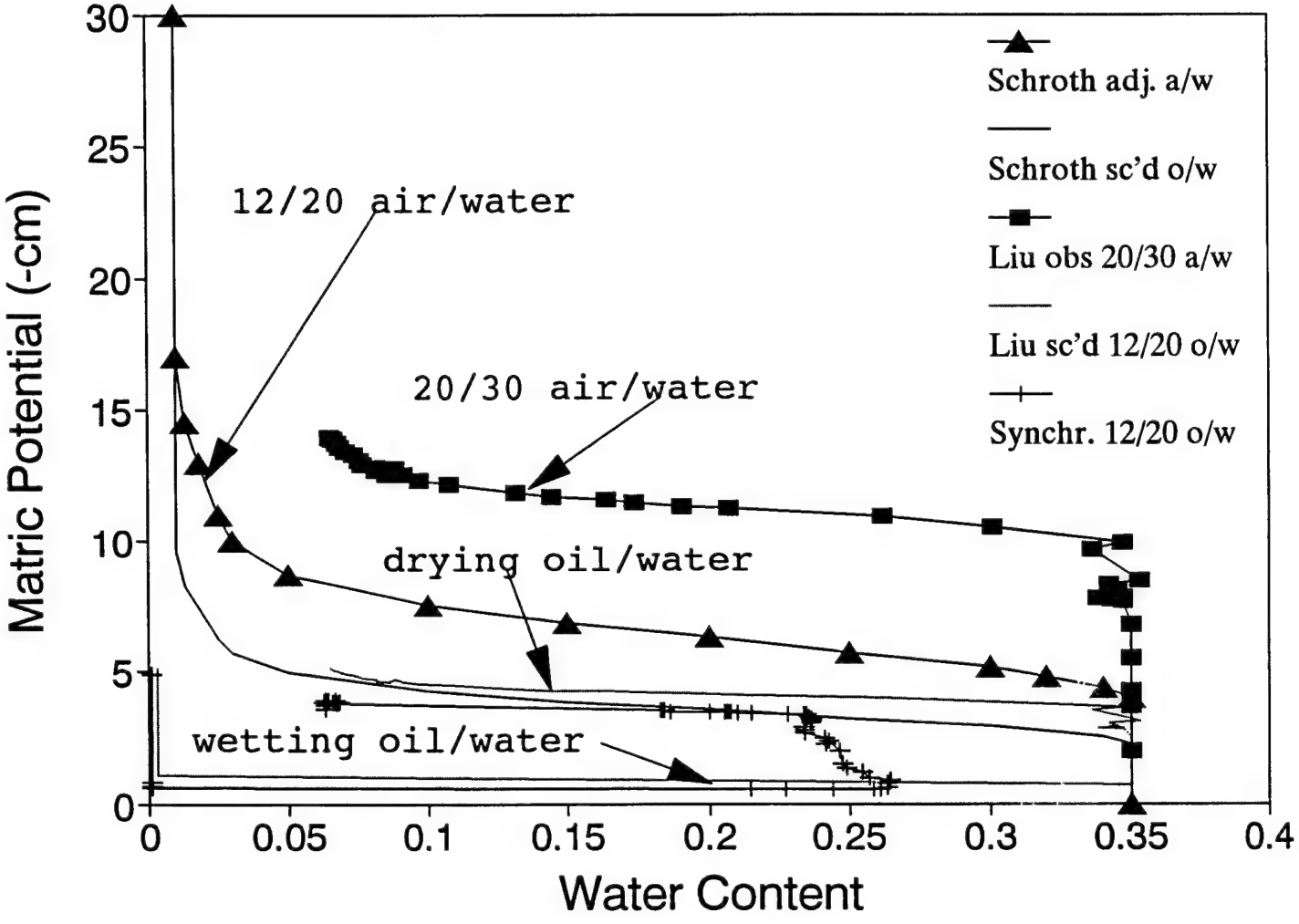
Matric Potential (-cm)
30
25
20
15
10
5
0
0
0.05
0.1
0.15
0.2
0.25
0.3
0.35
0.4
Water Content
12/20 air/water
20/30 air/water
drying oil/water
wetting oil/water
Schroth adj. a/w
Schroth sc'd o/w
Liu obs 20/30 a/w
Liu sc'd 12/20 o/w
Synchr. 12/20 o/w

Fig. 7

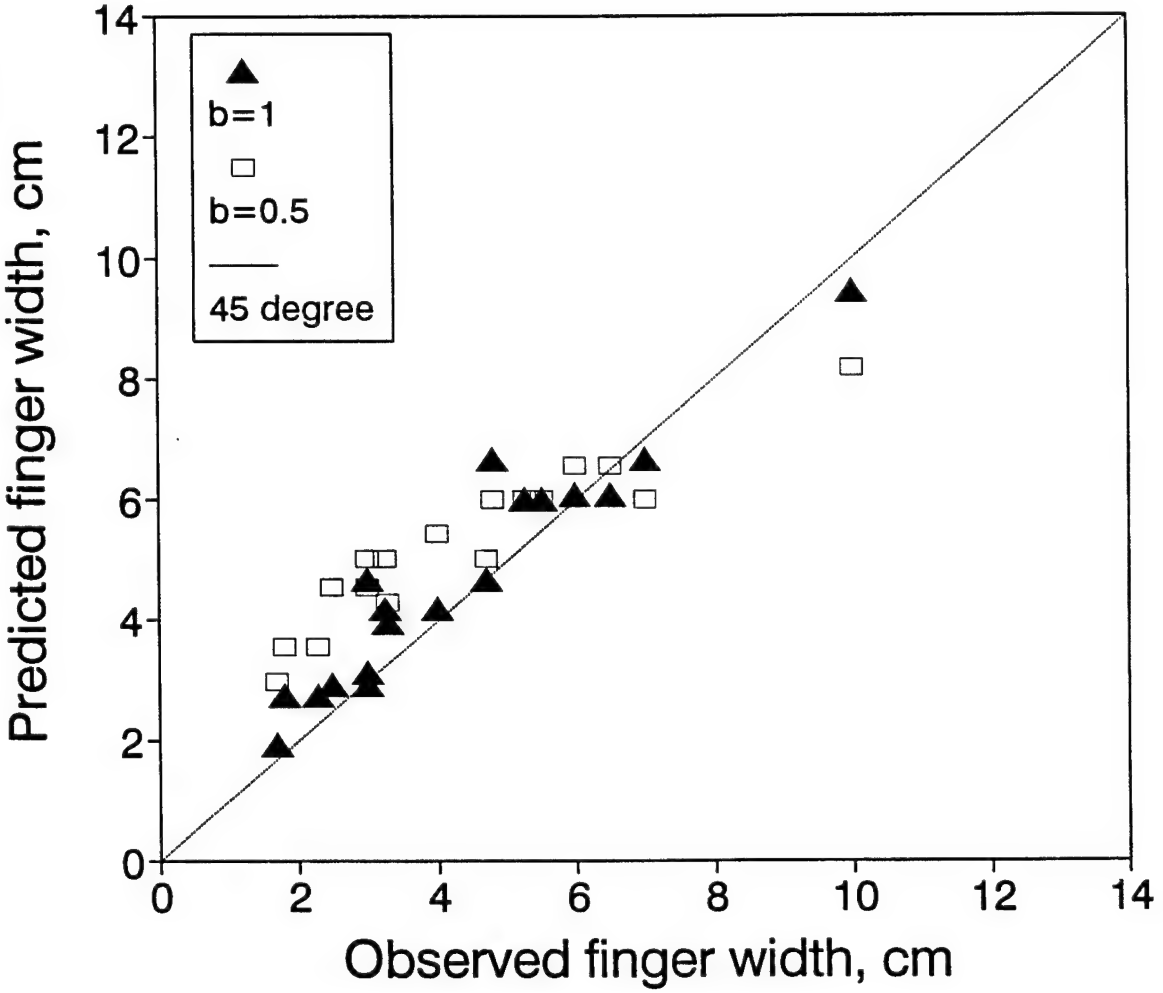

fingsumry.wq1

Fig. 4

APPENDIX C

VISUALIZATION BY LIGHT TRANSMISSION OF OIL AND WATER CONTENTS IN TRANSIENT TWO-PHASE FLOW FIELDS

C.J.G. Darnault, J.A. Throop, A. Rimmer,
D.A. DiCarlo, T.S. Steenhuis, and J.-Y. Parlange

Journal of Contaminant Hydrology (Accepted)

VISUALIZATION BY LIGHT TRANSMISSION OF OIL AND WATER CONTENTS IN TRANSIENT TWO-PHASE FLOW FIELDS

Christophe J.G. Darnault, James A. Throop, David D. DiCarlo,

Alon Rimmer, Tammo S. Steenhuis[1], and J.-Yves Parlange

Department of Agricultural and Biological Engineering

Cornell University, Ithaca, NY 14853

[1]Corresponding Author, Department of Agricultural and Biological Engineering, Riley-Robb Hall, Cornell University, Ithaca, NY 14853, Phone: 607-255-2489, Fax: 607-255-4080, Email: tss1@cornell.edu.

ABSTRACT

The difficulty of determining transient fluid contents in a soil-oil-water system is hampering an understanding of the system's flow characteristics. In this paper, we describe a light transmission method (LTM) which can rapidly obtain oil and water contents throughout a large two-dimensional flow field. By appropriately coloring the water with 0.005% FD&C blue #1, the hue of the transmitted light is found to be directly related to the water content within the porous media. Then, the hue provides a high resolution measurement of the water and oil contents in transient flow fields (such as unstable flow). Evaluation of the reliability of LTM was assessed by checking mass balance for a known water injection, and its utility in visualizing a whole flow field was exemplified for an unstable fingered flow by comparing fluid contents to those obtained with synchrotron x-ray radiation.

INTRODUCTION

The complexity of simultaneous flow of water and non-aqueous phase liquids (NAPLs) is little understood because few techniques permit accurate measurement of water and oil contents in transient flow fields. Mercer and Cohen (1990) noted that in situ fluid content measurements are needed to understand immiscible fluid flows in porous media and to perform effective subsurface remediation.

Most techniques available for visualization of oil and water fluid contents can measure only near steady state flow conditions. They include conventional x-ray and gamma ray radiation techniques used by, among others, Hopmans and Dane (1986), Lenhard et al. (1988), Dane et al. (1992), and Illangasekare et al. (1995). These measurements are slow because of the relatively long counting times and only one point can be measured at one time. Synchrotron x-rays (Liu et al., 1993; Rimmer et al., 1996) allow shorter counting times (in the order of seconds) but only regions of less than 0.5 cm^2 can be measured at one time. Tidwell and Glass (1994) have performed full field measurements using x-ray film, but recording times are too long for measuring transient flow phenomena.

Transient visualizations (but not a direct measurement of fluid contents) have been made in Hele-Shaw cells with smooth walls (Saffman and Taylor, 1958; Chuoke et al., 1959) or with imprints of porous media on glass (Schwille, 1988). The visualization method of Van Geel and Sykes (1994) allows measurement of liquid content near the wall of the slab chambers by relating the

gray level of the reflected light to water content. However, as they noted, the fluid content near the wall might not necessarily be the same as within the porous media.

Thus, there is a need for a method that allows full field moisture content visualization in two-phase liquid systems. This paper describes the development of such a technique by using light transmission through a two-dimensional slab chamber. By coloring the water phase with 0.005% FD&C blue #1 the hue content of the transmitted light is directly related to the water content. The technique is a new application of the method of Glass et al. (1989) for air-water systems in which the light intensity was directly related to water content. Unlike air and water, in the case of oil-water systems the refractive index of the two fluids is almost identical, making it impossible to measure liquid contents of each of the fluids from the light intensity measurements. A blue dye was chosen because it produced a wide color spectrum going from yellow for the oil saturated sand via green to blue for water saturated soil.

VISUALIZATION

Quantification of color differences can be complicated, because there are various ways to specify "color". The color for video cameras, color monitors and computer graphics is defined in terms of a vector with the three components of red, green, and blue intensities (RGB). Another system to specify the color vector involves hue, saturation, and intensity (HSI), which is used, for instance, by the Munsell color chart for soil classification. Hue is the attribute that describes the pure color and is what we are typically referring to when we use the term "color".

Saturation is the attribute that describes the degree to which the color is diluted with white. Intensity is the attribute which corresponds to the gray level (black and white) of the color image. The advantages of the HSI format is that it treats color roughly the same way that humans perceive and interpret color. Therefore, because color differences are apparent to the human eye for different water and oil contents, we expect that water content is directly related with hue rather than intensity or saturation.

Hue, H, in HSI format can be obtained from the RGB vector (R=red, G=green, and B=blue intensity, respectively, with values for each vector component ranging from 0 to 255) following (Wilson, 1988):

$$H = 255\left[\frac{1}{360}\left[Y - ARCTAN\frac{2R-G-B}{\sqrt{3}(G-B)}\right]\right], \qquad (1)$$

$$Y = 90 \quad for\ G>B,$$

$$Y = 270 \quad for\ G<B.$$

where Y is a constant depending on the green and blue intensity. This equation shows that if, as we expect, H is the best variable to measure water content, each of the components of the RGB vector is affected by the water content and the combination (2R-G-B)/(G-B) would be the relevant parameter in the RGB system to relate to water content.

MATERIALS AND METHODS

For fluid measurements in porous media, light transmission techniques involve placing a two-dimensional experimental chamber in front of an uniform light source and recording the

transmitted light (Glass and Nicholl, 1995). We used a light source composed of a bank of 24 florescent light bulbs in front of a white background. Experimental chambers had 1 cm thick polycarbonate walls with a 1 cm thick interior. The transmitted light was recorded with a Cohu Solid State Color Camera located 1 m in front of the chamber, with constant settings (zoom = 3 - 5 m and aperture = f 1.8) and stored on standard VHS tape in RGB format. Recorded images were converted from RGB to HSI format with an IBM compatible computer equipped with a DT2871 Color Frame Grabber and analyzed with a Color Tutorial (SP0228) V1.00 software, both from Data Translation, Inc., - 07839A 1988.

To obtain a calibration curve between hue value and oil-water content, a two-dimensional calibration chamber, consisting of compartments with known quantities of oil and water, was constructed (Figure 1). The oil used was Soltrol 220, an isoparaffine solvent composed of a mixture of alkanes C13 through C17 from the Phillips 66 Co. The water was colored with FD&C blue #1, at a concentration of 0.005% by weight. By trial and error, the color blue and the specific concentration of 0.005% were found to give the widest range of hue values. The calibration chamber had dimensions of 32.5 cm high, 26 cm wide, and 1 cm thick, and was divided into six cells of 3 cm high, 26 cm wide, and 1 cm thick. The walls consisted of a 1 cm thick Hyzod polycarbonate sheet, made by Sheffield Plastic, Inc. Cell walls were covered with black tape to avoid edge effects of transmitted light through the plastic walls. The cells were packed with 12/20 sieve size sand and water contents of 0, 20, 40, 60, 80, and 100% saturation (volumetric moisture content of 0.00, 0.07, 0.14, 0.21, 0.28, and 0.35 cm^3/cm^3, respectively). The remainder of the pore space was filled with oil. The coarse 12/20 sand was industrial

quartz (Unimin Corp.) with particle sizes between 0.85 and 1.5 mm, which was packed to a porosity of 35%. The 0 and 100% water saturations were obtained by dripping oil and water into the sand-filled cells, respectively. The 20, 40, 60, and 80% water saturations were made by mixing the required water and oil quantities in a beaker with the sand, stirring the mixture, loading the mixture in the cells, and then packing the cells by vibration.

For each cell, the hue was taken as the mean values present in a centered line of 100 pixels. A histogram of all the hue values located on the line was made for each cell. The mean hue values were plotted versus the corresponding water content to obtain a calibration curve.

Two types of experiments were conducted to illustrate the reliability and applicability of the method. The first one aimed to test the accuracy of the technique for a simple flow experiment from a point source to check the mass balance, while the second one illustrated the technique for a more complex flow produced by fingering, similar to the experiment of Rimmer et al. (1996) with synchrotron x-rays. These experiments were carried out in a two-dimensional slab chamber (Figure 2). The interior dimensions of the experimental chamber were 57 cm high, 51 cm wide, and 1 cm thick. Two metal bars were fixed at the top and middle of the chamber to prevent it from expanding while filling with oil. The walls consisted of 1 cm thick Hyzod polycarbonate sheets made by Sheffield Plastic, Inc. The experimental chamber was continuously filled with industrial quartz 12/20 sieve size sand through a funnel-extension-randomizer assembly to minimize segregation and heterogeneity (Glass et al., 1989). Extra sand was added to have a 10 cm sand layer in the funnel to achieve a natural packing in order to

avoid the movement of sand particles during the experiment. After packing, the top 2 cm of the sand was removed by sweeping to bring the sand height to 55 cm. The experimental chamber was saturated with oil to a height of 55 cm by adding Soltrol from the bottom at a constant rate of 8.4 ml/min. The oil level was kept constant and excess oil was drained through the bottom of the chamber via an overflow at the same level as the Soltrol upper level in the chamber. The experiments were performed at a constant temperature of 20°C.

The first test consisted of checking the mass balance. Water was injected with a flow rate of 2.8 ml/min at a point source located 3 cm below the oil-saturated 12/20 sand surface in the experimental chamber. The hue values were taken for all pixels constituting the area surrounding the finger and converted to water content.

For the second test, we measured fluid contents for unstable flow of water into oil-saturated sand. A set of three experiments were performed in the experimental chamber. The water was uniformly applied through a needle, attached to a cam driver which went back and forth at a repetition rate of 8 seconds, along the top, 1 cm above the oil-saturated 12/20 sand surface. Figure 2 depicts the experimental setup. Water fingers were observed under three different infiltration flow rates: 4.5, 7.5, and 10.4 ml/min.

RESULTS

Calibration of the Light Transmission Method (LTM)

Color differences were visible between the different cells of the calibration chamber: the oil-saturated cell appeared yellow, the water-saturated cell appeared blue and the oil-water saturated cells appeared varying shades of green. In each cell, the color was not completely uniform, slight spatial differences existed due to oil and water ganglia formation (Figure 1).

Inside each cell, the color attributes of pixels were correlated with water content in HSI and RGB formats. Using RGB format, even though the color went from yellow to green to blue, only the red component of the RGB vector showed any trend with water content. This trend, however, was not sufficient to give an unique relationship with water content. The difficulty in using RGB is the interdependence of color saturation with values of the components of the color vector (Wilson, 1988). In our case, the bright yellow (0% water) had approximately the same value for the blue component as the 100% water which was pale blue. Thus, even if the eye can see a difference in color, RGB is unable to pick out the colors in a simple predictable manner. In HSI format, the hue (representing the color for the human eye) is independent of the color saturation (Wilson, 1988) and, indeed, the histograms of hue values for the water content in each cell were found to be unique, whereas neither saturation nor intensity had significant correlation to water content. The distribution of hue values for the six different water contents is presented in Figure 3. The yellow oil-saturated cell had a hue value of about 43, and

the blue-green water-saturated cell had a hue value of about 86. The oil-saturated and water-saturated cells had the most uniform color, and the narrowest hue histograms. Only two of the histograms had overlapping hue values because of formation of some oil and water ganglia, but there was a difference in peak positions. The hue value increased with the water content and a linear regression provided a good fit with a R^2 of 97.8 % (Figure 4). The hue-water content equation is:

$$\theta = -0.9395 + 0.0222H \qquad (2)$$

where θ is the volumetric water content and H is the hue value calculated with Eqn. (1) from the recorded RGB color attributes. Note that the constants in Eqn. (2) are specific for our experimental setup. The system needs to be calibrated when different video cameras or particle sizes are used.

Accuracy, Utility, and Reliability of LTM

The LTM was evaluated with a mass water balance and synchrotron x-ray technique. The mass balance test consisted of measuring a known water volume in oil-saturated sand. The injected 20 ml of water generated a finger of dimensions approximately 10 cm long, 6 cm wide, and 1 cm thick in the experimental chamber. Hue values were obtained by analyzing all the 14400 pixels present in a surrounding area that contains the finger, and were converted to water content using Eqn. (2). The total amount of water calculated was 19.85 ml, which was within 1% of the amount of water applied.

As an application and to check the accuracy of LTM under transient flow conditions, water infiltrations into 12/20 oil-saturated sand were performed for three flow rates. An unstable wetting front formed with one or more fingers. An example of the fingered flow of water for the flow rate of 4.5 ml/min is presented in Figure 5. Before the first finger went down, a horizontal wetting front of about 2 cm deep formed. The finger was the bluest (highest value for hue) at the tip, indicating the highest water content. Figure 6 shows the finger water content profile after 15 and 20 minutes. LTM measurement indicated that after 15 minutes the water content at the finger tip was between 0.27 and 0.30 cm^3/cm^3, and the finger width ranged from 6 to 8 cm. At 20 minutes, the finger tip water content was between 0.26 and 0.28 cm^3/cm^3. Approximately 25 cm above the finger tip, the moisture content decreased to an average of 0.17 cm^3/cm^3. The horizontal water content profile at a depth of 48 cm at 20 minutes through the tip of the finger is shown in Figure 7. Both infiltration flow rates of 7.5 and 10.5 ml/min produced a wetting front instability that generated 2 and 3 fingers, respectively, with approximately the same characteristics as the one generated with 4.5 ml/min. The only difference was that the water content was slightly higher and the velocities sometimes slower (Table 1).

The above results were compared with available data from synchrotron x-ray measurements by Rimmer et al. (1996) with 12/20 oil-saturated sand and a flow rate of 2.3 ml/min through a point source (Figure 6). For the synchrotron measurements, unlike LTM, there is a fundamental relationship between the attenuation of x-rays and moisture content. Although slight differences existed in observed water contents, which have been caused by slight different experimental flow

rates, both methods follow the same finger behavior. The highest water content was measured at the finger tips: 0.265 cm^3/cm^3 for the x-ray radiation and 0.26 to 0.28 cm^3/cm^3 for the LTM. Also, in the transition zone behind the finger tip, the decrease in water content is similar over the zone that the synchrotron was available. In Figure 7, the moisture content in a horizontal profile at comparable locations is also very similar between the two methods.

DISCUSSION

The Light Transmission Method (LTM) was found to yield reliable fluid contents in transient oil-water flow fields as checked by the mass conservation experiment. Unstable fingered flow phenomena measured with LTM gave similar results as those with the synchrotron x-ray source. The advantage of the LTM is that it records the fluid contents of the whole flow in less than 0.05 seconds (the time it takes for a video camera to take an image). Synchrotron x-ray measurements can be taken also within one second but only at one location at a time. The disadvantage of LTM is that silica sand has to be used as porous media while synchrotron x-ray measurements are independent of the translucence of the porous media. The LTM when coupled with simultaneous pressure measurements will be useful in validating 1-D and 2-D computer codes for transient oil and water flow.

CONCLUSIONS

A method was developed that can measure full field average fluid contents for transient flows in soil-oil-water systems. Currently, there is a lack of such measuring techniques, hampering the development of theory and testing of two-phase models.

We found that by dying the water light blue and analyzing the flow field for this blue color in HSI format, we could determine the water content in the slab chamber filled with sand. RGB, which is used in recording color with video cameras, could not easily quantify the obvious color difference between yellow and blue. By using the HSI format, an unique relationship existed between the hue and water content. Comparison with moisture contents, determined with synchrotron x-rays, showed that the LTM can be successfully used for full field moisture contents in porous media consisting of silica sand.

ACKNOWLEDGMENTS

This work was sponsored by the U.S. Air Force Office of Scientific Research, under Grant No. F49620-94-1-0291.

REFERENCES

Chuoke, R.L., P. van Meurs, and C. van der Poel. 1959. The instability of slow, immiscible viscous, liquid-liquid displacement in permeable media. Petrol. Trans. AIME. 216:188-194.

Dane, J.H., M. Oostrom, and B.C. Missildine. 1992. An improved method for the determination of capillary pressure-saturation curves involving TCE, water and air. J. Contaminant Hydrology 11:69-89.

Glass, R.J., T.S. Steenhuis, and J.-Y. Parlange. 1989. Mechanism for finger persistence in homogeneous, unsaturated, porous media: Theory and verification. Soil Sci. 148(1):60-70.

Glass, R.J. and M.J. Nicholl. 1995. Physics of gravity fingering of immiscible fluids within porous media: An overview of current understanding and selected complicating factors. Geoderma 70(2-4):133-163.

Hopmans, J.W. and J.H. Dane. 1986. Calibration of a dual-energy gamma radiation system for multiple point measurements in a soil. Water Resources Research 7:1009-1114.

Illangasekare, T.H., J.L. Ramsey Jr., K.H. Jensen, and M.B. Butts. 1995. Experimental study of movement and distribution of dense organic contaminants in heterogeneous aquifers. J. Contaminant Hydrology 20:1-25.

Lenhard, R.J., J.H. Dane, J.C. Parker, and J.J. Kaluarchchi. 1988. Measurement and simulation of one-dimensional transient three-phase flow for monotonic liquid drainage. Water Resources Research 24(6):853-863.

Liu, Y., B.R. Bierck, J.S. Selker, T.S. Steenhuis, and J.-Y. Parlange. 1993. High intensity x-ray and tensiometer measurements in rapidly changing preferential flow fields. Soil Sci. Soc. Am. J. 57:1188-1192.

Mercer, J.W. and R.M. Cohen. 1990. A review of immiscible fluids in the subsurface: Properties, models characterization and remediation. J. Contaminant Hydrology 6:107-163.

Rimmer, A., D. DiCarlo, T.S. Steenhuis, B.R. Bierck, and J.-Y. Parlange. 1996. Preferential flow in an oil-water-sand system: A synchrotron x-ray study. Submitted.

Saffman, P.G., and G. Taylor. 1958. The penetration of a fluid into a porous medium or Hele-Shaw cell containing a more viscous liquid. Proc. Royal Soc. London A 245:312-331.

Schwille, F. 1988. Dense chlorinated solvents in porous and fractured media. Translated by J.F. Pankow. Lewis Publishers, Chelsea, MI. 146 pp.

Tidwell, V.C. and R.J. Glass. 1994. X-ray and visible light transmission for laboratory measurements of two-dimensional saturation fields in thin-slab systems. Water Resources Research 30:2873-2882.

Van Geel, P.J. and J.F. Sykes. 1994. Laboratory and model simulations of a LNAPL spill in a variably-saturated sand. 1. Laboratory experiment and analysis technique. J. Contaminant Hydrology 17:1-25.

Wilson, A. 1988. What color is color? The Electronic System Design Magazine. January: 38-44.

LIST OF TABLES

Pure water experiments	Number of fingers	Average width (cm)	Average velocity (cm/min)	Water content at the tip
4.5 ml/min	1	6-8	5.7	0.27
7.5 ml/min	2	5-6	#1 3.95 #2 4.48	#1 0.20-0.30 #2 0.25-0.30
10.4 ml/min	3	6	# 1 5.6 # 2 6.0	#1 0.25-0.30 #2 0.25-0.30 #3 0.30

Table 1

LIST OF FIGURES

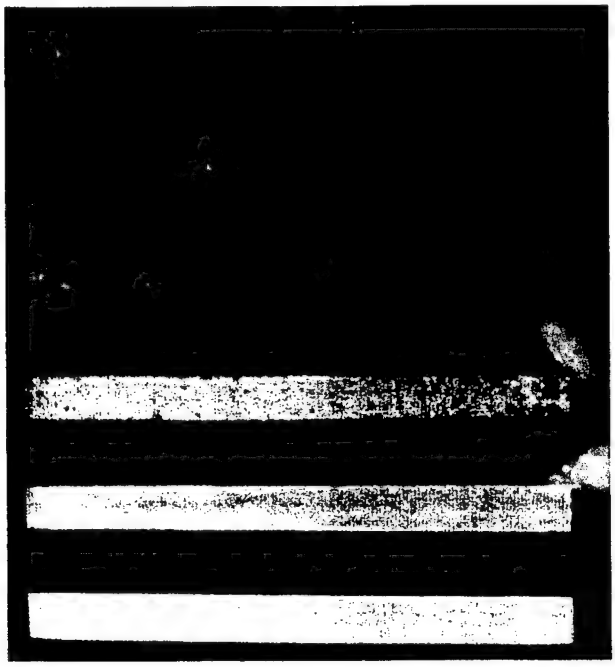

(Note: In actuality there are color differences between the cells which this picture does not represent)

Figure 1

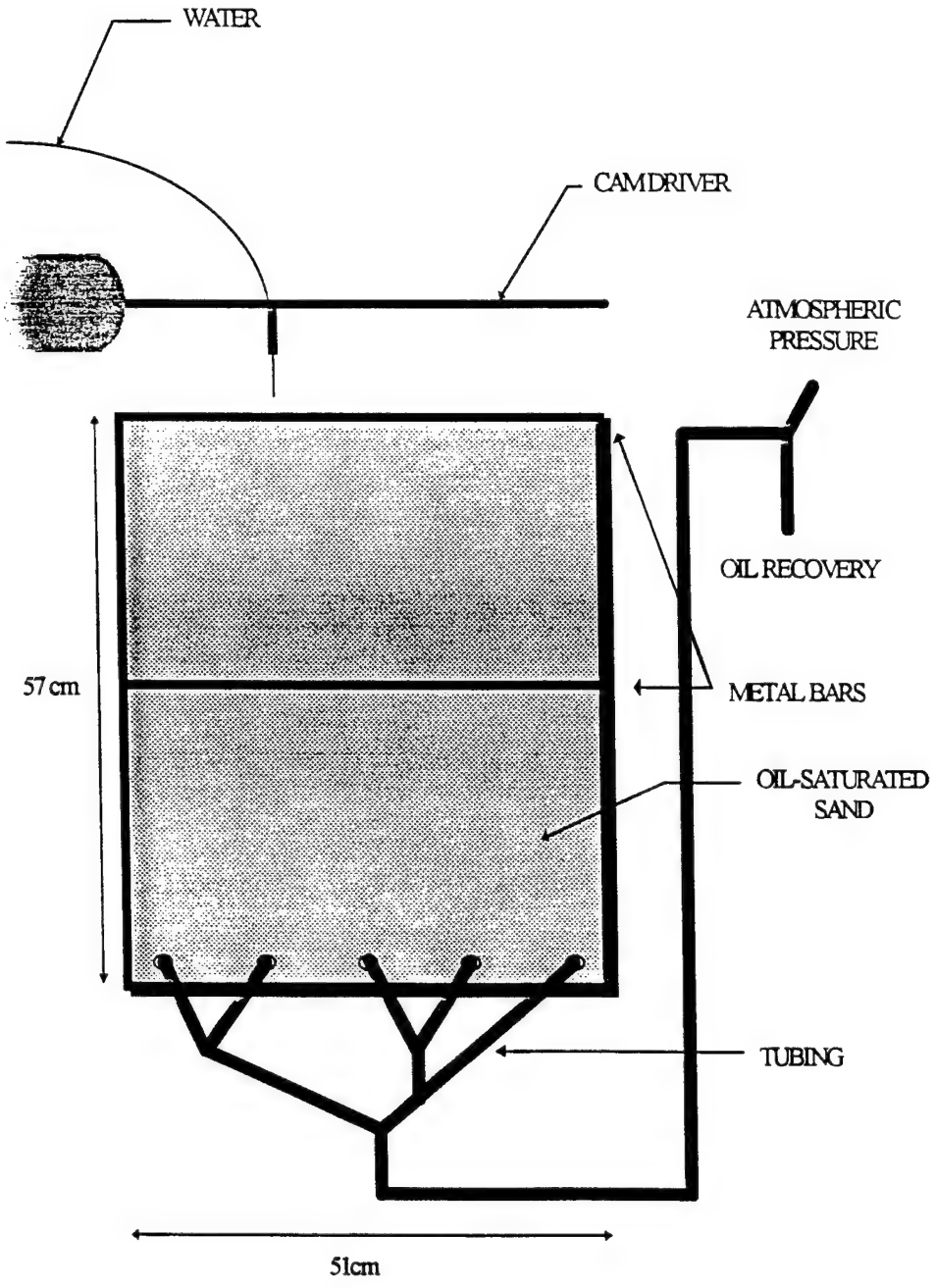
WATER
CAM DRIVER
ATMOSPHERIC PRESSURE
OIL RECOVERY
57 cm
METAL BARS
OIL-SATURATED SAND
TUBING
51cm

Figure 2

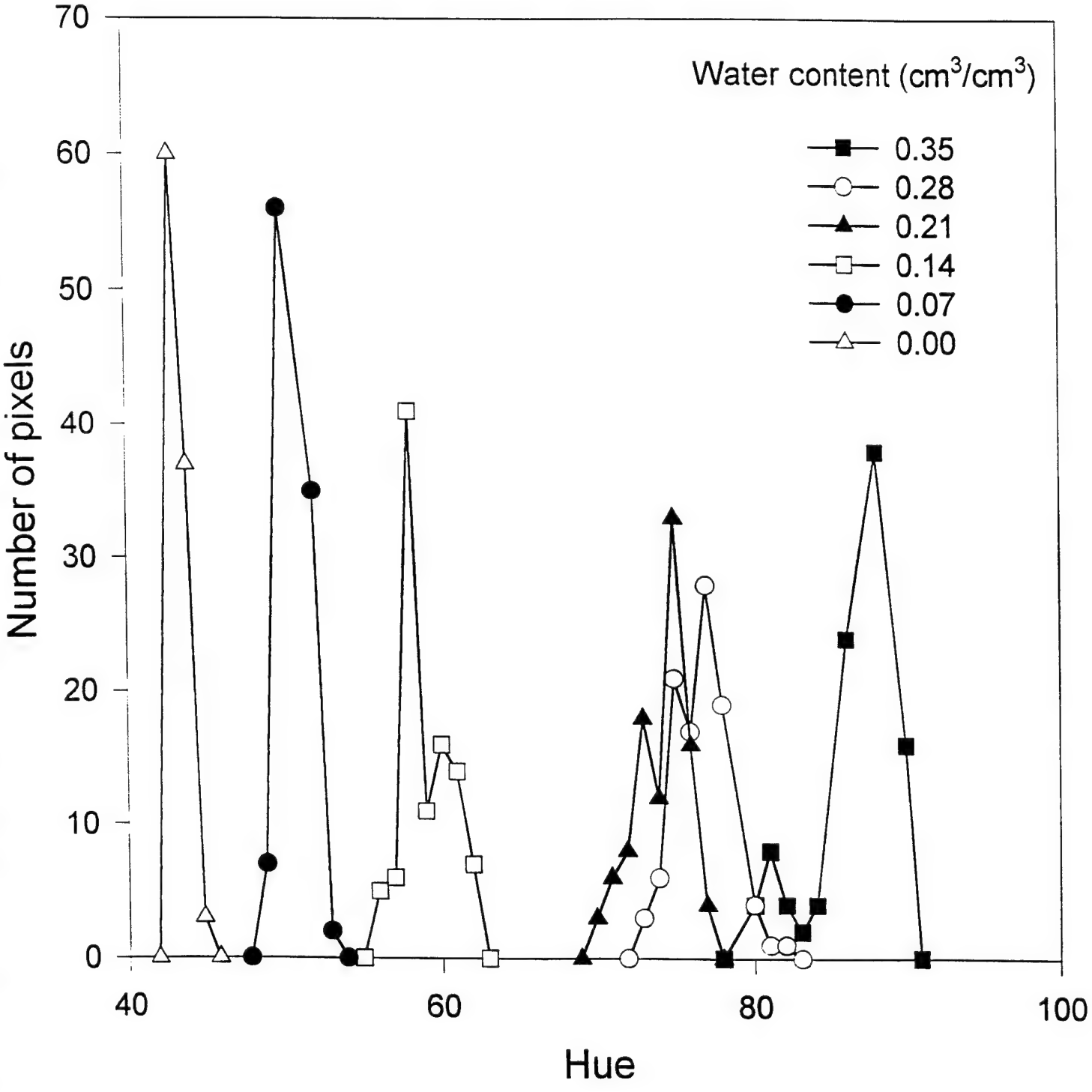
Water content (cm^3/cm^3)
0.35
0.28
0.21
0.14
0.07
0.00
Number of pixels
Hue
0
10
20
30
40
50
60
70
40
60
80
100

Figure 3

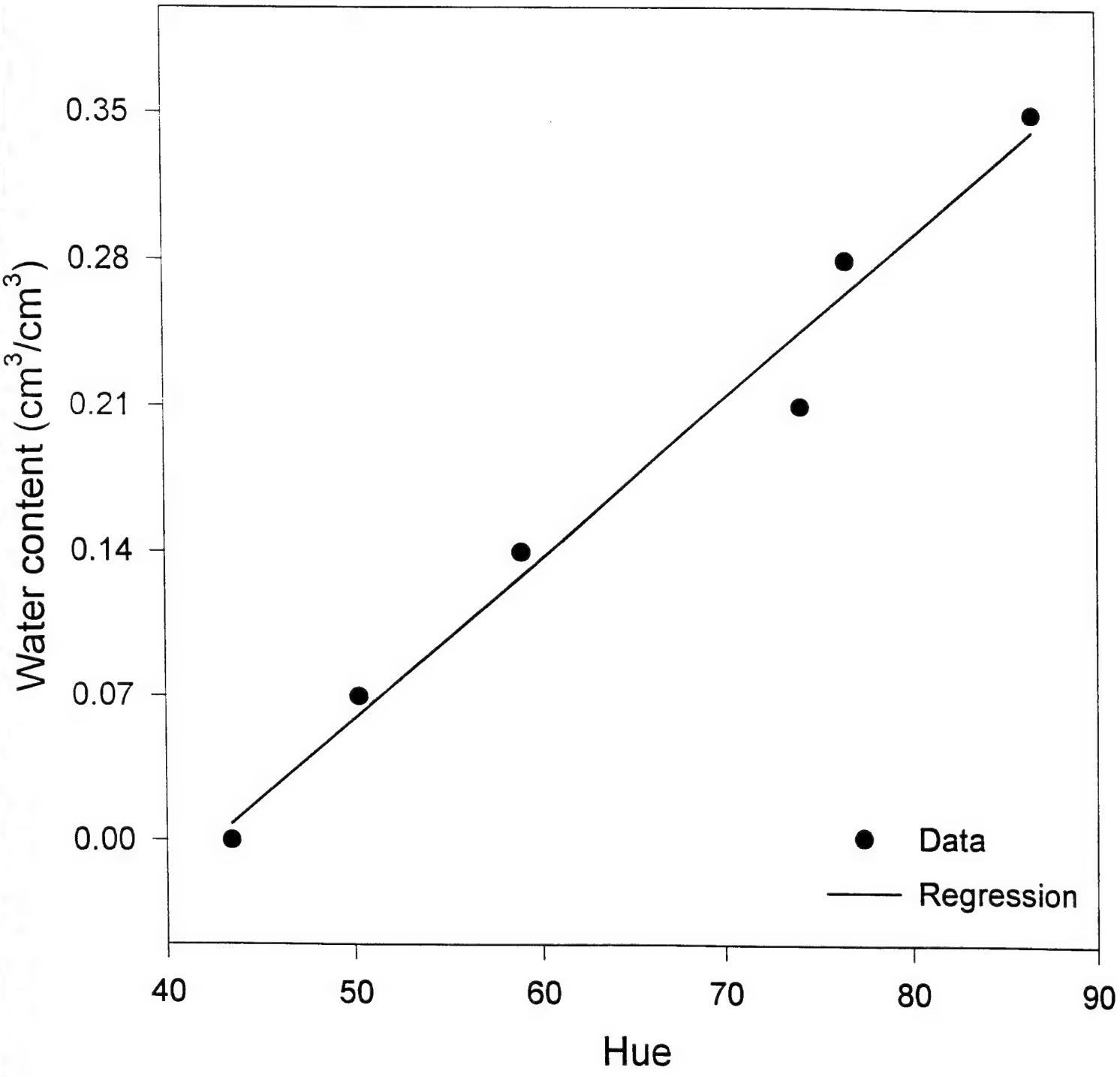
0.35
0.28
0.21
0.14
0.07
0.00
Water content (cm3/cm3)
40
50
60
70
80
90
Hue
Data
Regression

Figure 4

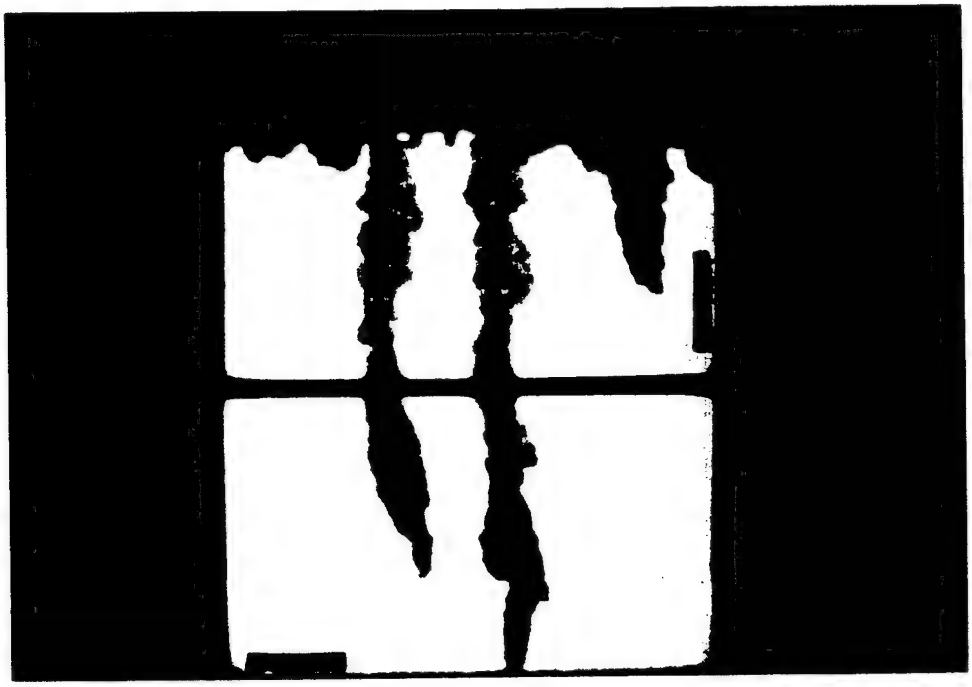

Figure 5

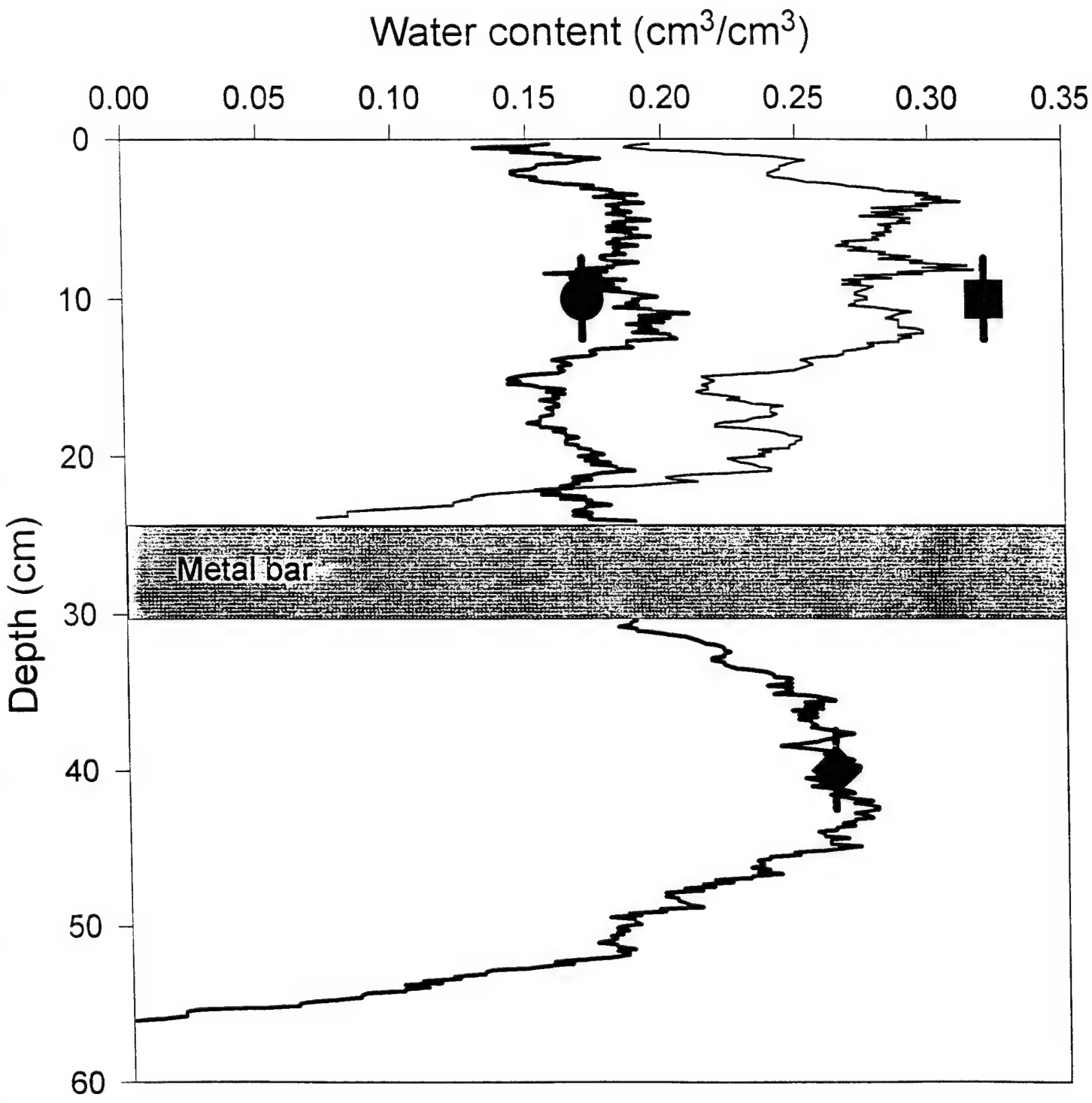
Water content (cm3/cm3)
0.00
0.05
0.10
0.15
0.20
0.25
0.30
0.35
0
10
20
30
40
50
60
Depth (cm)
Metal bar

Figure 5

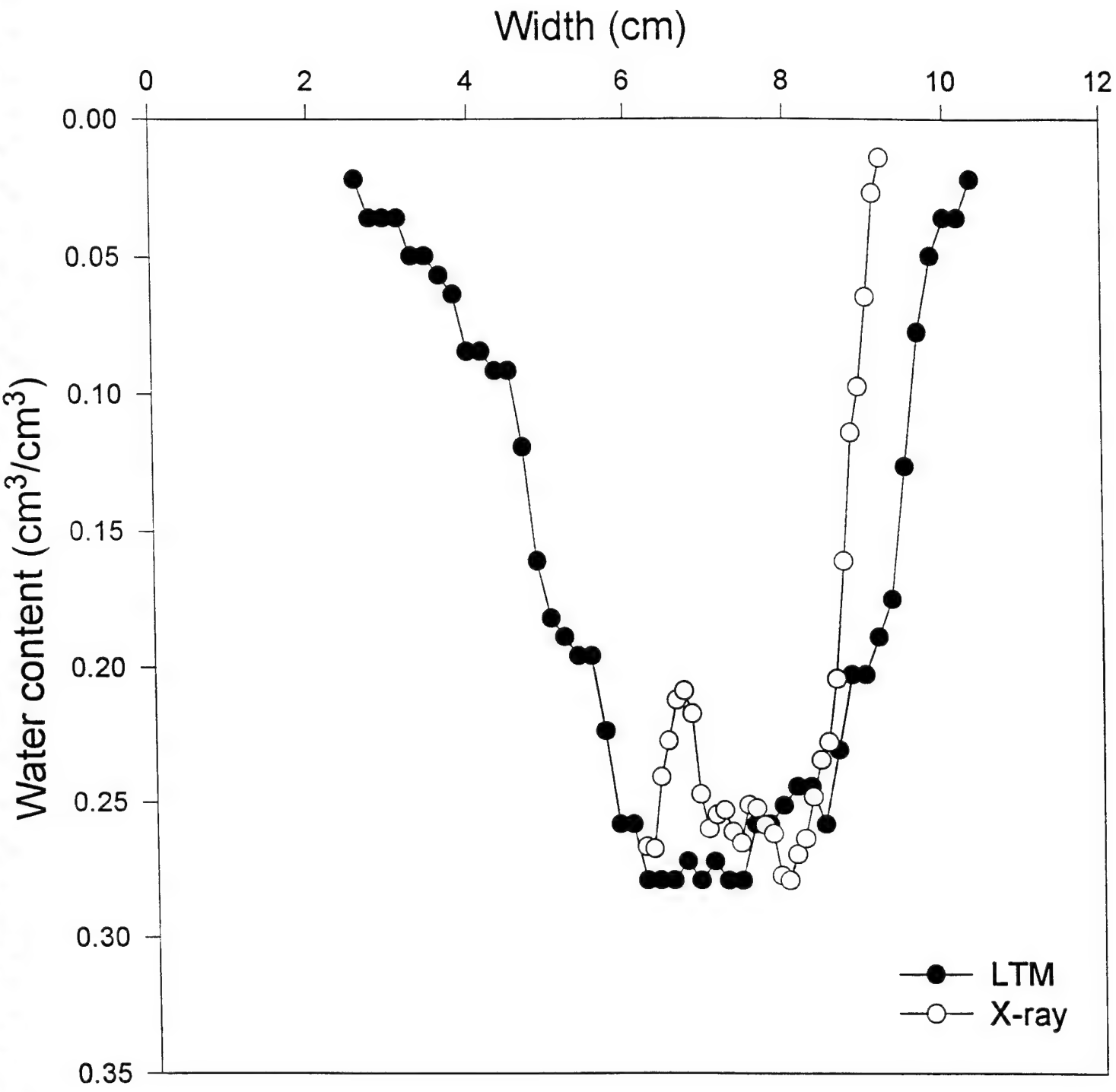
Width (cm)
0
2
4
6
8
10
12
0.00
0.05
0.10
0.15
0.20
0.25
0.30
0.35
Water content (cm3/cm3)
LTM
X-ray

Figure 7

APPENDIX D

HIGH-SPEED MEASUREMENTS OF THREE-PHASE FLOW USING SYNCHROTRON X-RAYS

D.A. DiCarlo, T.W.J. Bauters, T.S. Steenhuis,
J.-Y. Parlange, and B.R. Bierck

Water Resources Research 33(4):569-576

WATER RESOURCES RESEARCH, VOL. 33, NO. 4, PAGES 569–576, APRIL 1997

High-speed measurements of three-phase flow using synchrotron X rays

D. A. DiCarlo, T. W. J. Bauters, T. S. Steenhuis, J.-Y. Parlange, and B. R. Bierck
Department of Agricultural and Biological Engineering, Cornell University, Ithaca, New York

Abstract. Accurate monitoring of flow instabilities, which can occur when nonaqueous phase liquids (NAPLs) flow through porous media, is an important component of predicting the transport and fate of these compounds in the subsurface. In particular, flow situations in which three mobile phases (such as water, NAPL, and air) exist in the porous media are inherently complex. Unfortunately, the relatively low source intensities and the nontunable source energies make traditional dual gamma techniques unsuitable to study flow instabilities which can change within seconds. We present an alternate technique, which uses synchrotron X rays from the Cornell High Energy Synchrotron Source (CHESS) to measure three-phase fluid saturations on the time scale of seconds. Using the harmonic content resulting from X ray diffraction, we obtained a high-intensity X ray beam consisting of distinct tunable energies. Three-phase saturations were measured on 5-s timescales during fingering of light NAPL into regions of dry and water wet sandy soil. In the water wet soil the oil finger was less saturated, slower, and wider than the same finger in the dry soil. The results yield insights into the nature of three-phase preferential flow.

Introduction

Accurate measurements of multiphase flow in porous media are needed to understand and model subsurface transport of contaminants such as nonaqueous phase liquids (NAPLs). In particular, flow instabilities and the subsequent preferential flow patterns can dramatically affect the fate of NAPLs and the subsequent attempts at remediation. For quantitative studies of preferential flow it is imperative to obtain fast, accurate, and nondestructive measurements of various fluid saturations within the porous media. Nondestructive measurements of multiphase saturations can be achieved using dual-energy gamma radiation systems, but these techniques have been limited in speed [*Oostrom et al.*, 1995].

Attenuation of high-energy electromagnetic radiation, such as X and gamma rays, is directly related to the amount of fluid or solid in the path of the radiation, thus providing a means to obtain nondestructive fluid saturation measurements. Radiation sources and techniques have progressed over the years, providing quicker and more accurate saturation measurements. Decays of radioactive elements such as cesium (Cs) and americium (Am) produce monochromatic gamma rays, and the elements have been used as portable radiation sources for field and laboratory measurements [*Hillel*, 1980]. Combining and collimating Cs and Am sources allows them to be used for three-phase measurements [*Nofziger and Swartzendruber*, 1974; *Hopmans and Dane*, 1986; *Ferrand et al.*, 1986; *Lenhard et al.*, 1988; *Illangasekare et al.*, 1995]. Recently, *McBride and Miller* [1994] have developed a technique that obtains dual energies from an X ray tube. Both sources can yield accurate three-phase saturations but only over long timescales as enough photon counts are needed to overcome the random errors associated with counting statistics [*Gardner et al.*, 1972; *Oostrom et al.*, 1995]. Recently, synchrotron radiation sources have also been used for nondestructive measurements. The greater than 10,000-fold intensity increase over tube sources and radioactive elements produces fast two-phase saturation measurements and allows preferential flow to be precisely monitored in real time [*Liu et al.*, 1993].

In the first part of the paper, we present a general procedure for obtaining and using dual energies from a synchrotron X ray source. This procedure has been used to simultaneously measure water, NAPL, and air saturations in a sandy soil. For saturation data taken in 5-s time intervals, the measured variance in the volumetric content is approximately 0.01 cm^3/cm^3, which is comparable to the destructive oven drying technique. This technique can be applied to produce fast, precise monitoring of any three phases in porous media. In the second part of the paper, we present and analyze the saturations obtained when a light NAPL, hereafter referred to as oil, infiltrates through dry and partially water wetted soil.

Theory

For monochromatic radiation the attenuation of high-energy radiation is linearly related to the material within the radiation's path [*Cullity*, 1956],

$$A = \ln (T/I) = -\sum_i U_i x_i, \qquad (1)$$

where A is the measured attenuation defined as the natural logarithm of the transmitted intensity T, divided by the incident intensity I. The sum is over each material in the radiation's path, where U is the attenuation constant and x is the cumulative thickness of each material. The attenuation constants depend on the atomic constituents of each material and the energy of the radiation. In general, the attenuation decreases with increasing radiation energy and decreasing atomic

Paper number 96WR03958.
0043-1397/97/96WR-03958$09.00

number, with the exception of abrupt attenuation increases at atomic K and L electron energy levels.

Substituting in the relevant materials for multiphase measurements in a porous media of total thickness x,

$$A = -U_w\theta_w x - U_o\theta_o x - U_s\theta_s x - U_c + D. \quad (2)$$

Here x is the thickness of the experimental chamber, θ are the volumetric saturations, and the subscripts w, o, and s denote the water, oil (or NAPL), and soil phases, respectively. Attenuation by the chamber walls and the air between the detectors is given by the constant U_c. The term D is a constant offset that occurs if relative rather than absolute intensities are measured. Attenuation by the air inside the chamber can be considered negligible. In two-phase flow situations where there is only one independent quantity, for example, water and air in a partially saturated soil, the equation can be inverted to yield the fluid saturations in terms of the measured attenuation,

$$\theta_w = -\frac{A - A_0}{U_w x}, \quad (3)$$

where A_0 is the attenuation measured for the dry soil. Notice that only changes in the attenuation enter into the fluid determination, and knowledge of the individual contributions of D and U_c to the attenuation is unnecessary. In three-phase flow situations where three saturations are variable (water, oil and air, or water, soil and air), another independent measurement is needed to characterize the system. This can be provided by measuring the attenuation of radiation of a different energy. In a sample in which saturations of water, oil, and air are variable, the fluid saturations can be determined from the attenuation of the high (A_H) and low (A_L) energy radiation,

$$\theta_w = \frac{U_{OL}(A_H - A_{H0}) - U_{OH}(A_L - A_{L0})}{(U_{WL}U_{OH} - U_{WH}U_{OL})x} \quad (4)$$

$$\theta_o = \frac{U_{WH}(A_L - A_{L0}) - U_{WL}(A_H - A_{H0})}{(U_{WL}U_{OH} - U_{WH}U_{OL})x} \quad (5)$$

where the subscripts H and L denote the high- and low-energy attenuation constants and A_{H0} and A_{L0} are the high and low attenuations for the dry sand, respectively. These are the saturation equations for any dual-energy attenuation apparatus.

The advantages of synchrotron radiation can be demonstrated by studying the sources of variance in the above equations. The variance of the fluid saturations consists of systematic variances due to uncertainties in attenuation constants, dry attenuations, and chamber thickness, and temporal variances due to the finite counting times for the detectors. The systematic variances can be minimized by careful calibration, and the variance is typically dominated by the temporal variance [*Oostrom et al.*, 1995]. Using Poisson statistics for the detectors, photon intensities of R_H and R_L (photons per second), and a counting time of t (seconds), the variance of the attenuations are

$$\text{Var}(A_L) = \frac{1}{R_L t} \qquad \text{Var}(A_H) = \frac{1}{R_H t}. \quad (6)$$

For synchrotron sources the variance is typically twice this amount as counting uncertainties apply to both the incident and transmitted intensities. Using error propagation formulas, the variance in the fluid saturations can be calculated [*Oostrom et al.*, 1995],

$$\text{Var}(\theta_w) = \frac{1}{t}\left(\frac{U_{OH}^2}{R_L} + \frac{U_{OL}^2}{R_H}\right)\left(\frac{1}{(U_{WL}U_{OH} - U_{WH}U_{OL})x}\right)^2, \quad (7)$$

$$\text{Var}(\theta_o) = \frac{1}{t}\left(\frac{U_{WH}^2}{R_L} + \frac{U_{WL}^2}{R_H}\right)\left(\frac{1}{(U_{WL}U_{OH} - U_{WH}U_{OL})x}\right)^2. \quad (8)$$

Variances can be decreased by either increasing the counting times, the countable photon flux, or the denominator of the third term. For conventional dual gamma sources, long counting times are typically used for increasing precision. The high flux and tunable energies available at synchrotron sources allow the second two factors to be increased dramatically, thus lowering the variance, and decreasing the necessary counting times.

For dual-energy attenuation measurements, the advantages of large photon fluxes are more subtle than a brute increase in the counting rates. Typically, large photon fluxes allow ion chambers to be used as detectors for attenuation measurements. Ion chambers detect ionization currents produced when X rays are passed through an inert gas, and when used with synchrotron source fluxes are free from counting statistics associated with individual photon detectors. Unfortunately, the lack of energy resolution precludes ion chambers from being used for dual energy attenuation measurements. Scintillation or solid state detectors are still needed, both of which give linear results up to a maximum photon flux, but at a synchrotron source the detectors can be configured to run at their maximum rates for a wealth of experimental situations.

The advantages of tunable energies and attenuations are much greater than the pure increase in intensity. The attenuation of each fluid can be increased in a number of ways; doping the fluids with heavy elements, increasing the path length, or using lower energy X rays. For conventional radiation sources, fluid doping is often used, but any method of increasing the attenuation is limited as it cuts into the detected count rate. For synchrotron sources, increasing the attenuation is less limited as the large incident intensities assure plenty of transmitted photons. Also, in some situations the thickness of the chamber and fluid contents are fixed. In this case, the attenuations can be optimized by altering the energy of the X rays. This is impossible for conventional sources, but the white light emitted by synchrotron sources allows a choice from a continuum of X ray energies.

Most importantly, precision can be increased by selecting the X ray energies such that the specific oil and water attenuations combine to yield a large value for the denominator of the third term. This result is achieved if one fluid preferentially attenuates the low-energy X ray and the other fluid preferentially attenuates the high-energy X ray such that $U_{WL}U_{OH} \gg U_{WH}U_{OL}$. This situation occurs only when an element within one of the fluids has an absorption edge between the two working energies. The selection of energies above and below absorption edges is again trivial for synchrotron sources.

Materials and Methods

Figure 1 depicts a schematic diagram of the apparatus used on the F-2 beam line at the Cornell High Energy Synchrotron Source (CHESS). CHESS is a National Science Foundation funded synchrotron facility open to outside users through peer

reviewed proposals (CHESS Facility Description, available at http://www.chess.cornell.edu, 1995). The initial white X ray beam is reflected off a double-bounce Si(220) monochromator, producing a beam of two distinct energies. The multiple-energy beam entered the experimental hutch where it passed through a set of tantalum slits which defined a beam size of 1 mm vertical × 8 mm horizontal. Subsequently, the beam passed through a nitrogen-filled ion chamber, 70 cm of open air, the sample chamber, and another 70 cm of open air before hitting the beam stop at the end of the hutch. X ray intensities were measured with scintillation detectors pointing down at the X ray beam. The incident detector was placed 33 cm before the sample chamber, and the transmitted detector was placed 40 cm after the sample chamber. The individual components of the apparatus are discussed in detail below.

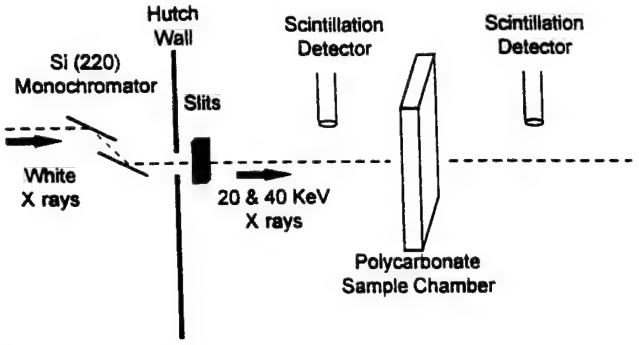

Figure 1. A schematic of the experimental set up at the F-2 hutch of CHESS. The monochromator transforms the white X ray beam into a multiple-energy beam. Scintillation detectors measure the intensity of both energy X rays by detecting air scattering from the main beam. The sample chamber is mounted on a movable platform allowing measurements from many different positions within the chamber.

Synchrotron Radiation

When relativistic charged particles are bent around a synchrotron ring they emit well-collimated X rays of a broad energy (white) spectrum. This is in contrast to radioactive decay sources which emit X rays with a well-defined fixed energy, and X ray vacuum tube sources which emit both X rays with a well-defined energy (corresponding to the characteristic emission lines of the target metal) and a low-intensity, broad energy, X ray background (bremsstrahlung). At the F-2 line at CHESS the radiation intensity is roughly constant from 9 to 40 keV and only drops by a factor of 2 at 60 keV (CHESS Facility Description, 1995). For absorption measurements the white radiation can be made monochromatic by diffraction from a pair of perfect silicon crystals. The wavelength λ of the X rays diffracted by the first crystal is dependent on the distance between the lattice planes d and the incident X ray angle θ, through Bragg's law [*Cullity*, 1956],

$$n\lambda = 2d \sin \theta \tag{9}$$

where n is an integer. This wavelength is related to the X ray energy,

$$E = hc/\lambda \tag{10}$$

where h is Planck's constant and c is the speed of light. The energies of the X ray beam can be varied by varying the angle of the monochromator. The second silicon crystal is placed below and downstream of the first crystal and set to an identical angle. This standard dual monochromator setup allows the energies to be varied without varying the spatial position of the beam.

The fundamental energy corresponding to $n = 1$ is the strongest reflection and typically the only one used. The higher harmonic energies, corresponding to $n = 2, 3, 4, \cdots$, are of lower intensity due to the smaller band pass of the monochromator crystal at higher-order crystal reflections (the band pass scales as approximately n^{-2}), and from the lower flux at higher energies in the incident beam. Harmonic energies are usually only observed at synchrotron facilities due to the broad energy spectra of the incident beam. In fact, harmonic energies are typically a nuisance as they destroy the monochromaticity of the beam, and various techniques can be used to suppress them. For dual-energy attenuation measurements the harmonics are extremely useful, as they can provide a simultaneous second (and possibly third!) attenuation measurement.

In our experiment we used a fundamental energy of 20 keV, but 12.5 keV was also tested in order to determine the most robust energy setting. When tuned to 20 keV, the low- and high-energy X rays were 20 and 40 keV, respectively. When tuned to 12.5 keV, the fundamental energy was eliminated by placing a 0.3-cm-thick aluminum plate in the beam path, and the low- and high-energy X rays were 25 and 37.5 keV, respectively. In either case, the energies were chosen to be above and below Iodine's absorption edge at 33.2 keV. As measured by the ion chambers, typical initial intensities were 10^{11} photons/s for the low-energy beam, and 10^{10} photons/s for the high-energy beam.

X ray Detection

As the X ray intensity is not constant for synchrotron sources, the incident and transmitted intensities of both energies must be accurately measured. Detection methods must have adequate energy resolution, enough counts for good statistics, and not destroy the incident beam. Also to reduce systematic errors, it is useful if the incident and transmitted detectors are of the same type.

We have used Na I(Tl) scintillation detectors, which count individual X ray photons at rates up to 10^6 counts/s with an energy resolution of 40% [*Thompson*, 1986]. Since the intensity of the beam was so great, the detectors were placed above the beam and pointed down at the passing beam. In this fashion, the detectors counted the X ray photons which were vertically scattered from the beams by the air in the hutch. Scattering by the air consists of elastic (Rayleigh) and inelastic (Compton) processes [*Cullity*, 1956]. At the working photon energies the energy loss due to 90° Compton scattering is less than 1 keV, much less than the difference in photon energies and the energy resolution of the detectors. More importantly, both processes are linear with the X ray intensity. To control the magnitude of the scattered flux into the detector a lead aperture and an aluminum attenuator were placed in front of each detector. The low- and high-energy photon flux scattered into the detectors are given by

$$I_{DL} = \{\sigma(\theta, E_L)\Omega \exp [-U_A(E_L)y]\}I_L, \tag{11}$$

$$I_{DH} = \{\sigma(\theta, E_H)\Omega \exp [-U_A(E_H)y]\}I_H, \tag{12}$$

where I_{DL} and I_{DH} are the low and high X ray intensities into the detector, I_L and I_H are the low and high intensities of the beam below the detector, σ is the air scattering cross section

and is a function of scattering angle θ (90° in this case) and X ray energy E, Ω is the solid angle of the aperture, U_A is the attenuation constant (cm^{-1}) of the attenuator in front of the detector and y is the thickness (centimeters) of the attenuator. Since the aluminum preferentially attenuates the low-energy X ray, by adjusting the attenuator thickness y and the aperture size Ω, we were able to obtain roughly 15,000 counts/s of high- and low-energy photons scattered into each detector. To eliminate stray radiation from entering the detector a circular lead flight tube was attached to the front of each detector. The incident detector was placed 10 cm above the beam, had a 3-cm flight tube, a 1.2-cm circular aperture, and a 0.6-cm-thick aluminum attenuator. The transmitted detector was placed 8.5 cm above the beam, had a 7-cm flight tube, a 2.2-cm circular aperture, and no attenuator. Throughout each experiment the configuration of the detectors was not altered as this would change the proportionality constants and destroy any previous calibration.

The output of each scintillation detector was fed through an attached preamplifier followed by a variable gain spectroscopy amplifier. The gains of the spectroscopy amplifiers were set such that the electronic pulses of average heights 3.4 and 6.8 V were produced for the 20 and 40 keV photons, respectively. The output from each amplifier was split and fed into two separate single channel analyzers, one analyzer recorded pulses between 2.5 and 4.5 V as 20 keV photons, the other recorded pulses between 5.2 and 7.7 V as 40 keV photons.

For any dual gamma setup there is a finite chance that a high-energy photon may elicit a detector response which will be counted in the low-energy photon bin, and vice versa. The sources of this "cross-binning" are different for synchrotron X rays than for traditional dual gamma apparatus and are worth discussing. In a traditional dual gamma apparatus using Am and Cs sources, the "cross-binning" is due to Compton scattering. When a 660 keV enters the scintillation detector, it may be Compton scattered out of the detector, leaving behind a Compton electron with energy ranging from 0 to 477 keV. The Compton electron subsequently produces scintillation light, resulting in a broad low-energy tail in the detected energy spectra. If the Compton electron happens to acquire 60 keV of energy, it will be detected as a 60 keV photon and will be mistaken for a Cs photon. For the lower photon energies used here, Compton scattering inside the detector does not cause errant readings. The maximum Compton electron energy created by a high-energy 40 keV photon is 5 keV, which will not be counted as a low-energy 20 keV photon. Instead the more likely source of cross-binning at these energies is due to the statistical spread in the small amount of primary electrons produced for each X ray, resulting in an energy full width at half maximum (FWHM) of 40%. Thus there still exists a finite chance that a 40 keV photon will produce a response in the detector that would be fit into the bin reserved for counting 20 keV photons. For our experimental parameters the expected chance of a high-energy photon being counted as a low-energy photon, and vice versa is approximately 1%. As shown in the appendix, the cross-binning creates an additional variance of 1% in the fluid concentrations.

Sample Chamber and Fluids

The sample chamber had 0.94-cm-thick polycarbonate walls and interior dimensions of 30 cm wide (x direction), 0.94 cm thick (y direction), and 55 cm tall (z direction). Attached to the bottom end was a manifold of five fluid ports, and the top end was left open to the atmosphere. The chamber was filled with clean, dry, sieved, quartz sand (Unimin Corporation) using a dual randomizing funnel. Grain sizes used were 12/20, 20/30, and 30/40, where the numbers correspond to the sieve sizes the sand passes through and does not pass through, respectively. To measure the fluid saturations at many points, the chamber was mounted on a movable platform which had a horizontal and vertical range of 25 and 50 cm, respectively, and a position repeatability of 0.01 cm.

Table 1. Measured Attenuation Constants of the Water and Oil Phases

Phase	Attenuation, cm^{-1}	
	20 keV	40 keV
Water	2.56	0.512
Oil	1.339	1.102

Distilled water doped with 50 g/L NaBr and FD&C blue dye was used for the aqueous phase, and Soltrol 220 (Phillips Company) doped with 77 g/L iodoheptane (Aldrich Chemical Company) and a red Sudan IV dye was used for the oil phase. Soltrol 220 has been widely used to study NAPL behavior [*Schroth et al.*, 1995]. The addition of the dopants raised the specific gravities of the fluids slightly to 0.825 and 1.040 g/cm^3, for the oil and water phases, respectively. Measured changes in the surface tensions were less than 1 dyne/cm (du Nouy ring method), with surface tensions of 28 and 72 dynes/cm for the oil and water phases, respectively, and an interfacial tension of 32 dynes/cm. Thus the oil phase was a spreading NAPL. Fluid attenuation constants were obtained using a polycarbonate chamber with five sequential cells of thickness 0.56 cm [*Lenhard et al.*, 1988]. The attenuation was measured for the empty chamber and after each cell was filled with either fluid. The measured attenuations were linear with fluid thickness, except at the highest thickness (corresponding to 2.8 cm of fluid, or a volumetric saturation of 3.00 cm^3/cm^3) where the transmitted count rates were smallest. Attenuation constants were calculated from the slope of the attenuation versus thickness curve. Table 1 lists the measured attenuation constants and their precision.

To test the precision and speed of the technique and to observe unstable three-phase flow, the saturations within an oil finger penetrating partially water saturated soil were measured. Initial attenuations of the dry sand-packed chamber were measured at various positions throughout the chamber. The chamber was then filled from below with water at a rate of 30 mL/min to a height of z = 40 cm, and subsequently drained at a rate of 20 mL/min until the water fringe was at a height of z = 12 cm. The chamber had three distinct regions, below z = 12 cm the sand pack was water saturated (θ_s = 0.37 cm^3/cm^3), between z = 12 cm and z = 40 cm the sand was drained to the residual water saturation (θ_R = 0.05 cm^3/cm^3), and above z = 40 cm the sand was dry. Oil was applied through a point source at the top of the chamber at a rate of 4 mL/min. A finger formed which moved quickly through the dry sand, and slowly through the partially wet sand before finally hitting the water table and spreading laterally. Figure 2 presents a sketch of the chamber during the finger infiltration. Temporal fluid saturations were measured in the water unsaturated and partially water saturated regions at positions z = 45 cm and z = 30 cm, respectively, as the finger traversed these regions.

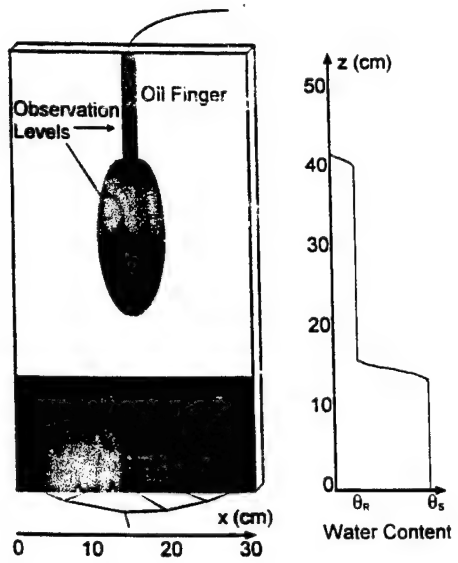

Figure 2. Front view of the experimental chamber during an oil infiltration. The oil was applied from a point source at the top and the water from the manifold of ports at the bottom. Initially, below $z = 12$ cm the sand pack was water saturated ($\theta_s = 0.37$ cm^3/cm^3), between $z = 12$ cm and $z = 40$ cm the sand was drained to the residual water saturation ($\theta_R = 0.05$ cm^3/cm^3), and above $z = 40$ cm the sand was dry. The initial approximate water content as a function of depth is sketched on the right. The finger became wider and slower when it entered the partially water saturated sand. Oil and water saturations were observed as a function of time at $z = 45$ cm and $z = 30$ cm.

Horizontal profiles of the finger were taken at $z = 30$ cm when the finger saturations had reached steady state.

Results and Discussion

Time Resolution

Figures 3 and 4 show the measured fluid saturations as the oil finger penetrated the initially dry and partially water saturated 20/30 sand, respectively. To resolve the tip of the finger passing through the observed region, attenuation data were accumulated over 5-s intervals. The predicted variances in the fluid contents due to the finite counting times can be calculated from (8) and (9). Even for the 5-s counting times the variances are only 0.01 cm^3/cm^3 and are depicted by the error bars in Figures 3 and 4. The scatter in the data roughly matches the predicted variance, implying that the expected precision has been achieved, and that the counting statistics are the precision limiting factor.

Figures 5 and 6 show the measured fluid saturations as the oil finger penetrated the initially dry and partially water saturated 30/40 sand, respectively. Data were accumulated over 3-s intervals, yielding slightly higher variances, but greater time resolution than for the results in Figures 3 and 4. The scatter in the data is slightly larger than expected from counting statistics, and was most likely caused by temporary cooling problems with the monochromator crystal.

It is instructive to compare the precision and speed of the above synchrotron X ray technique and other dual energy techniques. Using Am and Cs sources, *Nofziger and Swartzendruber* [1974] obtained a water precision of 0.01 cm^3/cm^3 when counting for 5 minutes, and 0.04 cm^3/cm^3 when counting for

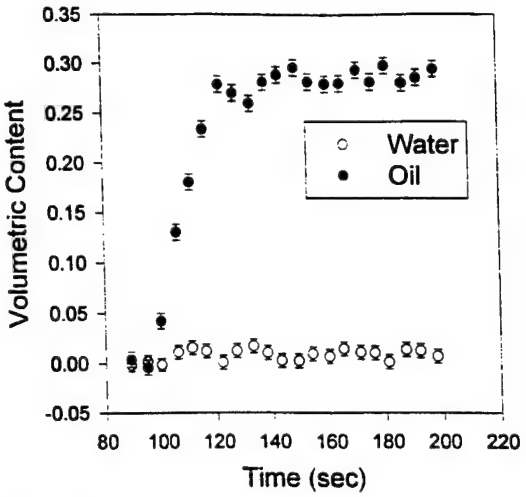

Figure 3. Water and oil contents versus time as the oil finger passes through initially dry 20/30 sand. Error bars depict the expected variance due to counting statistics as calculated from (8) and (9), and they roughly match the scatter in the data. The rapid rise of the oil content can be easily discriminated, and the oil level approaches saturation.

5 s. *Oostrom et al.* [1995] obtained water and oil precisions of better than 0.01 cm^3/cm^3 when counting for 60 s, with slightly worse precisions for a counting time of 30 s. Studies [*Okuda et al.*, 1996; *Imhoff et al.*, 1996] using the X ray vacuum tube apparatus described by *McBride and Miller* [1994] have reported precisions of 0.0024 cm^3/cm^3 for porosity and 0.005 cm^3/cm^3 for PCE saturation when counted for 6 s three separate times. It is unclear if this reported accuracy is from a dual-energy measurement or a single energy measurement, the latter of which is inherently more accurate, as the attenuations do not have to be decoupled. These comparisons are only rough as all the studies have used different fluids, dopants, and chamber thickness.

One of the strengths of the synchrotron technique can be seen from a comparison of Figures 4 and 6. In three-phase studies it can be important to know which phase is forced out

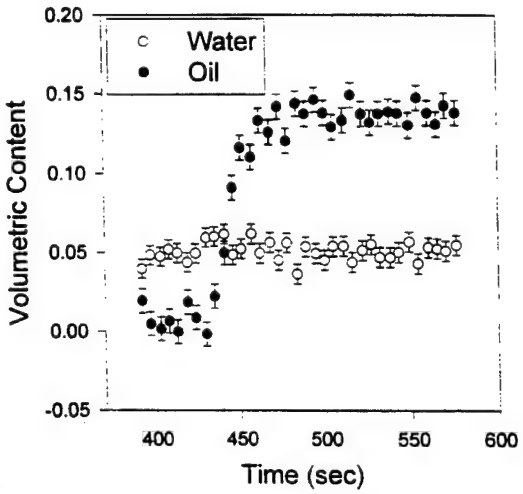

Figure 4. Water and oil contents versus time as the oil finger passes through partially water saturated 20/30 sand. The oil content rises less rapidly and to a lower saturation than in the dry sand. The water content is unaffected by the oil finger.

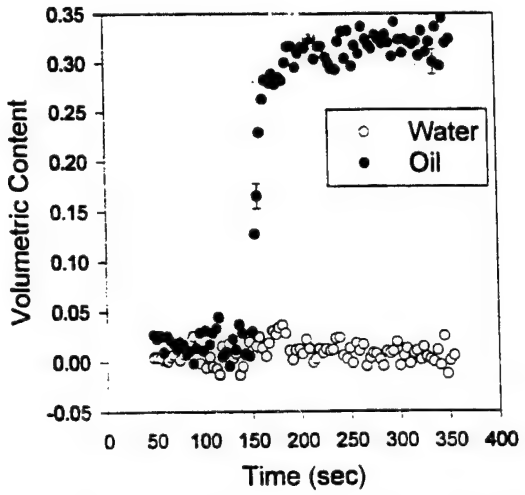

Figure 5. Water and oil contents versus time as the oil finger passes through initially dry 30/40 sand. Again, the oil rises rapidly to a value near saturation.

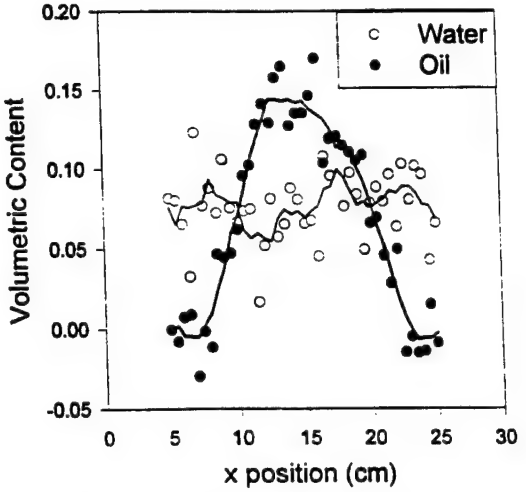

Figure 7. A horizontal scan through the oil finger in the partially water saturated 30/40 sand. The lines are moving averages of the saturations and are a guide for the eye. The extra scatter in the data is most likely due to local variations in the sand density due to the coarseness of the sand.

of a region when a third phase enters the region [*Kao and Hunt*, 1996]. For the 20/30 sand the water content remains constant as the oil finger passes implying that only air leaves the volume, but in 30/40 sand the water content is driven down slightly by the arrival of the oil finger. These small and fast saturation changes are easily observed.

Figure 7 shows the measured horizontal profile of the oil finger in 30/40 sand. In this case, the measured variance was much greater than expected for counting statistics. This variance was even greater in the coarser 12/20 and 20/30 sands. The extra scatter was most likely due to the variations in the soil attenuation A_0. The soil volume sampled by the X rays was only 0.08 cm^3, which was not much greater than the average grain size volumes for the 12/20 and 20/30 sand. Thus the sand density and porosity fluctuates on this length scale, causing fluctuations in the dry soil attenuation. If the sand settles and shifts slightly when wetted, the sand attenuation at each position can change, thereby creating more scatter in the data.

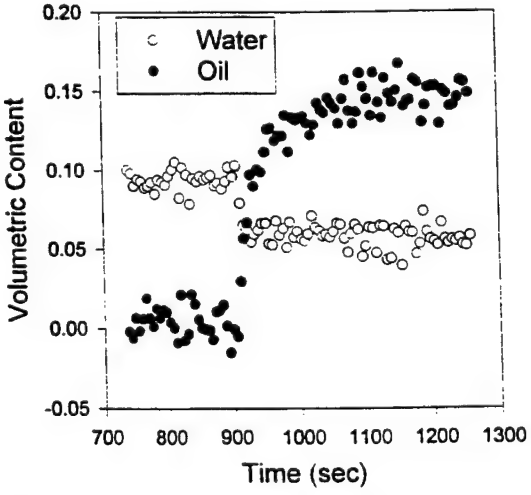

Figure 6. Water and oil contents versus time as the oil finger passes through partially water saturated 30/40 sand. The oil content rises to a lower saturation than in the dry sand, similar to that seen in 20/30 sand. As opposed to 20/30 sand, in this case the water content is driven lower by the oil finger.

Three-Phase Unstable Flow

Quantitative determinations of oil finger properties can be made using this technique. Finger widths were measured by taking the full width at half maximum (FWHM) in the horizontal profiles. Finger saturations were measured as the average near the center of the profile. These results are summarized in Table 2. In the initially dry region the oil saturation was close to full saturation (0.30 cm^3/cm^3) and the finger was 2.5–3.0 cm wide (FWHM). In the partially water saturated region the oil saturation was 0.15 cm^3/cm^3, roughly one half of the completely saturated value, the finger was 9.0–10.0 cm wide (FWHM), and the water saturation has a value of 0.05 cm^3/cm^3. So not only does the water remain when the oil finger passes, the initial water content creates a much lower oil saturation (and thus higher air situation) within the oil finger.

Comparisons can be made between this three-phase experiment and a similar two-phase experiment performed by *Liu et al.* [1991]. In Liu's experiment, finger properties were measured as a water finger passed from initially dry sand into partially water wetted sand. Similar qualitative effects were observed: in the initially dry sand the finger was 2.3 cm wide (FWHM) with a saturation of 0.35 cm^3/cm^3, while in the partially wetted sand the finger was 5.0 cm wide (FWHM) with a saturation of 0.24 cm^3/cm^3.

For either invading fluid the increase in the finger widths can be understood through the following argument. In the partially

Table 2. Summary of Oil Finger Properties in the 20/30 and 30/40 Sands for Both Regions

Sand Region	Finger Width, cm	Oil Saturation, cm^3/cm^3	Water Saturation, cm^3/cm^3
Dry 20/30	2.5	0.30	0.00
Dry 30/40	3.0	0.30	0.00
Water wetted 20/30	9.0	0.15	0.05
Water wetted 30/40	10.0	0.15	0.05

wetted sand the water forms menisci which in turn creates isolated islands of the water or air phases. The invading fluid has to either bypass these islands or force the water out of the pores, resulting in a decrease of the fluid conductivity. The initial water film covering the solid surfaces also enhances the lateral spreading of water and/or oil, the latter of which is a spreading fluid when in contact with water. The simultaneous decrease in conductivity (K) and increase in sorptivity (S) combine to increase the finger width. Experimentally, it is observed that the ratio of the finger widths between the dry and prewetted regions is greater for the oil finger (a factor of 3), than it is for the water finger (a factor of 2). This difference in ratios may be attributed to the fact that the water finger is miscible with the initial water in the soil, while the oil is immiscible. Thus the water flow is blocked or slowed by pores with entrapped air, while the oil flow is blocked by pores with entrapped air or entrapped water.

Although the air and water phases partially block the pores, the oil must replace one or both of these phases as it invades a region. For this experiment it appears that generally the oil only replaces the air as it invades the soil, leaving the water in place. The one exception is in the 30/40 sand where the oil finger causes the water saturation to decrease from 0.08 to 0.05 cm^3/cm^3. Here the final water saturation value is identical to the final saturation value for 12/20 and 20/30 sands. This saturation is also the value of the so-called irreducible water saturation for all the sands, roughly where the water conductivity becomes negligible.

Summary

Synchrotron radiation opens many possibilities to increase the speed of nondestructive measurements in porous media. For this particular experimental realization, better detector mounts and standard attenuators will make the detectors easier to configure. Faster electronics can be installed to increase the detectors' count rates and the precision further. Large improvements are possible by using custom monochromator crystals. Miscut monochromator crystals will inflate the beam in the vertical direction, thus diminishing the variances caused by coarse soils. One intriguing possibility is the use of a horizontally bent monochromator. This could produce focused dual energy X ray beams which will converge at the sample position but be separated in space elsewhere so that ion chambers can be used for detection. This would eliminate counting statistics and make attenuation measurements arbitrarily fast.

In summary, the power of synchrotron radiation has been used to increase the speed of dual radiation techniques in order to observe unstable three-phase phenomena. The dual energies were provided by the natural harmonic content of the monochromated beam, which can be tuned to the most appropriate energies. The advantages of the synchrotron method over dual gamma are the tunability of the energies and extraordinarily higher intensities. Tunability makes the method easily adaptable to maximize the accuracy for many different experimental requirements; for example, the energies can be chosen to be above and below any absorption edge. The high fluxes allow scintillation detectors to operate at their maximum efficiency. Also different X ray optic configurations may produce even faster nondestructive measurements. A limitation of synchrotron X rays is the variability of the source, and thus the incident radiation must be measured, slightly increasing the experimental error. The method is most applicable to unstable three-phase flow, where the real time saturation measurements of simple oil infiltrations illustrate how the initial water content makes the oil fingers less saturated, wider, and slower moving than fingers in dry sand.

Appendix

If these cross-binning probabilities are known, estimates can be made for the error that cross-binning introduces into the measured attenuations and attenuation constants. It is most instructive to observe how cross-binning changes the expected attenuations of known quantities of the pure fluids. The measured incident intensity I^M of each X ray can be related to the true incident intensity I of each X ray on the detector,

$$I_H^M = c_H^H I_H + c_H^L I_L \tag{A1}$$

$$I_L^M = c_L^H I_H + c_L^L I_L \tag{A2}$$

where c_i^j is the probability of a j energy photon being counted as an i energy photon. Assuming c_L^H/c_L^L, $c_H^L/c_H^H \ll 1$, and similar constants for the transmitted X rays, the difference between the measured attenuation and true attenuation can be expressed as

$$A_H^M = A_H + \frac{c_H^L}{c_H^H}\left(\frac{T_L}{T_H} - \frac{I_L}{I_H}\right). \tag{A3}$$

The calculation is identical for the low-energy attenuations. The true attenuation is linear with fluid concentration, while the cross-binning adds some nonlinearity to the measured attenuation. This nonlinearity results in an effective attenuation constant that varies with fluid concentration. To determine the magnitude of this nonlinearity, we differentiate the above expression with respect to the fluid concentration. Substituting in the dependence of the transmitted intensities on the water concentration yields the effective attenuation constant

$$\frac{\partial A_H^M}{\partial \theta_w} = U_{WH}^M = U_{WH} + (U_{WL} - U_{WH})\frac{c_H^L}{c_H^H}\frac{T_L(0)}{T_H(0)} \cdot [1 + (U_{WL} - U_{WH})\theta_w x + O(\theta_w x)^2], \tag{A4}$$

where $T(0)$ are the transmitted intensities with no fluid in the chamber. The first linear term gives the effective attenuation constant, and the second nonlinear term determines how the effective attenuation constant changes with fluid concentration. The percentage change in the measured attenuation constant between an empty and water-saturated chamber is

$$\frac{\Delta U_{WH}^M}{U_{WH}^M} = \frac{c_H^L}{c_H^H}\frac{(U_{WL}^M - U_{WH}^M)^2 \theta_w x}{U_{WH}^M}. \tag{A5}$$

Using the observed attenuation parameters and cross binning ratios for 20 and 40 keV radiation, the maximum deviation of the attenuation constants was 1%. For 25 and 37.5 keV radiation the cross binning ratios were greater, resulting in a maximum deviation of the attenuation constants of 2%.

Acknowledgments. We would like to thank Bill Millier, Edward Zhang, Christophe Darnault, Qun Shen, and the staff at CHESS for useful discussions and experimental assistance. This work was supported (in part) by the Air Force Office of Scientific Research, USAF, under grant/contract number F49620-94-1-0291. CHESS is supported by NSF grant number DMR-931-1772.

References

Cullity, B. D., *Elements of X-Ray Diffraction*, Addison-Wesley, Reading, Mass., 1956.

Ferrand, L. A., P. C. D. Milly, and G. F. Pinder, Dual-gamma attenuation for the determination of porous medium saturation with respect to three fluids, *Water Resour. Res.*, *22*, 1657–1663, 1986.

Gardner, W. H., G. S. Campbell, and C. Callissendorff, Systematic and random errors in dual energy soil and bulk density and water content measurements, *Soil Sci. Soc. Am. J.*, *36*, 393–398, 1972.

Hillel, D., *Fundamentals of Soil Physics*, Academic, San Diego, Calif., 1980.

Hopmans, J. W., and J. H. Dane, Calibration of a dual-energy gamma radiation system for multiple point measurements in a soil, *Water Resour. Res.*, *22*, 1109–1114, 1986.

Illangasekare, T. H., J. L. Ramsey Jr., K. H. Jensen, and M. B. Butts, Experimental study of movement and distribution of dense organic contaminants in heterogeneous aquifers, *J. Contam. Hydrol.*, *20*, 1–25, 1995.

Imhoff, P. T., G. P. Thyrum, and C. T. Miller, Dissolution fingering during the solubilization of nonaqueous phase liquids in saturated porous media, 2, Experimental observations, *Water Resour. Res.*, *32*, 1929–1942, 1996.

Kao, C. S., and J. R. Hunt, Prediction of wetting front movement during one-dimensional infiltration into soils, *Water Resour. Res.*, *32*, 55–64, 1996.

Lenhard, R. J., J. H. Dane, J. C. Parker, and J. J. Kaluarachchi, Measurement and simulation of one-dimensional transient three-phase flow for monotonic drainage paths, *Water Resour. Res.*, *24*, 853–863, 1988.

Liu, Y., T. S. Steenhuis, J.-Y. Parlange, and J. S. Selker, Hysteretic finger phenomena in dry and wetted sands, in *Preferential Flow*, edited by T. J. Gish and A. Shirmohammadi, pp. 160–172, Am. Soc. of Agric. Eng., St. Joseph, Mich., 1991.

Liu, Y., B. R. Bierck, J. S. Selker, T. S. Steenhuis, and J.-Y. Parlange, High intensity x-ray and tensiometer measurements in rapidly changing preferential flow fields, *Soil Sci. Soc. Am. J.*, *57*, 1188–1192, 1993.

McBride, J. F., and C. T. Miller, Nondestructive measurement of phase fractions in multiphase porous-media experiments by using x-ray attenuation, *Cent. Multiphase Res. News*, *1*, 10–13, 1994.

Nofziger, D. L., and D. Swartzendruber, Material content of binary mixtures as measured with a dual-energy beam of gamma rays, *J. Appl. Phys.*, *45*, 5443–5449, 1974.

Okuda, I., J. F. McBride, S. N. Gleyzer, and C. T. Miller, Physicochemical transport processes affecting the removal of residual DNAPL by nonionic surfactant solutions, *Environ. Sci. Technol.*, *30*, 1852–1860, 1996.

Oostrom, M., J. H. Dane, B. C. Missildine, and R. J. Lenhard, Error analysis of dual-energy gamma radiation measurements, *Soil Sci.*, *160*, 28–42, 1995.

Schroth, M. H., J. D. Istok, S. J. Ahearn, and J. S. Selker, Geometry and position of light nonaqueous-phase liquid lenses in water-wetted porous media, *J. Contam. Hydrol.*, *19*, 269–287, 1995.

Thompson, A. C., *X-Ray Data Booklet*, section 6-1, Lawrence Berkeley Lab., Berkeley, Calif., 1986.

T. W. J. Bauters, B. R. Bierck, D. A. DiCarlo, J.-Y. Parlange, and T. S. Steenhuis, Department of Agricultural and Biological Engineering, Cornell University, Ithaca, NY 14853.

(Received July 1, 1996; revised November 25, 1996; accepted December 19, 1996.)

APPENDIX E

WETTING AND NONWETTING FLUID DISPLACEMENTS IN POROUS MEDIA

A. Rimmer, J.-Y. Parlange, T.S. Steenhuis,
D.A. DiCarlo, C. Darnault, and W. Condit

Transport in Porous Media 25:205-215

Transport in Porous Media **25:** 205–215, 1996.

Wetting and Nonwetting Fluid Displacements in Porous Media

ALON RIMMER, JEAN-YVES PARLANGE, TAMMO S. STEENHUIS,* CHRISTOPHE DARNAULT and WENDY CONDIT
Department of Agricultural and Biological Engineering, Cornell University, Ithaca, NY 14853-5701, U.S.A.

(Received: 18 December 1995; in final form: 11 June 1996)

Abstract. The understanding of simple laminar flow in tubes has often been used to interpret the more complicated flow in porous media. A study of the motion of two immiscible liquids in closed tubes with relatively large diameter (> 0.3 cm i.d), was conducted in order to examine the influence of wetting and nonwetting liquids on the flow behavior. The results indicate that the wetting properties of the fluids with regard to the tube wall have a major efffect on the formation and motion of long bubbles. A physically based model was used to predict the velocity and the conditions for no motion of bubbles and drops in tubes. These results were used to interpret the nature of oil and water flow in porous media. Experiments in which the wetting liquid was displaced by the nonwetting, or vice versa, were conducted by injecting the displacing liquid at a constant flux at the center of a two-dimensional chamber saturated with the displaced liquid. The influence of wetting-nonwetting characteristics on the quantity of liquid displaced, the shape of the interface between the two liquids, and the interpretation of the no motion radius in a closed tube to the case of a porous medium are discussed. It would appear that the no motion radius gives a good indication of the minimum width of a nonwetting penetrating finger and the maximum width of nonwetting ganglia left by drainage.

Key words: oil and water, NAPL, bubbles, slugs, entrapped fluid, immiscible displacement, ganglia, vadose zone, soltrol.

1. Introduction

Contamination of soils, sediments, and groundwater with non-aqueous phase liquids (NAPLs) is one of the most widespread environmental problems. For example, the volume of contaminants of 130 Department of Energy facilities in the United States exceeds 2,500 billion liters with a projected life cycle costs greated than 300 billion dollars (DOE, 1995; Wilkins *et al.*, 1995).

In situ remediation is one of the few viable treatment technologies that offer the potential for cost-effective clean up. Multiphase models (Bear and Bachmat, 1990) have been used with limited success to optimize in situ remediation. One of the problems is that the complex interactions of the system parameters is not well understood and, therefore, cannot be modelled accurately. This paper addresses the interactions of wetting properties of the pore wall and the liquid. Two investigations are carried out. First, the motion of two immiscible liquids in a cylindrical tube

* Corresponding author. e-mail: tss1@cornell.edu

with various diameters is investigated. Then, we apply these results to explain observation of fluid distribution in porous media.

2. Flow in a Single Tube

THEORY: Past research for movement of two fluids in closed tubes has been mainly described by the movement of a light fluid (gas) bubble rising through a more dense fluid (liquid) (see review of Fabre and Liné, 1992). In cases where the motion of two immiscible liquids is considered, the wetting properties of both liquids and tube wall greatly influence the formation and shape of the bubble or drop. This influence has not been studied systematically in the past. Zukoski (1966) described gas bubbles movement in closed tubes in detail, and made a few casual remarks on the present problem of two immiscible liquids, mostly on the velocity of propagation and very little on wetting properties.

Following early work on gas bubbles (Dumitrescu, 1943; Davies and Taylor, 1950; Tung and Parlange, 1976; Bendiksen, 1984), the stream function ψ, of the flow outside the axis-symmetric bubble in a closed tube is expressed in terms of Bessel functions of the first kind and first order $J_1(k_n r a^{-1})$

$$\psi = -\tfrac{1}{2}Ur^2 + Uar \sum_{n=1} A_n J_1\left(\frac{k_n r}{a}\right) \exp\left(\frac{k_n x}{a}\right), \tag{1}$$

where k_n is the nth root, U is the velocity of the bubble or drop, a is the tube radius and r is the distance from the axis. In these early theories, different number of coefficients, A_n, and physical approaches were used to predict both the bubble shape ($\psi = 0$), and the bubble velocity. Davies and Taylor (1950) obtained a solution by retaining only the first term of the series expansion, which would result in a velocity increase when surface tension is taken into account, contrary to experimental observations. According to Fabre and Liné (1992), Dumitrescu (1943) was the first to give the solution by retaining three terms in the series expansion of the potential flow around a prescribed spherical front ignoring surface tension. Bendiksen (1984) followed the method of Dumitrescu taking into account surface tension.

Tung and Parlange (1976) calculated the coefficients $A_1 = 0.2516, A_2 = -0.0040$, and $A_3 = 0.0064$ in the series (Equation (1)), using an expansion of ψ for x and r small near the tip of the bubble and by satisfying the boundary condition of a constant pressure along the surface of the gas bubble, and the maximum velocity principle of Garabedian (1957) (Figure 2). The predictions of Tung and Parlange (1976) and Bendiksen (1984) of the velocity of an air bubble in a liquid both describe very well the experimental results of Zukoski (1966) and others (Fabre and Liné, 1992), but the first model is simpler, and slightly better as it satisfies Garabedian's conditions.

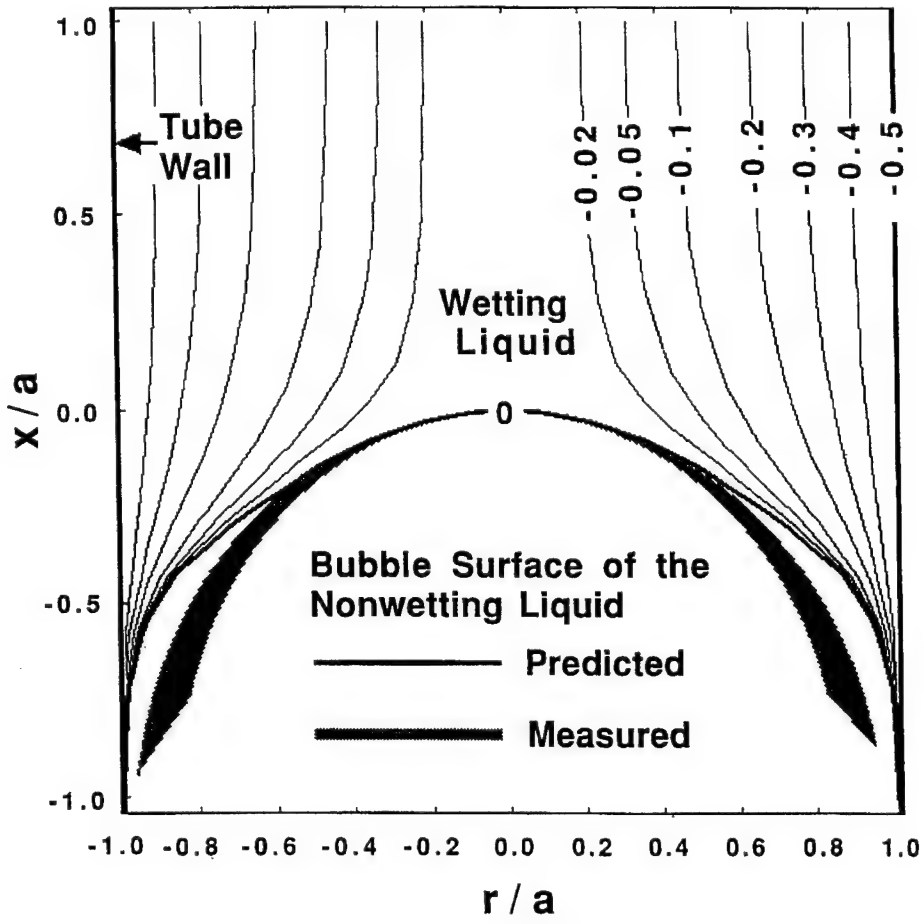

Figure 1. Contour plot of the stream function ψ (Equation (2)) as a function of r, the distance from the center of the tube, and x, the vertical coordinate measured from the tip of the bubble, using the coefficients $A_1 = 0.2516$, $A_2 = -0.0040$, and $A_3 = 0.0064$. $\psi = 0$ (thick line) indicates the calculated surface of the bubble, while the measured and scaled bubble (or drop) shapes fall into the shaded area.

The velocity of the nonwetting liquid bubble rising in a heavier wetting medium, or a liquid drop falling through a lighter medium is calculated using Bernoulli's equation for the wetting liquid (w) and the nonwetting bubble (nw) along the streamline separating the two fluids (indicated by '0' of Figure 1)

$$\text{(w)} \quad P_{\mathrm{w}} + \rho_{\mathrm{w}} g x + \frac{\rho_{\mathrm{w}} q_{\mathrm{w}}^2}{2} = C_{\mathrm{w}}, \tag{2a}$$

$$\text{(nw)} \quad P_{\mathrm{nw}} + \rho_{\mathrm{nw}} g x + \frac{\rho_{\mathrm{nw}} q_{\mathrm{nw}}^2}{2} = C_{\mathrm{nw}}, \tag{2b}$$

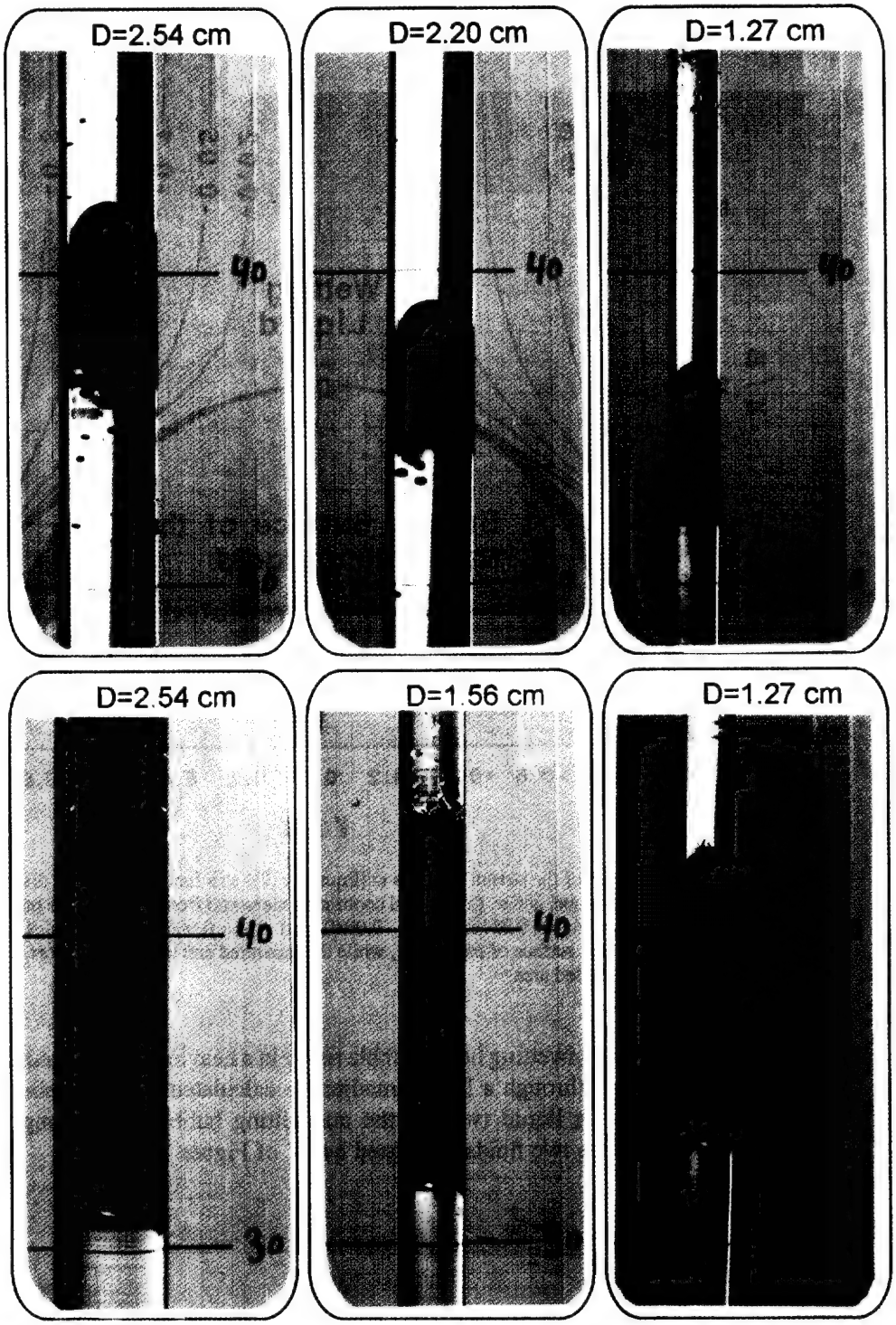

Figure 2. Oil bubbles in water (red, top of the figure) and water bubbles in the oil (gree-blue, bottom). In the smaller diameters (right) instability and distortions in the interface are smaller and occur further downstream from the bubble tip.

Table I. Nondimensional parameters of flow in closed tubes: Re: bubbles velocities, described in terms of Reynolds number; σ^*: the dimensionless surface-tension parameter; U^*: the dimensionless velocity.

System	Diameter (cm)	Re	σ^*	U^*
Glass-water-oil	1.27	296	0.435	0.214
	1.65	726	0.267	0.354
	2.20	1436	0.145	0.457
	2.54	1890	0.109	0.483
Acrylic-oil-water	0.60	0	1.947	0.000
	1.27	84	0.435	0.246
	1.56	169	0.287	0.363
	1.90	231	0.193	0.368
	2.54	426	0.109	0.441

where P is the pressure, q is the tangential liquid velocity along the surface of the bubble, g is the gravitational acceleration, ρ is the density, C is a constant, and x is measured along the vertical axis, positive upstream with zero at the bubble nose (Figure 1). Subtracting Equation (2b) from Equation (2a), imposing the boundary conditions at the bubble nose (i.e., $x = 0$ and $q = 0$), and using the surface tension, σ, to describe the pressure differences at the bubble nose, results in

$$\Delta\rho g x + \tfrac{1}{2}(\rho_{\mathrm{w}} q_{\mathrm{w}}^2 - \rho_{\mathrm{nw}} q_{\mathrm{nw}}^2) = \sigma(R^{-1} - R_0^{-1}), \tag{3}$$

where $\Delta\rho$ is the positive density difference of the two immiscible liquids, R^{-1} is the curvature of the slug surface, and R_0^{-1} the value of the curvature at the bubble nose. (Note that we used $C_{\mathrm{nw}} - C_{\mathrm{w}} = 2\sigma/R_0$ in Equation (3), resulting from Equations (2a) and (2b) applied at the stagnation point, $x = q = 0$.) As long as no significant circulation is created within the liquid bubble by the outside liquid then $q_{\mathrm{nw}} \cong 0$ (we could just as easily have considered the other limiting case when $q_{\mathrm{nw}} \cong q_{\mathrm{w}}$, however anticipating our experimental results we found that $q_{\mathrm{nw}} \cong 0$, and we limit our theory to this case). By introducing the coefficients that were already calculated by Tung and Parlange (1976), Equation (3) can be written in the form

$$\frac{\rho_{\mathrm{w}} U^2}{\Delta\rho g a} = 0.272 - 0.472\frac{\sigma}{\Delta\rho g a^2}, \tag{4}$$

which describes the velocity at which a bubble rises or a drop falls. Interestingly it shows exactly the same nondimensional parameters as used previously by Zukoski (1966), based on his experimental observations.

3. Materials and Methods

Tests were carried out with two immiscible liquids, water and oil (Soltrol 220), and two types of tubes (glass and acrylic). Tubes were 100 cm long and varied in inside diameter from 0.6 to 2.54 cm (Table I).

Initial experiments showed that in an oil-water system, the water wetted preferentially the glass and the Soltrol wetted preferentially the acrylic. Bubbles and drops were formed by a sudden overturn of the tubes. In some cases flexible tubes with shutoff valves were used to store the heavier liquid at the top or the light liquid on the bottom, and bubbles or drops were initiated after the valve was opened. To view the bubbles/drops the wetting fluid was kept transparent and the nonwetting fluid was colored. Blue dye FD&C #1 was used for water in the acrylic and Sudan IV (red) for Soltrol in the glass tubes. Most consistent bubbles and drops were formed when tubes were partly filled (80–90 %) by the wetting liquid first, and completed with the nonwetting liquid. If the nonwetting liquid occupied most of the tube the wetting liquid moved erratically along the walls, probably because the nonwetting liquid left some smear along the walls.

Bubble/drop velocity was obtained by measuring the time required for the bubble/drop to move 30 cm. Pictures of the bubbles/drops in different diameter tubes were taken (Figure 2) in order to obtain the shapes of the bubbles and drops. The pictures were scanned into a graphic software and were scaled to the same size by overlapping the lines of the tube walls.

Soltrol-water surface tension was 32.84 dyne cm^{-1} measured with a Model 21 Fisher Surface Tensiomate. The Soltrol viscosity was 3.64 centipoise [gr cm^{-1} sec^{-1}] based on data supplied by Phillips Chemicals Company data.

4. Results and Discussion

Bubbles/drops formed in the glass and acrylic tubes with different diameters are shown in Figure 2. In all cases, the wetting fluid flowed along the wall and the nonwetting fluid in the center. Thus the oil moved upward as a bubble in the glass tube (Figures 2a, b, c) and the water moved downward as a drop in the acrylic tube (Figures 2d, e, f). The experimental bubble/drop nose shapes, compared to the predicted shape (Figure 1), indicate that the zero stream line prediction (Equation (1)) is accurate for $r < a/2$, and diverges increasingly from the actual shape as r increases, in agreement with Tung and Parlange (1976). We also found, in agreement with Zukoski (1966), that: (a) bubble length and initiation method did not affect the bubble velocity, which was measured with standard deviations of less than 5% (see also Figure 3), and (b) an instability in the two liquids interface was observed mainly for the large diameter tubes (Figure 2, left) for both the oil bubble in water and the water drop in the oil. The instability did not affect the velocity as long as large-amplitude waves were restricted to positions at least one tube radius

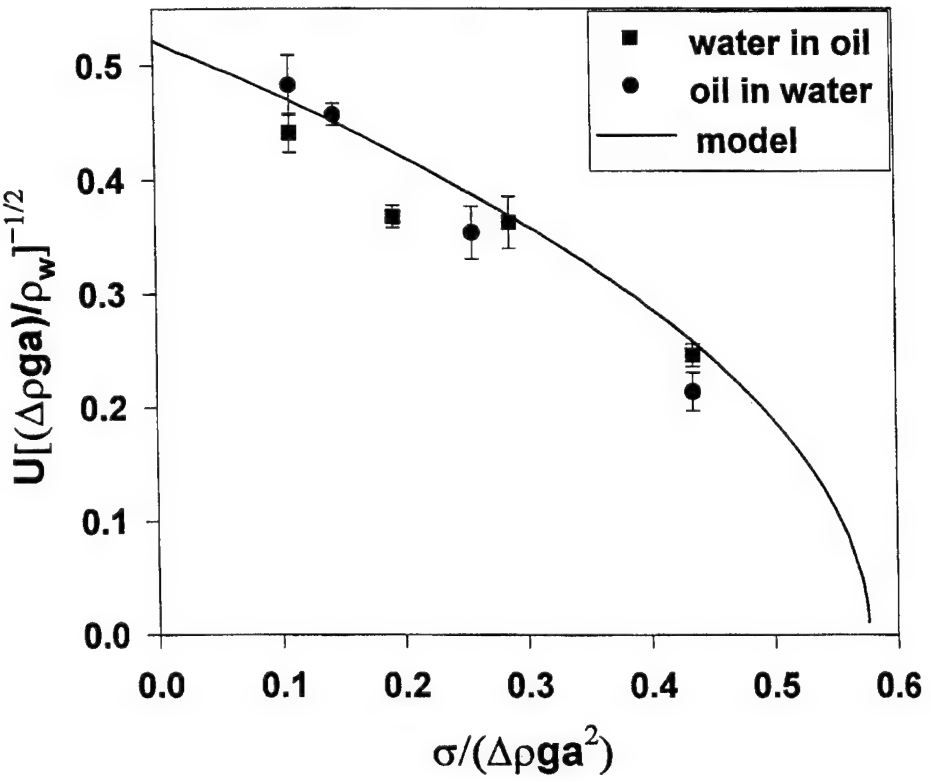

Figure 3. Dimensionless velocities, U^*, and standard deviations as a function of the dimensionless surface-tension parameter, σ^*, compared with the predicted velocity model (Equation (3)).

downstream of the bubble nose. With the smaller diameter the distortions were smaller and occurred further downstream from the tip.

The bubble/drop velocities, described in terms of Reynolds number, Re, the dimensionless velocity, U^*, and the dimensionless surface-tension parameter, σ^*, are given by

$$\mathrm{Re} = \frac{Ua\rho_w}{\mu_w}, \qquad U^* = U\left[\frac{\Delta\rho}{\rho_w}ga\right]^{-(1/2)}, \qquad \sigma^* = \frac{\sigma}{\Delta\rho g a^2}, \tag{5}$$

and shown in Table I. U^* was plotted as a function of σ^* and compared with the predicted velocity model (Equation (4)) in Figure 3. The good agreement between the predicted and measured results indicates that (a) the wall-liquids wetting relationship determines whether a bubble or a drop will be formed, but while formed, it does not affect its velocity, and (b) the assumption of no movement inside the bubble/drop is indeed the preferred assumption for modeling purposes. This assumption was also confirmed by tiny [< 0.25 mm] dust particles floating inside the bubble/drop, allowing us to observe that no significant circulation is

created within the liquid bubble by the outside liquid. The model predicted no movement of the bubble for $\sigma^* \cong 0.57$ which corresponds to $a \cong 0.55$ cm for our liquids, and indeed, no movement of the water bubble in the oil was observed in tubes with a < 0.55 cm.

There are many other experiments, mainly of gas bubbles in liquid, which could be added to Figure 3 (Zukoski, 1966; Fabre and Liné, 1992). However, none involve oil/water, which is of interest here, and the case of gas bubbles is already known to satisfy Equation (4) for that particular case with the same accuracy as shown in the present figure (Tung and Parlange, 1976). Thus, these earlier experiments would add nothing useful.

5. Applications to Porous Media

It is of interest to investigate how the model for single tubes applies to a porous media and provides some qualitative insight to the observed flow patterns. As in the single tube experiments we performed a series of experiments with two immiscible fluids, and hydrophobic and hydrophilic solid phases.

The porous medium consisted of 0.8–1.2 mm glass beads. Glass is hydrophilic. The glass beads were made hydrophobic by spraying them with Silicon lubricant spray. The beads were packed in two two-dimensional chambers ($27 \times 27 \times 1$ cm). One chamber had glass walls and held the glass beads. The other chamber was made of acrylic and contained the hydrophobic beads.

Each chamber was saturated with either oil or water (always noncolored). After placing the chamber horizontally, the invading liquid was injected in the center of the chamber at a rate of 1 cm^3/min. The invading liquid was colored with FD&C blue #1 for the water and Sudan red IV for the Soltrol. The resident fluid leaves the chamber through six outlets at the edge of the chamber. Photographs of the invading liquid were taken at intervals ranging from 2 to 5 min.

The two cases where water displaced the oil are presented in Figures 4a and 4b. In Figure 4a, the medium was hydrophilic resulting in a smooth front for the intruding water. In Figure 4b, the medium was hydrophobic and the water which is nonwetting forms a finger-like front. Oil displacing water in a hydrophobic medium resulted in a similar pattern as the smooth front in Figure 4a and oil displacing water in a hydrophilic media gave a finger structure as shown in Figure 4b. When water was injected in Soltrol in the hydrophilic medium only 15% of the pore space was filled with oil. When water was injected into oil in the hydrophobic medium at least 90% was filled with oil. Clearly a continuous smooth invading front is more efficient at removing the resident fluid.

If we calculate the tube diameter for which the flow is zero, from Equation (4), we find that this is approximately 5 mm. The smallest finger width observed is exactly of the same order. This is well above the pore size of our porous media with the Soltrol-water system. Thus, nonwetting fluid in different pores reconnect to form pathways of a size of around 6 mm or more, i.e., independently of the pore

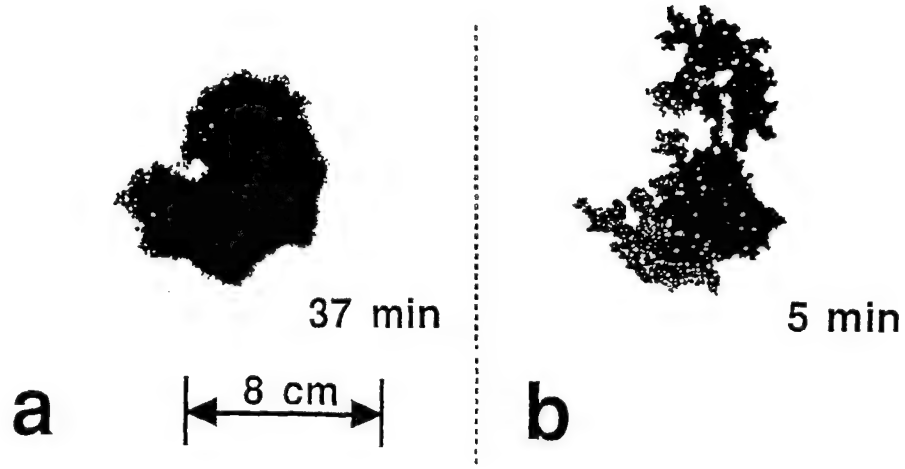

Figure 4. Prints of the colored fractions formed by injecting a constant flux of colored water to the oil saturated chamber, using two types of porous medium: (a) hydrophilic, (b) hydrophobic. The numbers indicate the time (min) elapsed from the beginning of the injection.

size distribution. However, it is also clear that the exact shape and dimension of the invading fingers is affected by the pore distribution, so that the 6 mm prediction is only a semiquantitative prediction, which should be very useful, for instance, to estimate the surface of contact between the two fluids when the intruding fluid is nonwetting.

After lifting the chamber the fluids always moved readily. Fluid movement eventually stopped after it had reached the configuration similar to the one shown in Figure 5. Observe that the width, i.e., the smaller characteristic dimension of all ganglia is less than 6 mm (only two near the top of Figure 5 are even close to 6 mm). Both results are consistent with flow in a single tube. During imbibition the flow requirement imposes that the pathway be larger than 6 mm. After drainage stops the dimension of the ganglia in the direction perpendicular to the flow must be less than 6 mm. As drainage proceeds the exact size of the ganglia left behind will depend on the connections between the entrapped fluid and the main pathway. This point was made before, e.g., see the excellent discussion by Powers et al. (1992). Here we suggest in addition that ganglia have a maximum size. It is interesting that ganglia formation and movement has been discussed in the past (e.g., see Payatakes and Dias (1984) or Adler and Brenner (1988)) but not in relation to pathway dimensions as discussed here.

Thus it seems that the minimum size for movement in the single tube experiment provides some indication of the order of magnitude of the width of pathways and maximum size ganglia in a porous medium left by drainage and minimum finger size during imbibition, which will normally be greater than the pore size. Experiments are currently underway to examine the effects of surfactants on this ganglion and

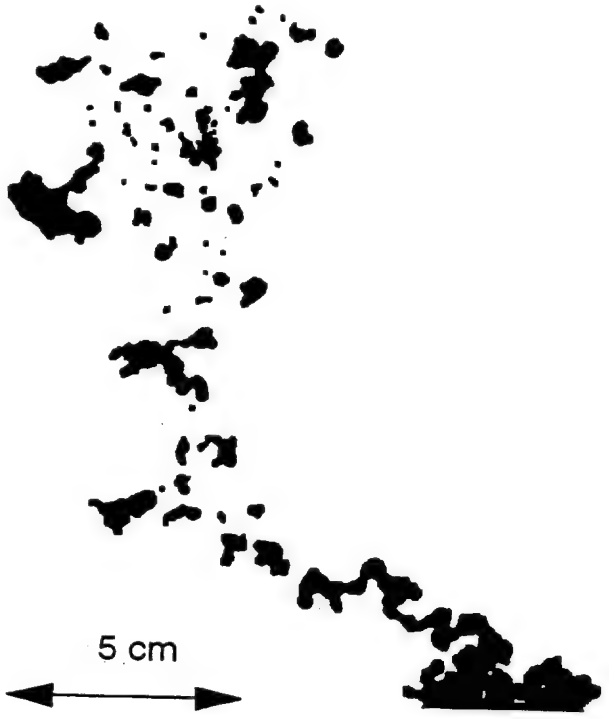

Figure 5. Trapped water in the hydrophobic porous material. Picture was taken after the chamber from Figure 1b was placed in a vertical position and allowed to drain.

pathway width, to check whether Equation (4) still holds, and quantify the effect of surfactant in promoting soil remediation.

6. Conclusions

Based on the study of wetting and nonwetting liquids motion in tubes, we expect more efficient displacement when the wetting liquid displaces the nonwetting liquid in a porous medium. Smooth wetting fronts are expected if the displacing liquid is the preferentially wetting liquid. Finger-like shapes with a width larger than a characteristic length are observed if the displacing liquid is nonwetting. Finally, lumps of the nonwetting fluid having a width smaller than the same characteristic length can be readily entrapped in the porous medium when gravity alone is the cause of motion. The characteristic length in both cases is given by $[\sigma/\Delta\rho g\sigma^*]^{1/2}$.

References

Adler, P. M. and Brenner, H.: 1988, Multiphase flow in porous media, *Ann. Rev. Fluid Mech.* **20**, 35–59.

Bear, J. and Bachmat, Y.: 1990, *Introduction to Modeling of Transport Phenomena in Porous Media*, Kluwer Acad. Publ., Dordrecht, The Netherlands.

Bendiksen, K. H.: 1985, On the motion of long bubbles in vertical tubes, *Int. J. Multiphase Flow* **11** 797–812.

Davies, R. M. and Taylor, G. I.: 1950, The mechanics of large bubbles rising through extended liquids and through liquids in tubes, *Proc. Roy. Soc. London A* **200**, 375–390.

DOE,: 1995, Closing the circle on splitting the atom: The environmental legacy of nuclear weapons production in the United States and what DOE is doing about it, The U.S. Department of Energy, Office of Strategic Planning and Analysis, Washington, DC.

Dumitrescu, D. T.: 1943, Strömung an einer Luftblase in senkrechten Rohr, *Z. Angew. Math. Mech* **23**, 139–149.

Fabre, J. and Liné, A.: 1992, Modeling of two-phase slug flow, *Ann. Rev. Fluid Mech.* **24**, 21–46.

Garabedian, P. R.: 1957, On steady-state bubbles generated by Taylor instability, *Proc. Roy. Soc. London A* **241**, 423–431.

Payatakes, A. C. and Dias, M. M.: 1984, Immiscible microdisplacement and ganglion dynamics in porous media, *Rev, Chem. Eng.* **2**, 85–174.

Powers, S. E., Abriola, L. M. and Weber, J. W.: 1992, An experimental investigation of nonaqueous phase liquid dissolution in saturated subsurface systems: Steady state mass transfer rates, *Water Resour. Res.* **28**, 2691–2705.

Tung, K. W. and Parlange, J.-Y.: 1976, Note on the motion of long bubbles in closed tubes-influence of surface tension, *Acta Mech.* **24**, 313–317.

Wilkins, M. D., Abriola, L. M. and Pennel, K. D.: 1995, An experimental investigation of rate-limited nonaqueous phase liquid volatilization in unsaturated porous media: Steady state mass transfer, *Water Resour. Res.* **31**, 2159–2172.

Zukoski, E. E.: 1966, Influence of viscosity, surface tension and inclination angle on motion of long bubbles in closed tubes, *J. Fluid Mech.* **20**, 821–837.

APPENDIX F

PREFERENTIAL FLOW IN WATER REPELLENT SOILS

T.W.J. Bauters, D.A. DiCarlo, T.S. Steenhuis, and J.-Y. Parlange

Submitted to Soil Science Society of America Journal

PREFERENTIAL FLOW IN WATER REPELLENT SOILS

Tim W.J. Bauters, David A. DiCarlo, Tammo S. Steenhuis and Jean-Yves Parlange

Department of Agricultural and Biological Engineering

Cornell University, Ithaca, NY 14853

Abstract

Predicting the occurrence of preferential flow is crucial as preferential flow causes faster downward movement of water and solutes, which may result in groundwater contamination. The effects of water repellency on preferential flow were studied by varying the silane coating on a silica sand. Uniform rain on the non-coated substrate resulted in a stable wetting front and no preferential flow, while the coated sands produced an unstable wetting front and preferential flow. The occurrence of preferential flow was directly linked with the soil's water repellency, and its pressure-saturation relationship. In addition, the front velocity and the water entry pressure increased linearly with a higher degree of water repellency of the sand.

Introduction

Soils which have hydrophobic properties (also called water repellent soils), can resist or retard surface water infiltration (Brandt, 1969). This affects plant growth and surface water distribution. These soils can be found in Florida, Arizona and California (DeBano, 1969), as well as abroad, in New Zealand, England, Australia (Bond, 1969) and the Netherlands (Hendrickx et al., 1988; Dekker and Ritsema, 1994). Water repellent soils may be more prevalent than is commonly acknowledged (Bond, 1964; Gilmour,1968; DeBano, 1969; Marshall and Holmes, 1979; Nakaya, 1982; Dekker and Ritsema, 1996). Some researchers suggest that repellency is the norm rather than the exception (Dekker, 1988; Dekker and Jungerius, 1990; Wallis and Horne, 1992). The degree of repellency may vary between soils.

Besides the retardation or resistance of surface water infiltration, water repellent soils have been associated with preferential flow paths (Jamison, 1945; Bond, 1964; Gilmour, 1968). Preferential flow paths create spatial variability in soil moisture affecting plant growth and surface distribution (Dekker and Ritsema, 1994). In addition, preferential flow allows much faster transport of water and solutes, thus creating greater potential for groundwater contamination.

In this paper, the effects of water repellency on preferential flow by varying the silane coating on a silica sand is systematically studied. Uniform rain on the non-coated substrate resulted in a stable wetting front and no preferential flow, while the coated sands produced an unstable wetting front and preferential flow. A direct link between the soil's water repellency, its pressure-saturation relationship, and the occurrence of preferential flow was found.

Materials and Methods

Blasting silica sand (W.F. Saunders & Sons, Inc.) was used as the substrate to analyze the effect of repellency. Table 1 shows the screen analysis for this sand. Different degrees of water repellency were added to the sand through the following procedure. An ethanol solution containing 5% octadecyltrichlorasilane (100 ml OTS (Fisher Scientific) in 2 liter ethanol) was mixed for 5 hours with 25 kg of blasting sand which produced an extremely water repellent sand after drying (Bradford and Leij, 1996). A basis sand batch was made by mixing 3 kg of the extremely repellent sand with 45 kg regular non-repellent sand. This basis sand was than diluted with regular sand to achieve different degrees of repellencies (Table 2). The most repellent sand tested was achieved by mixing the undiluted repellent sand with 10 kg of regular sand. In Table 2, the first number in the notation for the batches refers to the amount, in kg, used of the basis repellent sand (except for the most repellent sand) and the second number refers to the amount, in kg, of the regular sand. The degree of repellency defines the amount of highly repellent sand (the sand that was mixed with OTS in an ethanol solution) versus the total amount of sand used.

Besides the ratio of repellent to non-repellent sand, the water drop penetration time (WDPT) was used to quantify the degree of repellency. The WDPT test consists of randomly applying a single water drop (0.05 ml) onto the sand surface and measuring the amount of time (in seconds) it takes to infiltrate the soil (Letey, 1969). The WDPT for the different batches is shown in Table 2 (Letey, 1969; King, 1981.)

A polycarbonate slab chamber was built to observe and quantify the preferential flow phenomena (see Figure 1). The interior dimensions of the chamber were 42 cm wide, 61 cm tall and 0.8 cm thick with 1 cm polycarbonate walls. Seven high speed tensiometers, to measure water pressures, were threaded into the chamber at a height of 32 cm and 6 cm horizontal spacing. Each tensiometer consisted of a flat stainless porous plate (0.8 cm diameter, 2 micrometer pore size) sealed in a hollow brass housing (Selker et al., 1992a). The tensiometers were inserted so the porous plate was flush with the inside of the chamber, to minimize their effect on packing and fluid flow. Each tensiometer was filled with de-gassed water and attached through a stiff nylon tube and a three-way valve to a pressure transducer and a vertical water tube. By turning the valve the transducer could be connected to the vertical tube for calibration, or to the tensiometer for measurement. The output of the transducers was read by a data acquisition system, consisting of a personal computer with a DAS-800 card (Keithley Metrabyte), and a multiplexer to process in total 16 incoming channels.

The chamber was filled under a hopper with three randomizing screens (Glass et al., 1989a). Before every filling, an extension of 15 cm was put on top of the chamber to remove the always poorly packed top section and to also achieve an homogenous packing in the chamber.

Using this chamber, the soil characteristic curves were determined for all the sands. The drying curves were obtained through the following procedure. A peristaltic pump pumped the water in at 0.4 cm/min until the water reached a height of 45 cm. After pausing for 30 minutes, the chamber was drained by pumping the water out at 0.4 cm/min until the water fringe reached a height of 7 cm. After 24 hours, the front panel of the chamber was removed and the sand column was

segmented in 1 cm levels. Each segment was weighed, dried for 24 hours at 105° C, and weighed again. This procedure was practiced on the left and right side of the chamber, which resulted in 2 drying curves per experiment, those two where then averaged to obtain the drying curve. The wetting curves were also determined in the chamber; a constant head was connected to the bottom of the chamber and left connected for 24 hours till equilibrium was reached. The chamber was again taken apart to section the sand and determine the water saturation.

For infiltrations, the packed chamber was placed in front of a fluorescent light bank and the tensiometers were attached to the data acquisition system. As wet sand transmits more light than dry sand (Glass et al., 1989b), light transmission was used to observe the position and velocity of the wetting front. The experiments were recorded by a black and white camera (Panasonic, TV Camera WV 1850) and a video cassette recorder (Panasonic AG 6720). The recorded experiments were than digitized with a frame grabber from Data Translations and analyzed with Global Labs Imaging software.

The water application system consisted of a peristaltic pump driven point source which was translated back and forth across the soil surface by a rotating cam shaft. To eliminate the possible flow down the side edges of the chamber, gutters were installed to prevent rain from impacting within 2 cm of the chamber edges. Infiltrations were conducted with an irrigation rate of 0.16 cm/min. Experiments with infiltration rates between 0.058 cm/min and 0.19 cm/min all produced similar results.

Results

Figure 2 shows the averaged drying soil characteristic (or pressure-saturation) curves for the five different sands. The curves were very similar over most of the range of water contents with statistical differences (curves more than 2 standard deviations apart) only for water saturations between 10-40 %. In this region, the more repellent the sand the less water it holds at a particular negative pressure.

Figure 3 shows the averaged wetting soil characteristic (or pressure-saturation) curves for the five different sands. As opposed to the drying curves, the wetting curves varied much more with the degree of water repellency, with two types of differences between the curves. First, the water entry pressures increased with the degree of repellency. Second, the slope of the repellent curves was flatter than that from the pure sand. For the repellent sands the actual wetting slope may be slightly sharper than that measured. By sectioning the chamber every centimeter, we may have taken a chunk of wet sand and a chunk of dry sand at the same time. Thus, an abrupt wetting front in the water repellent sands will still appear as having a minimum slope.

Major differences between the different water repellent sands were observed when water was infiltrated into the sands. For the non-water repellent sand, the water moved downward in a uniform stable front, while for the repellent sands, the water moved downward in preferential flow paths. In the higher repellent sand the water ponded before it moved downwards in the fingers. To gain insight into this phenomena, we measured front velocity, front width (for finger flow), and water pressures within the front.

Figure 4 shows the time series of the pressure at the tensiometers as the wetting front passed in the non-water repellent sand. The front hit the tensiometer at T=3259 sec, and the pressure at the front reached -11.8 cm. Pressures before the front were meaningless as the sand is air dry and there is no connection to the water in the soil. Behind the front the pressure remained -11 cm. Once the infiltration was stopped, the pressure decreased till -26 cm and gradually went till -30 cm.

Figure 5 shows the equivalent time series of the pressure in the 5.6 % water repellent sand. The front hit the tensiometer at T= 2199 sec, and the pressure at the front reached 3.6 cm. Immediately behind the front, the pressure quickly began decreasing before settling at -12 cm. Once the infiltration was stopped, the pressure further decreased till -27 cm and gradually moved till -30 cm. This post infiltration pressure decrease drops at a rate which was much higher than in regular sand.

Figure 6 depicts the measured water pressure at the wetting front (error bars indicate the standard deviations) versus % repellency of the sand. The water entry values measured from the static wetting curves are also shown. These pressures are seen to be closely related, and both clearly increased with the degree of repellency. This increase was roughly linear, as a linear regression resulted in $R^2 = 91$ and 97% for the wetting front pressures and water entry values, respectively. A positive water entry pressure was required when the degree of repellency rose above 5%, which implied a ponding layer on top of the sand grains. This ponding was also related to the WDPT test. The WDPT for those 5% repellent sands was > 600 sec, consequently there was positive

entry pressure necessary for infiltration, thus we might expect that a water droplet of a couple of mm high would never penetrate the repellent sand grains.

Figure 7 gives the finger velocity versus % repellency and the fitted linear regression line (error bars indicate the standard deviation of the measured points). The finger velocity was measured, starting 5 cm below the sand surface and stopped 5 cm before reaching the bottom. The finger velocity increased linearly with the degree of repellency ($R^2 = 98\%$.)

Figure 8 depicts the observed front width at the wetting front versus % repellency. The error bars indicate the standard deviations. The finger width was measured in 5 cm intervals starting at the distribution layerBecause the wetting front for the non-repellent sand is uniform, the width was not depicted. Widths at the wetting front for the various degrees of repellencies, except the highest one; were found to be around 3 cm. The width for the highest degree of repellency was 5.8 cm or nearly double the width compared to the other front widths.

Discussion

In this section, we will discuss how different degrees of repellency affected the wetting and drying pressure-saturation curves and, in turn, how these curves can be related to the observed infiltration properties. Ideally, this should give us an insight in the likelihood of preferential flow in soils from the observed degree of wettability, or non-wettability.

Repellency affects the wetting pressure-saturation curves of the soil much more than the drying

pressure-saturation curves (Figure's 2 & 3). The similarities in the drying curves imply that once the soil grains are wetted, the soil acts like a normal non-repellent soil. Only when the soil is drained to less than 40 % saturation does the water start leaving some portions of the soil drier and, thus, the repellency starts affecting the water retention. Conversely, on the initial wetting, the soil begins dry and the water repellency reaches its full effect. Thus, the greater the water repellency the greater the hysteresis in the soil's pressure-saturation relationship.

Importantly, we find that these drying and wetting pressure-saturation relationships can be related to the fingering properties. First of all, Figure 3 and Table 3 show that the water entry pressures measured from the wetting curve match the water pressure observed from the tensiometers directly behind the infiltrating front. The behavior of the infiltrations differ from this point, depending on the repellency of the soil. For the non-water repellent soil, the wetting front is uniform and stable, and Figure 4 shows that the pressure behind the front remains the initial wetting pressure. This implies that the water at all positions behind the front is driven by a unit gradient, and that the conductivity equals the downward flux. Thus, in the case of an uniform wetting front, the soil *wets* to the water content such that the unsaturated conductivity $K(\theta)$ equals the downward flux.

For the water repellent soil, the wetting front is unstable, and Figure 5 shows that the pressure at the tip is quickly dropping from the initial wetting pressure. This drop in pressure for unstable fronts was first elucidated by Raats (1973). The final pressure behind the wetting front is seen to be roughly the pressure at the knee in the drying curve. Thus, in the case of the unstable wetting front, the soil ***dries*** to the water content such that the unsaturated conductivity $K(\theta)$ equals the

downward flux. Since the flow is through preferential paths, the flux in each wetting path is greater than the overall applied flux. Interestingly, the water pressure behind the unstable front is less than the water pressure behind the stable front, even though the soil behind the unstable front is exhibiting a higher conductivity (and is likely to be more saturated) than the soil behind the stable front.

Clearly, the pressures inside the infiltrating fronts can be directly related to the measured pressure-saturation curves for each soil. These curves can also be related to the stability of the wetting front, the velocity of the fingers, and the width of the wetting front.

The finger velocity increases linearly with the degree of repellency of the sand. This is, at first, contradictory: the higher the repellency, the more the sand resists the infiltration of water. A simple argument on how repellency enhances fingering is given as follows. Previously, Weitz et al. (1987) have found that the velocity of the fluid/fluid interface (the water front in this case) increases with the pressure drop at the interface. For our case, as the sand is more repellent, a higher water pressure must be reached before water can enter it. But once water enters the sand and coats the grains all the sands have more or less the same drying properties. The flow then proceeds normally (same conductivity and P-S relationship) and, thus, the major pressure drop is taken up at the interface and the front velocity is higher. Finger velocity is important, as for a constant flux, the greater the velocity the fewer the fingers. Also, Selker et al. (1992b) have shown that the saturation profile within the finger can be related to the finger velocity and soil conductivity.

The stability of the wetting front for different repellencies can be understood heuristically as follows. Since Saffman and Taylor (1958), it has been known that for gravity-driven displacements, the front is unstable whenever the flux is less than the soil's unsaturated conductivity:

$$q < K(\theta) \tag{1}$$

When the wetting pressure-saturation curve has little or no slope (the repellent sands), the wetting front is very abrupt and directly behind it the saturation is very high. This leads to a high conductivity and the instability criterion is satisfied. However, when the wetting pressure-saturation curve has an appreciable slope (the non-repellent sand), the wetting front is not as abrupt and directly behind it there is a range of saturations. Thus we observe a situation where the soil wets only to a saturation such that the conductivity equals the flux, and the instability criterion is not satisfied.

The slope of the wetting curve has been more quantitatively related to the finger width (and, in turn, front stability) by Liu et al. (1994) through:

$$d \cong \frac{2\pi\theta_f\left(\frac{dh}{d\theta}\right)}{\eta + 1.5}, \tag{2}$$

where: $d =$ finger width

$\theta_f =$ the moisture content at the fingertip

$\left(\frac{dh}{d\theta}\right)$ = the slope of the soil moisture characteristic curve

η = is the exponent in the Brooks and Corey (1964) conductivity saturation relationship:

$$\eta = \frac{2}{\lambda} + 3 \qquad (3)$$

with λ a positive index related to the pore size distribution of the soil.

This predicts that the flatter the main wetting curve, the smaller the finger and the increased likelihood of instability. This trend is replicated in our data. Table 4 shows the measured front width versus the predicted front width (with n= 3.3 and $\theta_f = 100$). These predictions do not match the measured finger widths very well. This might be due to the extreme small slope of the wetting curve. As mentioned earlier, the wetting curves were determined by sectioning every centimeter, which might be large to accurately define the wetting front. Nevertheless, the following trend can still be deducted: repellent sands, which finger, have wetting curves much flatter than the non-repellent sands, which do not finger. The large finger width for the most repellent sand contradicts the trend, however, the observed finger was possibly two smaller fingers traveling together as the wet portion of the tip was observed to be splitting into two. However, the finger reached the bottom before anything further could be noticed.

In summary, we have shown that by making identical soils water repellent, unstable water fronts and preferential flow patterns are created where none existed before. Water repellency directly affects the soil's pressure-saturation relationship, and these changes are represented in the preferential flow characteristics. Finger velocity and water entry pressure are both linearly related to the water repellency of the sand, but the finger widths show a less definitive trend. This implies

for field soils, that water repellency, or lack thereof, plays a controlling roll in the creation of preferential flow, and groundwater pollution such as was shown already experimentally by Hendrickx et al. (1993.)

Figure captions

Figure 1: A schematic of the experimental chamber. Water was infiltrated from a cam-driven point source at the top. Pressure readings were made by the row of seven tensiometers.

Figure 2: The averaged drying curves for identical sands with different degrees of repellency. The drying curves statistically differ only between 10-40% saturation. The arrow indicates the trend for the more repellent sands.

Figure 3: The averaged wetting curves for identical sands with different degrees of repellency.

Figure 4: A time series of the measured tensiometer pressure in regular sand.

Figure 5: A time series of the measured tensiometer pressure in 5.6% water repellent sand. Notice the sharp drop in pressure after the finger hit the tensiometer, this is the typical property for unstable wetting fronts (Raats, 1973.)

Figure 6: The water entry pressure obtained from the wetting pressure-saturation curves and the tensiometer readings directly behind the front versus % repellency. The error bars indicate the standard deviation for the tensiometer measurements. The line is a linear regression on the tensiometer measurements and has a R^2 of 91%.

Figure 7: The front velocity is depicted versus the % water repellency. The error bars indicate the standard deviations. The line is a linear regression and has a R^2 of 98%.

Figure 8: The finger widths versus % repellency. The error bars indicate the standard deviations.

References

Bond, R. D. 1964. The influence of the microflora on the physical properties of soils. Field studies on water repellent sands. Aust. J. Soil Res. 2:123-131.

Bond, R. D. 1969. The occurrence of water-repellent soils in Australia. Proc. Symp. Water Rep. Soils, Univ. Calif., Riverside. pp: 1-6.

Bradford, S.A., and F.J. Leij. 1996. Predicting two- and three-fluid capillary pressure-saturation relationships of porous media with fractional wettability. Water Resour. Res. 32(2):251-259.

Brandt, G.H. 1969. Water movement in hydrophobic soils. Proc. Symp. Water Rep. Soils, Univ. Calif., Riverside. pp: 91-115.

Brooks, R.H., and A.T. Corey. 1964. Hydraulic properties of porous media. Hydrology paper 3, Colorado St. Univ., Fort. Collins.

Debano, L.F. 1969. Observations on water-repellent soils in Western United States. Proc. Symp. Water Rep. Soils, Univ. Calif., Riverside. pp: 17-29.

Dekker, L.W. 1988. Verspreiding, oorzaken, gevolgen en verbeterings mogelijkheden van waterafstotende gronden in Nederland. Rep. 2046, Soil Survey Inst., Wageningen, Netherlands.

Dekker, L.W., and P.D. Jungerius. 1990. Water repellency in the dunes with special reference to the Netherlands. Catena Suppl. 18: 173-183.

Dekker, L.W., and C.J. Ritsema. 1994. How water moves in a water repellent sandy soil 1. Potential and actual repellency. Water Resour. Res. 30(9):2507-2517.

Dekker, L.W., and C.J. Ritsema. 1996. Preferential flow paths in a water repellent clay soil with grass cover. Water Resour. Res. 32(5):1239-1249.

Gilmour, D.A. 1968. Water repellence of soils related to surface dryness. Aust. Forestry 32:143-148.

Glass R.J., T. S. Steenhuis, and J.-Y. Parlange. 1989a. Wetting front instability 2. Experimental determination of relationships between system parameters and two-dimensional unstable flow field behavior in initially dry porous media. Water Resour. Res. 25(6):1195-1207.

Glass R.J., T. S. Steenhuis, and J.-Y. Parlange. 1989b. Mechanism for finger persistence in homogeneous, unsaturated, porous media: Theory and verification. Soil Science 148(1): 60-70.

Hendrickx, J.M.H., L.W. Dekker, E.J. van Zuilen, and O.H. Boersma. 1988. Water and solute movement through a water repellent sand soil with grasscover. In: Validation of Flow and Transport Models for the Unsaturated Zone, P.J. Wierenga and D. Bachelet, Editors. International Conference and Workshop Proceedings. Ruidoso, NM. May 23-26, 1988.pp. 131-146.

Hendrickx, J.M.H., L.W. Dekker, and O.H. Boersma. 1993. Unstable wetting fronts in water-repellent field soils. J. of Env. Qual. 22:109-118.

Jamison, V.C. 1945. The penetration of irrigation and rain water into sandy soil of Central Florida. Soil Sci. Soc. Amer. Proc. 10:25-29.

King, P.M. 1981. Comparison of methods for measuring severity of water repellence of sandy soils and assessment of some factors that affect its measurements. Aust. J. Soil Res. 19:275-285.

Letey, J. 1969. Measurement of contact angle, water drop penetration time, and critical surface tensions. Proc. Symp. Water Rep. Soils, Univ. Calif., Riverside. pp: 43-47

Liu, Y., Steenhuis, T.S., and J.-Y. Parlange. 1994. Closed form solution for finger width in sandy soils at different water contents. Water Resour. Res. 30:949-952.

Marshall, T.J., and J.W. Holmes. 1979. Soil Physics. Cambridge University Press, Cambridge.

Nakaya, N. 1982. Water repellency of soils. Min. Agr., For. and Fish., Japan. JARQ 16(1):24-28.

Raats, P.A.C. 1973 Unstable wetting fronts in uniform and nonuniform soils. Soil Sci. Soc. Amer. Proc. 37:681-685.

Saffman, P.G., and G. Taylor. 1958. The penetration of a fluid into a porous medium or Hele-Shaw cell containing a more viscous liquid. Proc. Royal Soc. London. A 245:312-331.

Selker, J.S., P. Leclerq, J.-Y. Parlange, and T.S. Steenhuis. 1992a. Fingered flow in two dimensions 1. Measurement of matric potential. Water Resour. Res. 28(9): 2513-2521.

Selker, J.S., T.S. Steenhuis, and J.-Y. Parlange. 1992b. Fingered flow in two dimensions 2. Predicting finger moisture profile. Water Resour. Res. 28(9):2523-2528.

Wallis, M.G., and D.J. Horne.1992. Soil water repellency. Adv. Soil. Science.20:91-146.

Weitz, D.A., J.P. Stokes, R.C. Ball, and A.P. Kushnick. 1987. Dynamic capillary pressure in porous media: Origin of the viscous-fingering length scale. Phys. Rev. Let. 59 (26):2967-2970.

Table 1: The screen analysis (by weight) of the blasting silica sand provided by manufacturer, W.F. Saunders & Sons Inc.

Screen (lines / inch)	% Retained	Cumulated
20	Trace	Trace
30	0.8	0.8
40	14.1	14.9
50	38.6	53.5
70	28.4	81.9
100	11.0	92.9
Through 100	7.1	100.0

1 Table 2: The WDPT for the different batches (Letey, 1969; and King, 1981.)

Water Repellent Ratios		**WDPT (Water Drop Penetration Time)**	
Batch type	% Water Repellency	WDPT	Description
Regular	0	<0.5	Wettable (<5 sec)
10+10	3.13%	40	Slightly water repellent (5-60 sec)
10+2.5	5.00%	2400	Severely water repellent (600-3600 sec)
6+0.6	5.60%	>3600	Extremely water repellent (>3600sec)
1+10	9.00%	>3600	Extremely water repellent (>3600sec)

Table 3: Water entry pressures measured with tensiometer and water entry values from the wetting curves.

% Water Repellency	Water Entry Pressure Data From The Fingertip (cm)		Water Entry Pressure Data From Wetting Curves (cm)
	data	standard deviation	
Regular	-9.3	1.3	-9.2
3.13%	-2.2	0.7	-3.0
5.00%	-1.5	1.0	-1.0
5.60%	3.6	NA	2.0
9.00%	5.6	0.9	5.0

1 Table 4: Measured versus predicted finger widths.

2

% Water Repellency	Measured Widths (cm)	Predicted Widths (cm)
Regular	NA	16.4
3.13%	2.1	3.6
5.00%	2.8	2.6
5.60%	2.7	3.1
9.00%	7.1	1.3

3

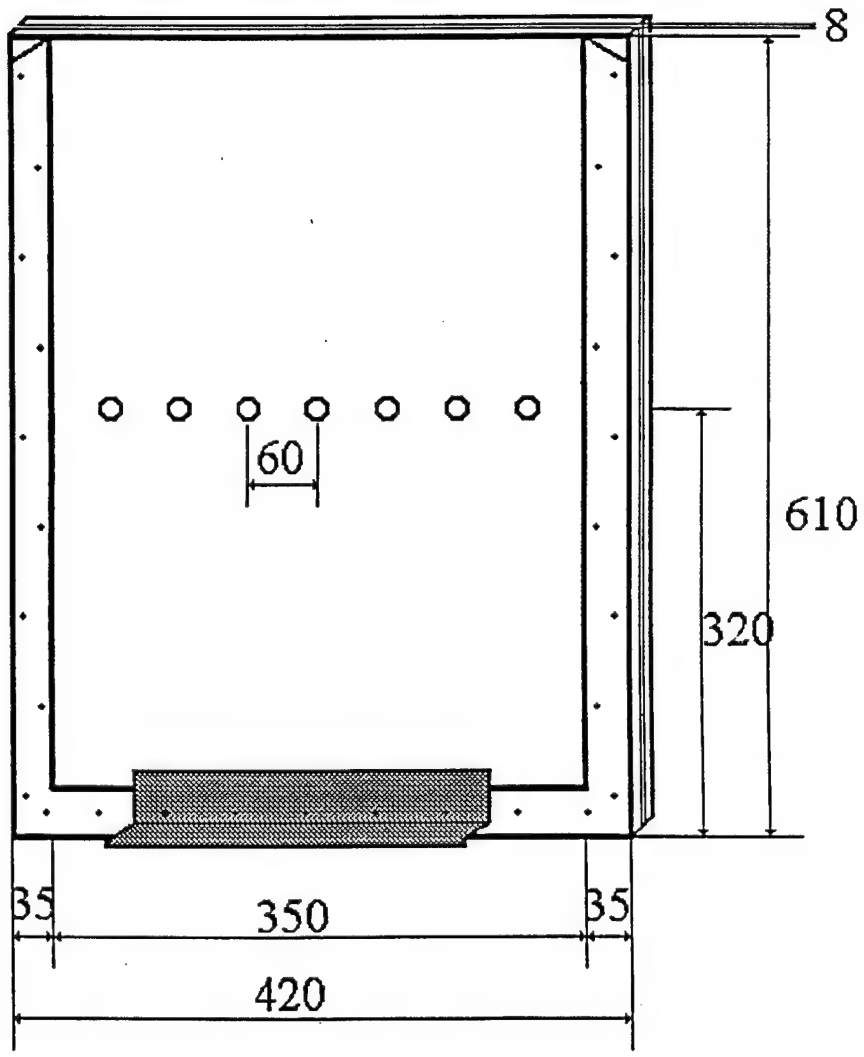

F.G. 1

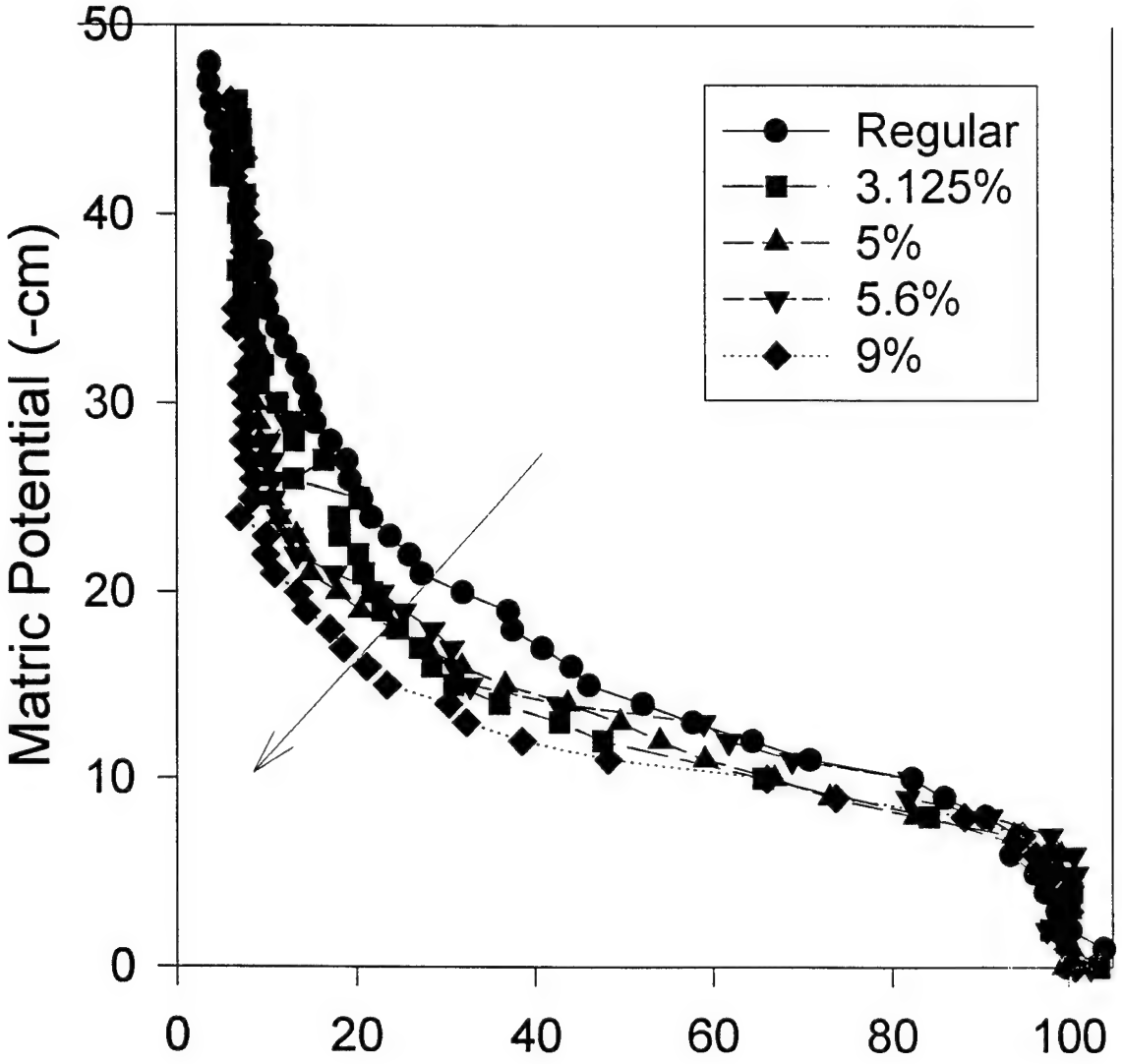
Matric Potential (-cm)
50
40
30
20
10
0
0
20
40
60
80
100
Regular
3.125%
5%
5.6%
9%

Fig 2.

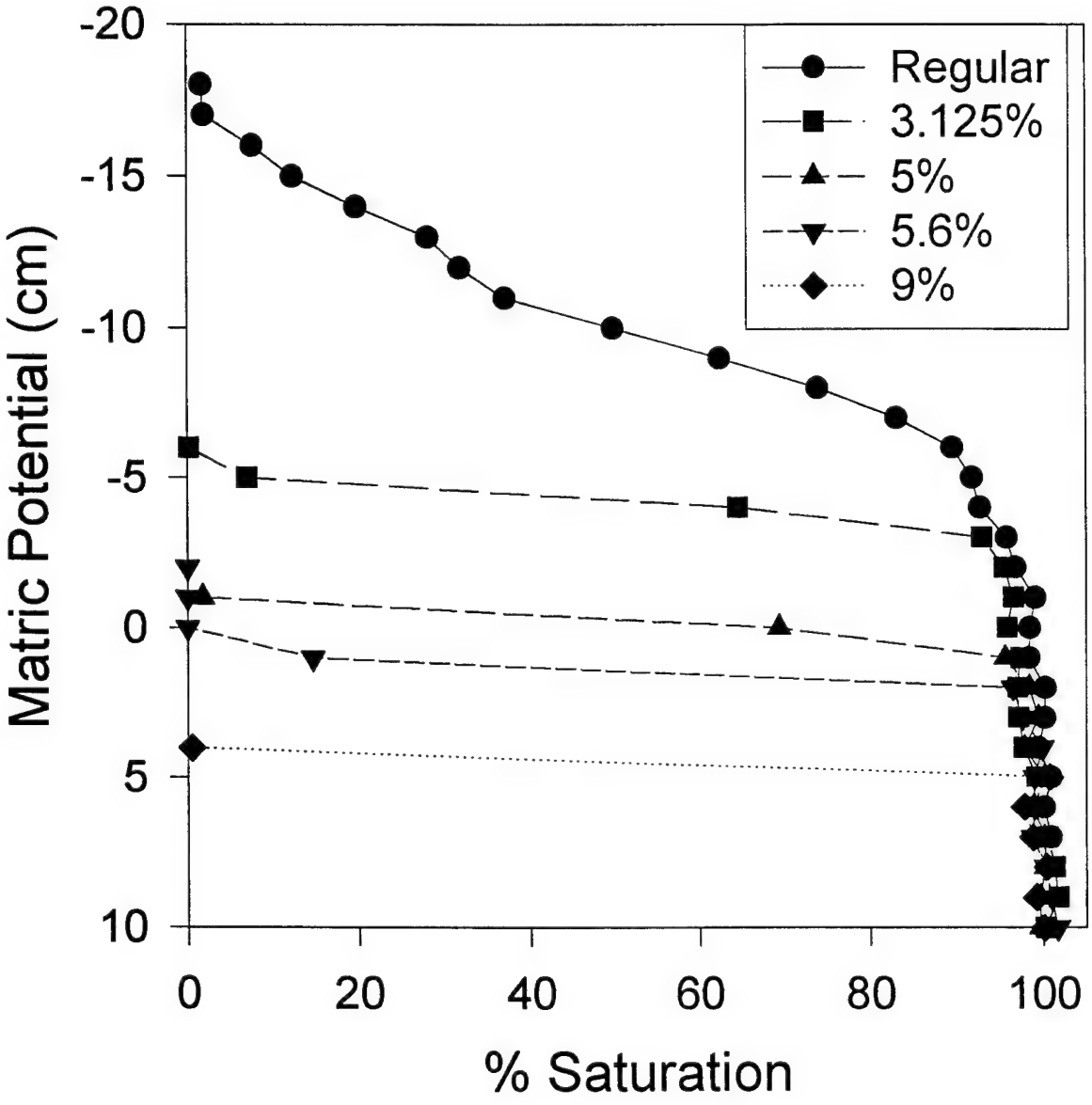
-20
-15
-10
-5
0
5
10
Matric Potential (cm)
0
20
40
60
80
100
% Saturation
Regular
3.125%
5%
5.6%
9%

Fig. 3

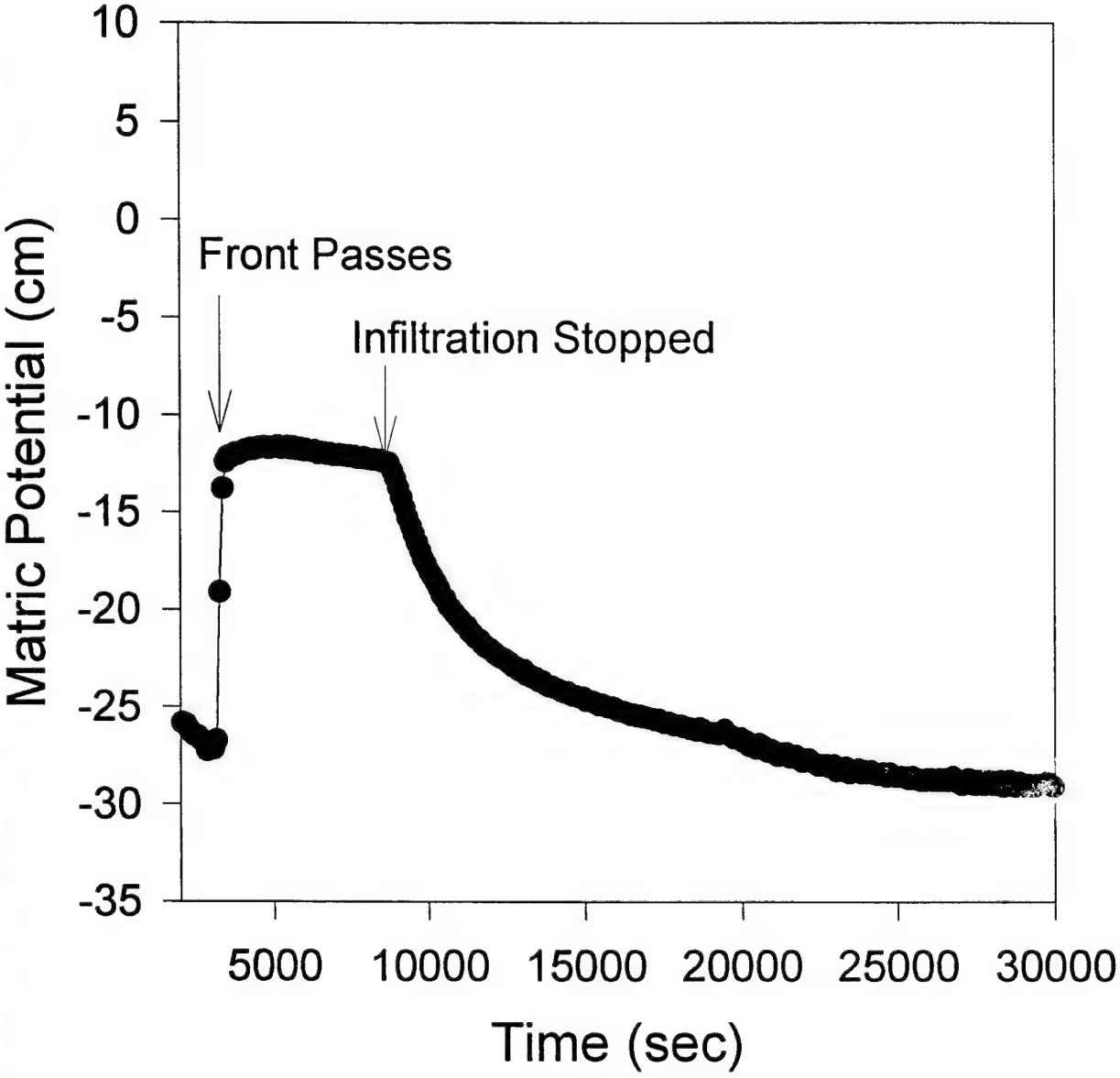
10
5
0
-5
-10
-15
-20
-25
-30
-35
Matric Potential (cm)
Front Passes
Infiltration Stopped
5000
10000
15000
20000
25000
30000
Time (sec)

Fig 4.

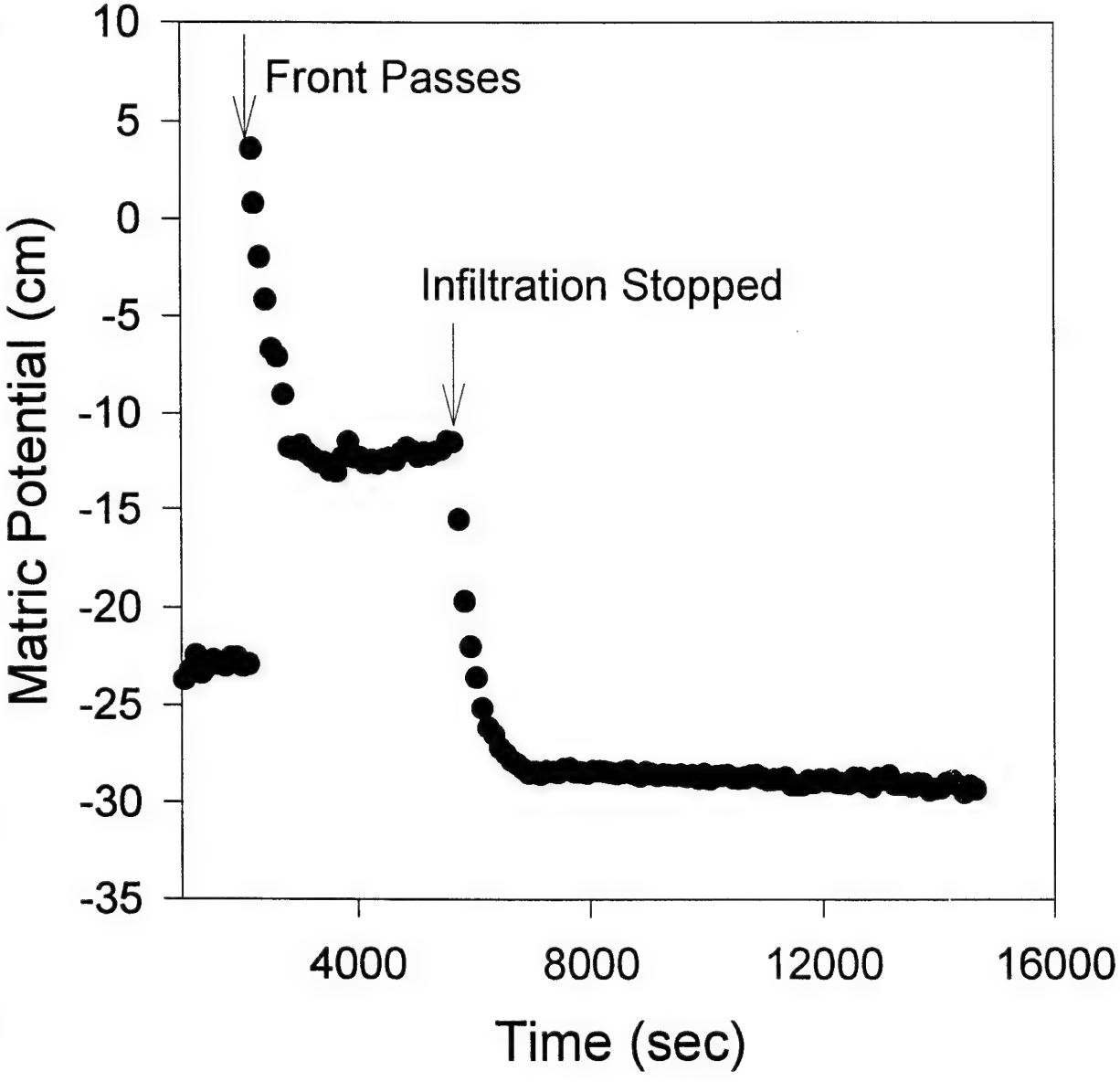
10
5
0
-5
-10
-15
-20
-25
-30
-35
Front Passes
Infiltration Stopped
Matric Potential (cm)
4000
8000
12000
16000
Time (sec)

Fig 5

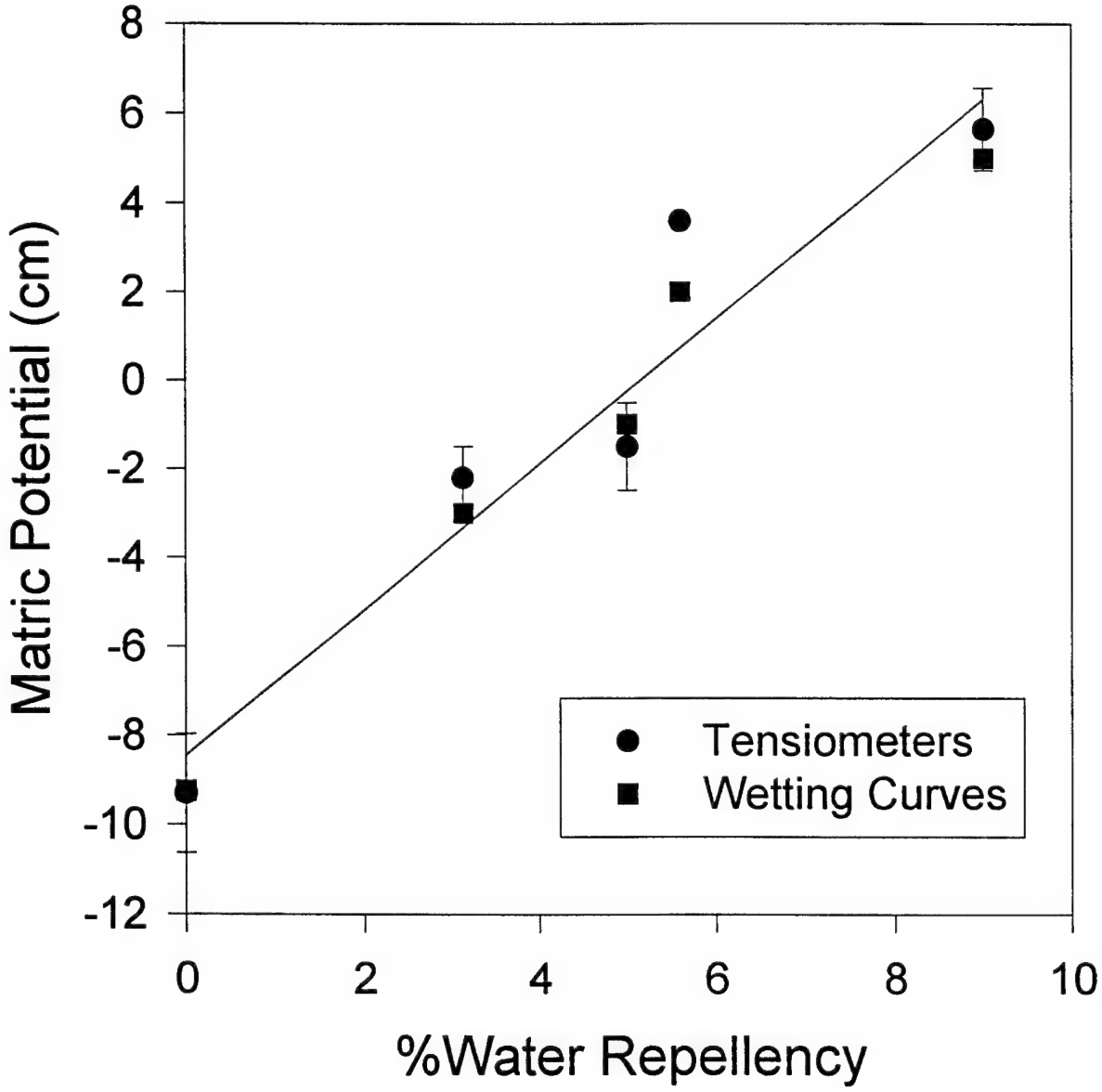
Matric Potential (cm)
8
6
4
2
0
-2
-4
-6
-8
-10
-12
0
2
4
6
8
10
%Water Repellency
Tensiometers
Wetting Curves

Fig 6

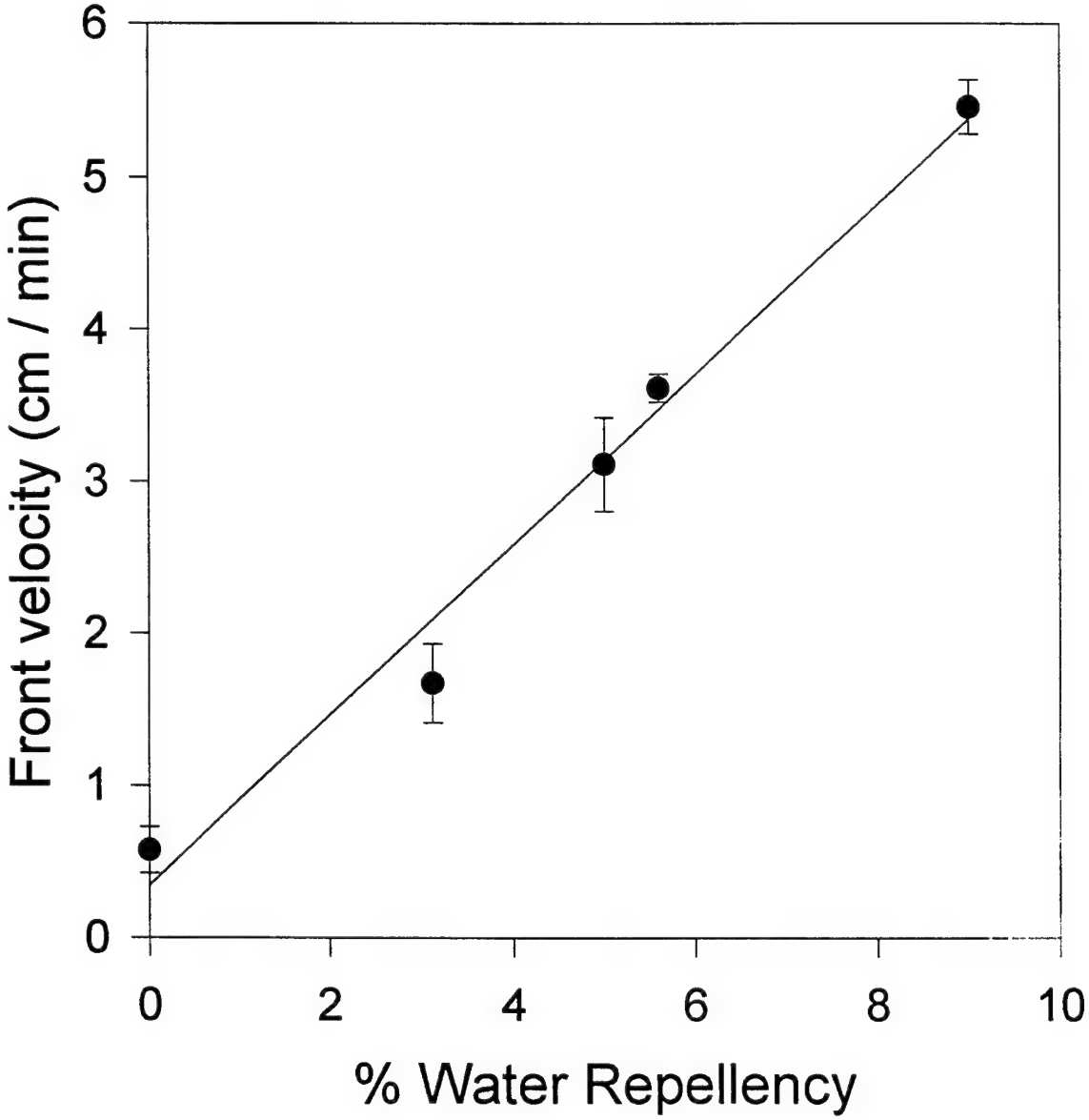

Fig-7

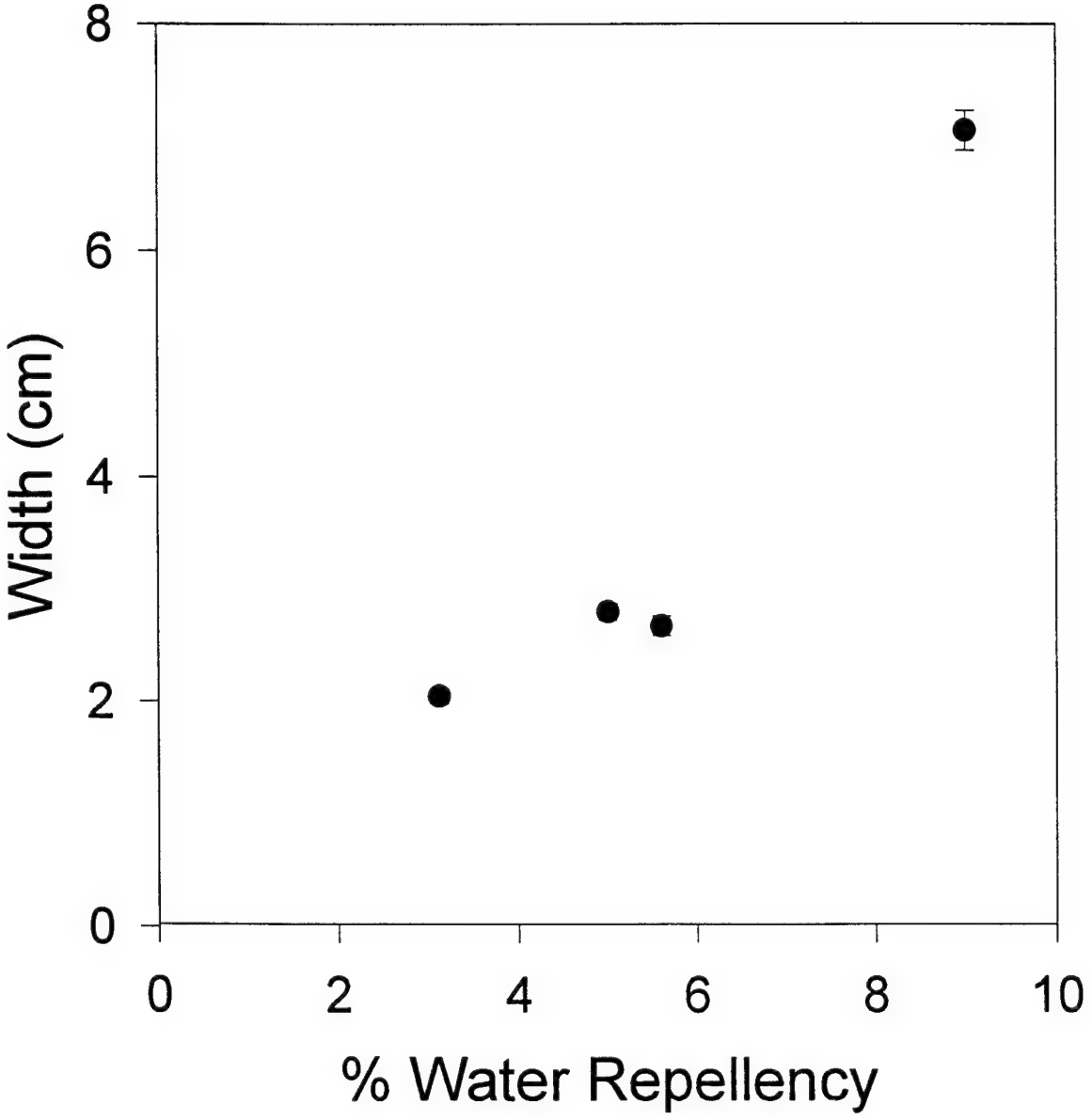

Fig. 8

APPENDIX G

SURFACTANT INDUCED CHANGES IN GRAVITY FINGERING THROUGH A LIGHT OIL

D.A. DiCarlo, T.W.J. Bauters, C.J.G. Darnault,
E. Wong, B.R. Bierck, T.S. Steenhuis,
and J.-Y. Parlange

Submitted to Water Resources Research

Surfactant Induced Changes in Gravity Fingering of Water Through a Light Oil

D. A. DiCarlo, T. W. J. Bauters, C. J. G. Darnault, E. Wong, B. R. Bierck, T. S. Steenhuis*, and J.-Y. Parlange

Department of Agricultural and Biological Engineering

Cornell University, Ithaca, NY 14853

Abstract

Gravity driven preferential flow (fingering) can greatly affect how one fluid displaces another in the subsurface. Using synchrotron x-rays and miniature tensiometers, we have studied the internal properties of these preferential flow paths when water, with and without surfactants, infiltrating an oil saturated porous media. Water pressure and saturation decrease behind the front, similar to fingers in air-dry sand, with quantitative differences for different surfactants. Using a formulation originally described for water infiltrating air-dry sand, we find that the finger widths, pressure drops within the fingers, finger tip lengths, and finger splitting dynamics can all be related to the interfacial tension between the fluids.

* Corresponding Author

Concurrently, soil scientists have been interested in preferential flow during infiltration events, when the flow rate is slow and the fingering is driven by density effects. (hillel?) In the case of water infiltrating air dry soil, Parlange and Hill (1976) accounted for the capillary effects of the porous media by treating the wetting front as diffuse. The resultant expression for the finger dimensions includes the sorptivity S of the soil which is a function of the unsaturated conductivity and the capillary pressure-saturation relation. Recently this has been extended to water infiltrating oil-saturated soils by Chandler et al. (1997) with the assumption that the flow is slow enough to eliminate viscous effects.

Most experimental studies have focused on fingering in Hele-Shaw cells or at the outside wall of thin sands due to the difficulty in "seeing" inside a complete porous media. Viscous fingering has been studied as a function of front velocity, interfacial tension, and wettability in Hele Shaw cells (Homsy 1987) and at the wall of thin glass bead packs (Stokes et al., 1986). Of particular interest is the use of surfactants or detergents in the aqueous phase, which are used for enhanced oil recovery or remediation. By altering the interfacial tension with a surfactant, the preferential flow properties change dramatically. There has been a wealth of work in the very low interfacial tension limit, as fingers themselves are observed to be unstable and split. (Bensimon 1986, Homsy 1987)

Inside real porous media the fluid saturation at and behind the interface can show wide variations and affect the scale of the preferential flow. (Glass 19??, Selker et al., 1992b). In this paper, we have used synchrotron x-ray attenuation to measure accurately and quickly fluid saturations

during fingering within a two-dimensional slab of a three-dimensional porous media. Along with fast measurements of the fluids pressures, a better understanding of the dynamics of fingering can be resolved. By using sands already well characterized for fingers through dry sand, we find that the fingers through oil are qualitatively similar and the quantitative differences can be directly related to the interfacial tension and the density differences of the fluids. Thus, the same physics of unstable fluid displacements can be used to describe and predict gravity driven fingered flow for many fluid pairs.

Theory

We wish to obtain expressions for finger width and the fluid energy state (pressure) inside the finger for the case of water with a surfactant infiltrating a oil saturated column. The capillary pressure ($P_{w/nw}$, also known as the suction in soil science), which is the pressure difference between the non-wetting (P_{nw}) and wetting (P_w) phase, is related to the pore radius (r) through the Laplace equation,

$$P_{w/nw} \equiv P_{nw} - P_w = \frac{2\sigma_{w/nw}\cos(\phi_{w/nw})}{r}, \qquad (2)$$

where the subscript w/nw refers to each particular wetting and non-wetting fluid pair, σ is the interfacial tension of the pair, and ϕ is the contact angle. Thus in a fixed porous medium, the capillary pressure-saturation (P-S) relationship for a fluid pair will scale with the interfacial tension between the fluid pair, as long as the contact angles are similar. In particular, the two-

phase water-oil P-S relationship can be related to the two-phase water-air P-S relationship through,

$$P_{w/o}(\theta_w) = \frac{\sigma_{w/o}}{\sigma_{w/a}} P_{w/a}(\theta_w). \quad (3)$$

In general, the higher the capillary pressure, the less saturation of the wetting phase. Also the relation is always hysteritic depending if the wetting fluid is entering (wetting) or leaving (drying) a particular portion of the porous media.

From Parlange and Hill (1976) and Chandler et al. (1997) the scaling of finger width into the water and oil system is then given by,

$$\frac{d_{oil}}{d_{air}} = \frac{\frac{\sigma_{w/o}}{\sigma_{w/a}}}{1 - \frac{\rho_o}{\rho_w} - \frac{u(\theta_f - \theta_i)}{K_w}} \quad (4)$$

where d_{oil} is the finger width for the water oil system, d_{air} is the finger width for the water-air system, and $K_w = kg/\mu$ is the water conductivity behind the wetting front. This expression has been derived in the low velocity limit, where the effects of viscosity of the displaced fluid are assumed to be negligible.

We also wish to understand the fluid state within the preferential flow path. For water infiltrating an air dry soil, Selker (1992b) provided a description of the water saturation behind a moving gravity driven finger. We follow their arguments for the case of water infiltrating an oil-saturated soil.

Starting with the one-dimensional Richard's equation

$$\frac{\partial \theta_w}{\partial t} = \frac{\partial}{\partial z}\left(K(\theta_w) \frac{\partial (\psi_w - \psi_o)}{\partial z} \right), \tag{5}$$

where z is the vertical distance (positive downward), K is the unsaturated conductivity and ψ_w and ψ_o are the total water and oil potentials in units of pressure head (cm of water), respectively. This assumes that when preferential flow occurs that the oil moves under much smaller pressure gradients than the water, as the oil can move through the whole matrix and the water is confined in the flow path. This has been observed to be true for water and soltrol, but must break down for oils of high viscosity.

For water infiltrating a less dense oil the potential difference is the sum of the gravitational and capillary potentials,

$$\psi_w - \psi_o = \left(\frac{\rho_w - \rho_o}{\rho_w} \right) z + P_{w/o}(\theta_w). \tag{6}$$

It is experimentally observed that the saturation profile within the finger translates downward at a constant velocity v, and thus the water saturation can be expressed as $\theta(z-vt)$. Defining $\eta=z-vt$, substituting Eq. (6) into Eq. (5) and integrating converts the partial differential equation into

$$v\theta_w = K(\theta_w)\left(1 - \frac{\rho_o}{\rho_w} - \frac{dP_{w/o}}{d\eta}\right) \tag{7}$$

which relates the water saturation, the finger velocity, the unsaturated conductivity, and the capillary pressure inside the finger. This expression can be used to calculate the extent of the finger tip, and the unsaturated conductivity among other things.

At a particular time t, the capillary pressure within the finger path is given by

$$\frac{dP_{w/o}}{dz} = 1 - \frac{\rho_o}{\rho_w} - \frac{v\theta_w}{K(\theta_w)}. \tag{8}$$

Since a column of water at rest has $dP/dz = 1$, the above equation predicts that the water saturation within the finger will appear as a hanging water column scaled by the right hand side of Eq (8). For well-sorted soils, the lower portion of a water column (or equivalently the pressure - saturation relation) has a region of constant saturation between the water entry pressure and the non-wetting fluid entry pressure. This region of constant has been observed in fingers in air-dry soil. Since the saturation is constant, by integrating Eq. (8) we obtain a prediction for the length of the tip region for water fingers through oil-saturated sand,

$$z_{tip} = \frac{P_{w/o}(o.e.) - P_{w/o}(w.e.)}{\left(1 - \frac{\rho_o}{\rho_w} - \frac{v\theta_w}{K(\theta_w)}\right)} \quad (9)$$

where z_{tip} is the expected length of the finger tip, and $P_{w/o}$(w.e) and $P_{w/o}$(o.e.) are the water-entry and oil-entry pressures, respectively. Assuming the pressure-saturation scaling in Eq. (3), z_{tip} can be calculated from the known water and air entry values in the water and air system, the densities, the finger velocity and saturation, and the conductivity of the soil.

If the fluid pressures are also measured, it is possible to obtain measurements for the unsaturated conductivity using Eq. (7).

Materials and Methods

Experiments to observe and measure finger properties were performed in two different two-dimensional chambers uniformly packed with sand. The sample chambers both had 0.94 cm thick polycarbonate walls, interior thickness' of 0.94 cm, and heights of 55 cm, but different widths of 30 cm and 51 cm. Attached to the bottom end of each chamber was a manifold of 5 fluid ports, and the top end was left open to the atmosphere. Chambers were packed as follows. The bottom of the chamber was filled to a height of 17 cm with Soltrol 220 (Phillips Company), a non-toxic light NAPL. Clean, dry, sieved, quartz sand (Unimin Corporation) was dropped through the top using a dual randomizing funnel in a single pour to minimize layering. During packing and for one

minute afterwards, the chamber was vibrated to enhance settling. Grain sizes of 12/20 and 20/30 sand were used, where the numbers correspond to the sieve sizes the sand passes through and does not pass through, respectively. This produced a tight oil-saturated pack with minimal entrapped air and a porosity of 37%. Water fingers in these sand packs had uniform widths and velocities throughout the chamber.

The aqueous solutions used in the experiments consisted of either water or water with a dissolved surfactant. Four commonly available surfactants were used, Alfonic 810-4.5 Ethoxylate (CONDEA Vista Company) and Surfynol 485 (Air Products and Chemical, Inc.) are ionic surfactants, and Neodol (R) 25-7 (Shell Chemical Company) and Poly Sodium Vinyl Sulfonate (Air Products and Chemical, Inc.) are non-ionic. The names have been abbreviated throughout the text as alfonic, surfynol, neodol, and sulfonate, respectively. The surfactants were mixed with water to a 1 % by weight solution. Interfacial tensions between each solution and soltrol 220 were measured using a ring (du Nouy ring method) tensiomat. For all the aqueous solutions, 0.005 % of FD&C blue # 1 were added to aid in the visual inspection of water positions.

Infiltrations of the aqueous solution were performed by applying the aqueous solution to the top of the chamber either uniformly and through a point source. Uniform applications were performed in the wider chamber (width = 51 cm). The application system consisted of a peristaltic pump driven point source, which a rotating cam shaft moved continuously across the soil surface. Uniform application rates were 2.25, 6.0, and 10.0 cm/hour. Oil was removed from the bottom of the chamber through a constant head overflow system at the height of the soil surface. For

uniform applications, the chamber was placed in front of a light source and the infiltrations were observed visually.

Point source applications were performed in the smaller chamber (width = 30 cm). In this case, the water application system was set up to keep the fluid content in the chamber constant. This consisted of a fixed peristaltic pump which applied the solution through a tube and needle at 2 ml/min. The other end of the pump tubing was connected to the bottom of a stoppered 250 mL Erlenmeyer flask containing the aqueous solution, which was in turn connected to the bottom of the chamber, thus pulling an equal amount of oil out of the chamber. Using this system to withdrawal oil from the bottom of the chamber as water was being applied to the top maintained a constant fluid level and therefore kept the oil pressure constant.

For the point source infiltrations, fluid contents were measured using synchrotron x-ray attenuation. The dual energy attenuations were obtained at the F-2 beam line of the Cornell High Energy Synchrotron Source using a set-up described in detail elsewhere (DiCarlo et al. 1997). The chamber was mounted on a movable platform which had a vertical and horizontal range of 50 and 25 cm, respectively, and a position repeatability of 0.01 cm. In this experiment we used x-ray energies of 25 and 50 KeV. As the system consisted of two fluids, only the 25 KeV x-ray attenuation was used to obtain the water saturation, with the 50 KeV x-ray was used to calibrate out any possible soil motions. For two fluid measurements the water saturation is related to the attenuation through,

$$\theta_w = -\frac{A - A_0}{(\mu_w - \mu_o)x} \qquad (10)$$

where A is the measured attenuation, A_0 is the attenuation through the oil saturated soil, x is the thickness of the chamber, and μ_w and μ_o are the measured 25 KeV attenuation constants for the water and oil phases, respectively.

Fluid attenuation constants were obtained using a polycarbonate chamber with 5 sequential cells of thickness 0.56 cm. (Lenhard, et al., 1988) The attenuation was measured for the empty chamber and after each cell was filled with either fluid. The measured attenuations were linear with fluid thickness, and the attenuation constant was given by the slope.

Water and oil pressures were obtained using 4 miniature tensiometers (Selker et al., 1992a) placed in a line 40 cm above the bottom of the chamber. The water tensiometers were 2 cm left of the horizontal center and on the center (on the front of the chamber) , while the oil tensiometers were 2 cm right of the horizontal center and on the center (on the rear of the chamber). Each tensiometer consisted of a hollow brass housing, with one end connected to the soil through a 0.8 cm diameter porous plate, and the other end connected to a pressure transducer through a rigid plastic tube and a three-way valve. The other port of each three-way valve was connected to a vertical reservoir of water. Prior to each experiment the valve was opened the reservoir, and the transducers were calibrated using different water heights in the reservoir. Water tensiometers were filled with de-gassed water, and had a sintered glass porous plate (Ace Glass) of maximum pore size 70-100 μm. Oil tensiometers were filled with soltrol 220 and had a sintered stainless

steel porous plate (Mott metallurgical) of pore size 20 μm. As water preferentially wets the glass plate, and oil preferentially wets the stainless steel plate, each tensiometer provided a connection to their particular fluid within the sand pack. The capillary pressures were obtained by subtracting the water pressure from the oil pressure.

Finger widths were found by analyzing tracings from the experiments and from horizontal attenuation scans through the finger. Tracings were done on 1 cm graph paper taped on the back of the chamber. While the finger was infiltrating, the finger was then traced at one minute intervals. The width was then measured from the paper tracings every 5 cm vertical. Horizontal attenuation scans were performed after the finger had reached the bottom of the chamber, and widths of the fingers were taken to be the full width at half maximum of the water saturation in the finger. Both procedures produced similar results and the reported widths are an average of the two procedures.

Results

Uniform Water Application

Due to the difficulties in applying water uniformly at the synchrotron and lack of control of the finger positions, only qualitative results were obtained for the uniform applications. When the aqueous solution was applied uniformly to the top of the oil saturated 12/20 sand pack, for every solution the water moved through the soil pack in preferential paths. The experiments were

repeated for three infiltration rates ranging from 2.2 to 13 cm/hour. The widths of the fingers and the pattern of the fingers varied for each surfactant used.

For pure water, the observed preferential flow moved through the chamber at constant velocity and with constant widths between 5 and 8 cm. The flow paths are sketched in Figure 1a. No splitting or merging was observed. Higher infiltration rates just produced more fingers; infiltrations of 5.6, 9.4, and 13 cm/hour produced 1, 2, and 3 fingers respectively.

For the surfactant solutions, sulfonate produced only 2 fingers for an infiltration rate of 2.2 cm/hour and produced 5 fingers for an infiltration rate of 10 cm/hour. Similarly to the water solution, these fingers did not merge and remained the same width and velocity throughout the chamber. The surfynol solution initially produced 10 fingers for all flow rates with widths of roughly 2 cm. Only a few fingers merged and 6-8 fingers remained at a depth of 50 cm with roughly the same 2 cm width. The low interfacial tension solutions containing alfonic and neodol were much different. Each initially produced 20 fingers of widths 1 cm or less for all flow rates. Many of these fingers quickly merged and produced fewer and faster moving fingers. Typically, the finger merging occurred twice for each infiltration, a primary merge at a depth of 10-20 cm, and a secondary merge at a depth of 40-50 cm. Fig 1b shows the sketch of the flow for the neodol solution.

Point Source Applications

All point source applications of the aqueous fluids produced preferential flow paths. Water, sulfonate, and surfynol each produced one single finger with uniform width and visually similar to the fingers observed for the uniform applications. Neodol and alfonic, however, exhibited different behavior from that observed in the uniform applications. Neodol began as one main finger, but small fingers quickly began to splinter off the main finger. These other fingers remained small and did not grow continuously during the experiment. Alfonic, similar to neodol, had many fingers which splintered off the main finger, but the fingers continued to grow and became the same size as the main finger, if not larger. The entire chamber became filled with alfonic fingers, and the entire finger pattern closely resembled a large net. The fingers were extremely diffuse and pervasive, especially when compared to the one water finger. Table 1 lists the widths and velocities of the main fingers. In general, water fingers were the widest followed by sulfonate, surfynol, neodol, and alfonic.

Pressure and saturation measurements were taken within the finger for each solution. Figure 2 shows the water saturation and capillary pressure between the water and oil phases in the initial finger versus time when the invading aqueous solution is distilled water. Both data points were taken at z = 40 cm (40 cm above the bottom of the chamber). The behavior is qualitatively similar to that seen for water preferentially flowing through air-dry sand. The finger has a tip with a relatively constant water saturation of 0.30 cm^3/cm^3, behind which the water saturation quickly

drops to 0.17 cm^3/cm^3 where it levels off. The capillary pressure of the is lowest at the finger tip (0.5 cm) and rises continuously after the tip before leveling off at 4 cm.

Figure 3 shows the water saturation and capillary pressure within the finger when the invading aqueous solution contains 1 % by weight surfynol. The same qualitative features as seen in the water finger are present: highly saturated tip, and saturations decreasing and pressures increasing behind the tip. But, an additional feature produced by surfactants is a slow increase in the water saturation of roughly 0.03 cm^3/cm^3 well behind the finger tip. This feature is associated with an decrease in the capillary pressure after the initial increase. Other than the slow increase at the end, the saturations in the finger are quantitatively similar for the surfactant fingers with a tip saturation of approximately) 0.30 cm^3/cm^3 and saturation directly behind the tip of 0.17 cm^3/cm^3. The surfactant fingers are quantitatively different in the actual length of the nearly saturated region, and the pressure rise behind the tip.

Identical sets of water saturation and pressure data were taken for the other surfactant solutions and for a coarser sand pack of 12/20 sand. Table 1 lists the finger widths, finger velocities, finger pressure rises, and the lengths of the saturated tips for all of the data sets. The finger properties show definite trends with the interfacial tension of the fluids. As the interfacial tension between the solutions is lowered by the surfactants, the pressure rises behind the wetting front decrease, the finger widths decrease, and the lengths of the saturated tips decrease.

Discussion

Due to the qualitative similarity between the fingers observed here and those observed in water infiltrating air-dry sand, we will analyze the data in the framework developed for the latter case. If this formulation is correct, the finger properties such as the finger widths, the pressure drop behind the finger and the length of the finger tips should be scaled through the above equations.

Figure 5 shows the finger width versus the interfacial tension for the 12/20 and 20/30 sand. The lines are the predicted scaling relation in Eq. 4 with the slope determined by the widths of the water fingers through air-dry sand (2.0 cm for 12/20 sand and 2.5 cm for 20/30 sand). The trend in the observed data follows the theoretical predictions; with the smallest fingers occuring with solutions of alfonic and neodol, which have the smallest interfacial tension values. At these low interfacial tensions, is also where the predictions differ the most, with the fingers being wider than predicted. This is not surprising as we have rarely observed fingers of widths smaller than 1.5 cm, and never smaller than 1 cm. Thus it appears that the scaling is roughly true, except that there appears to be some minimum finger width. Clearly the theory must break down at the pore scale and thus must have a length scale smaller than which it is not appropriate.

The simultaneous measurements of pressure and saturation allow us to quickly obtain the pressure-saturation relationship for this water oil system. Figure 5 shows the measured relationship from the water infiltration and the re-infiltration into 12/20 sand. As the wetting process is very abrupt, both curves are on drying branches of the P-S relationship.

Once the fingers are formed, hysteresis in the above pressure-saturation relation plays a large part in the stability of the fingers. The water does not enter the oil saturated sand until the capillary pressure decreases to 0.5 cm, at which the water enters at a saturation of 0.30 cm^3/cm^3 (point A). Behind the finger tip the capillary pressure increases and the water saturation decreases (point B). Since the capillary pressure behind the finger tip quickly becomes much greater than the water entry pressure, the water is confined within the finger and cannot spread. The finger remains at point B until the water is turned off after which the capillary pressure increases and water saturation decreases further (point C). On a reinfiltration the old finger core wets quickly to point D, where it remains until the water is turned off after which it dries to point E. Again, on reinfiltration the capillary pressure remains greater than the water entry pressure and the water finger does not expand.

These pressure drops differ for each surfactant used. Figure 6 shows the maximum pressure drop inside the finger (Point A to Point B) versus the interfacial tension of the fluids. The line shown is the predicted dependence on interfacial tension. The observed data correlates well over the variety of surfactants used and for the water into air dry sand case.

The pressure data can give us insight into the finger patterns for different fluid pairs. For viscous fingering, it has been known for some time that at low interfacial tensions, the finger pattern becomes very unstable or "chaotic" with large amounts of finger splitting. (Bensimon et al., 1986). For gravity driven fingers, we also observe finger splitting at the lowest interfacial

tensions. This splitting can be understood in terms of the water entry pressure of the soil and the pressure rise inside the finger tips. For large interfacial tensions, the pressure rise within the finger is large, and the pressure behind the tip of the finger becomes greater than the water-entry pressure. Therefore there will not be enough pressure for the finger to expand, and the width will not increase. This is what is observed for infiltrations of surfynol, sulfonate, and water. For small interfacial tensions (e.g. neodol and alfonic), however, the pressure rise within the finger is small, and the pressure behind the tip of the finger remains close to or at the water-entry pressure. Therefore there will be enough pressure for the finger to expand, and splitting and secondary fingers can occur. This is what is observed for infiltrations of neodol and alfonic.

What is the role of viscosity in these gravity driven fingers? In measurements of the oil pressure directly outside the finger path, we observe no change in the oil pressure as the finger passes (Chandler et al. 1997). Thus for soltrol and water with a viscosity ratio of $\mu_o/\mu_w = 4$, the major pressure changes are in the water phase and the assumption that the oil acts inviscidly (oil movement with little or no pressure gradients) during preferential flow appears to be valid. Although there are no observed effects of oil viscosity in the bulk oil phase, other effects can be attributed to oil viscosity. The most prominent of these viscous effects is that the finger is not completely saturated with water, unlike fingers in the water and air system. This is most likely due to the oil not being able to move out of all the pores fast enough during the infiltration because of its viscosity. The lower saturation in the tip also affects the behavior of the finger behind the tip, as the lower tip saturation yields a water conductivity of roughly half of the saturated conductivity.

Behind the finger tip, the water saturation drops and oil re-enters the finger path. Viscosity may affect the time scale over which this proceeds, and thus the tip length of the finger tip. Figure 7 plots the measured length of the finger tip versus that predicted in equation (9). The predictions were made by assuming that the pressure difference between the oil entry and water entry values scales with interfacial tension, the water saturation was 0.30 cm^3/cm^3, and the conductivity at this saturation was measured separately to be 0.45 cm/sec for 12/20 sand and 0.15 cm/sec for 20/30 sand. The trend is followed well by the data, but the observed finger widths are generally higher than the predicted widths. This is what would be expected if the displaced fluid has an appreciable viscosity, as the viscosity will limit the rate at which oil can return into the finger path thus making the finger longer. We have only used an oil of one viscosity, it would be interesting to see how the tip length

Summary

In summary, when water is gravitionally driven through an oil-saturated sand pack, fingers occur which resemble those seen when water infiltrates a dry sand pack. As opposed to viscous fingers in Hele-Shaw cells, behind the fingers tips oil re-enters the finger paths, and the capillary pressure - saturation relationship controls the spread of the fingers. These phenomena are described well by the theory developed for fingers from water infiltration with important scaling by the density differences, and the interfacial tensions, with the viscosity of the oil playing a minor role.

Possible future work involves looking into observing the crossover from gravity to viscosity driven fingers in porous media. Even with the oil being more 4 times more viscous than the water, the pressure drops occur inside the water finger. Future work consists of answering questions such as: Is the re-entry of the fluid behind the finger a signature of gravity driven fingers? Is the lateral expansion of fingers depend on if viscous or gravitational forces are dominating? And what is the role of pressure saturation relation in viscous fingering, as it is usually assumed that the interface is abrupt?

Acknowledgments

We would like to thank Edward Zhang, Qun Shen, and the staff at CHESS for useful discussions and experimental assistance. This work was supported (in part) by the Air Force Office of Scientific Research, USAF, under grant/contract number F49620-94-1-0291. CHESS is supported by NSF grant number DMR-931-1772.

Table 1:

12/20 sand

Fluid	Interfacial Tension (dynes/cm)	Finger Width (cm)	Finger Tip Length (cm)	Pressure Drop (cm of H_2O)	Finger Velocity (cm/sec)
Water	24	4.8	10.2	4.0	0.03
Sulfonate	21	2.8	8.0	2.6	0.055
Surfynol	9	2.4	8.0	1.5	0.06
Neodol	4	2.2	4.0	<0.2	0.09
Alfonic	3	1.6	3.5	<0.2	0.09

20/30 sand

Fluid	Interfacial Tension (dynes/cm)	Finger Width (cm)	Finger Tip Length (cm)	Pressure Drop (cm of H_2O)	Finger Velocity (cm/sec)
Water	24	5.1	25	3.5	0.022
Sulfonate	21	4.2	28	3.5	0.025
Surfynol	9	5.0	13	1.8	0.03
Neodol	4	2.1	6	0.5	0.043
Alfonic	3	1.9	6	<0.5	0.045

Summary of the internal finger properties for each infiltrating fluid and for both sand sieve sizes.

Figure Captions:

Fig. 1. Sketch of fingering patterns when a aqueous solution is infiltrated uniformly on an oil-saturated sand. a) water, b) water with neodol as a surfactant.

Fig. 2. Water saturation and capillary pressure inside a water finger infiltrating oil saturated 12/20 sand. The highest saturation and capillary pressures are at the tip of the finger.

Fig 3. Water saturation and capillary pressure inside a surfynol solution finger infiltrating oil saturated 12/20 sand. The pressure changes behind the tip are smaller than for the water case, and the saturation of the surfynol solution rises slightly after the finger tip.

Fig. 4. Capillary pressure - saturation relationship obtained from the water finger into oil-saturated 12/20 sand. The drying from A to B takes place in the initial finger, drying to point C occurs when the infiltration is stopped. Point D is reached on re-infiltration, and point E after the re-infiltration is stopped.

Fig. 5. Finger widths versus interfacial tension for the five solutions and two sands used. The solid and dotted lines are the expected scaling from fingers in air-dry 12/20 and 20/30 sand, respectively.

Fig. 6. Pressure drops behind the finger tip versus interfacial tension for the five solutions and two sands used. The solid and dotted lines are the expected scaling from fingers in air-dry 12/20 and 20/30 sand, respectively.

Fig. 7. Measured finger tip length versus the predicted tip length from Eq. 8. Tip lengths are slightly higher than predicted by the 1:1 solid line.

References:

Bensimon, D., L. P. Kadanoff, S. Liang, B. I. Shraiman, and C. Tang, Viscous flows in two dimensions, Rev. Mod. Phys., 58, 977-999, 1986.

Chandler, D. G., Z. Cohen, E. Wong, D. A. DiCarlo, T. S. Steenhuis, and J.-Y. Parlange, Unstable fingered flow of water into a light oil, submitted to Water Resour. Res.

Chuoke, R. L., P. van Meurs, C. van der Poel, The instability of slow, immiscible, viscous liquid-liquid displacements in permeable media. Trans. AIME, 216, 188-194, 1959.

DiCarlo, D. A., T. W. J. Bauters, T. S. Steenhuis, J.-Y. Parlange, and B. R. Bierck, High-speed measurements of three-phase flow using synchrotron x-rays, Water Resour. Res., ??

Glass, R. J., T. S. Steenhuis, and J.-Y. Parlange, Wetting front instability. 2. Experimental determination of relationships between system parameters and two-dimensional unstable flow field behavior in initially dry porous media, Water Resour. Res., 25, 1195-1207, 1989.

Homsy, G. M., Viscous fingering in porous media, Ann. Rev. Fluid Mech., 19, 271-311, 1987.

Liu, Y., T. S. Steenhuis, and J.-Y. Parlange, Formation and persistence of fingered flow fields in coarse grained soils under different moisture contents, J. Hydrology, 159, 187-195, 1994.

Lenhard R. J., J. H. Dane, J. C. Parker, and J. J. Kaluarachchi, Measurement and simulation of one-dimensional transient three-phase flow for monotonic drainage paths, Water Resour. Res. 24, 853-863, 1988.

Parlange, J.-Y., and D. E. Hill, Theoretical analysis of wetting front instability in soils, Soil Sci., 122, 236-239, 1976.

Saffman, P. G., and G. I. Taylor, The penetration of a fluid into a porous medium or Hele -Shaw cell containing a more viscous liquid, Proc. R. Soc. London Ser. A 245, 312-329, 1958.

Selker, J. S., P. Leclerq, J.-Y. Parlange, and T. S. Steenhuis, Fingered flow in two dimensions. Part 1: Measurements of matric potential, Water Resources Res., 28, 2513-2521, 1992.

Selker, J. S., J.-Y. Parlange, and T. S. Steenhuis, Fingered flow in two dimensions. Part 2: Predicting finger moisture profile, Water Resources Res., 28, 2523-2528, 1992.

Stokes, J. P., D. A. Weitz, J. P. Gollub, A. Dougherty, M. O. Robbins, P. M. Chaikin, and H. M. Lindsay, Interfacial stabillityu of immiscible displacement in a porous media, Phys. Rev. Lett. 57, 1718-1721, 1986.

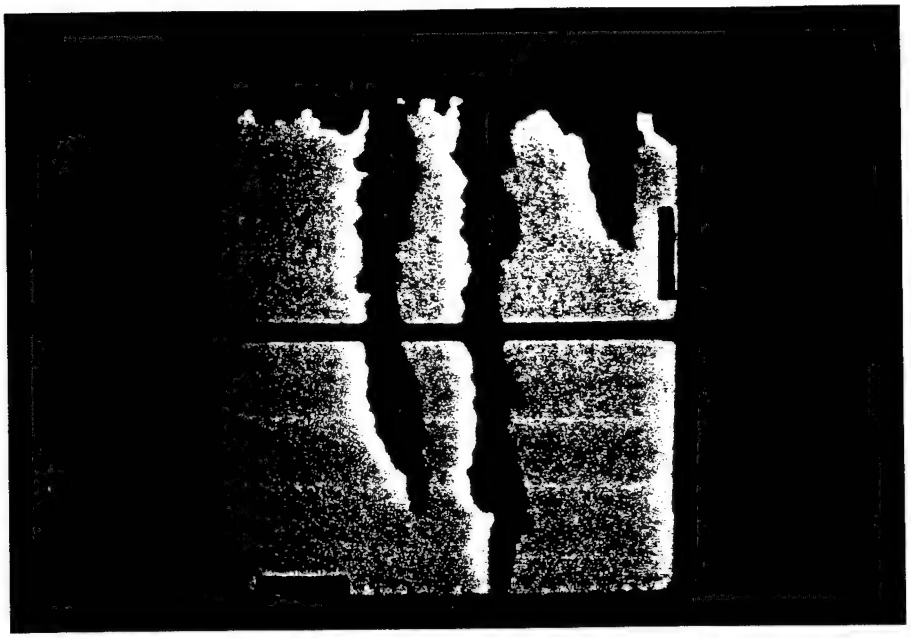

(a)

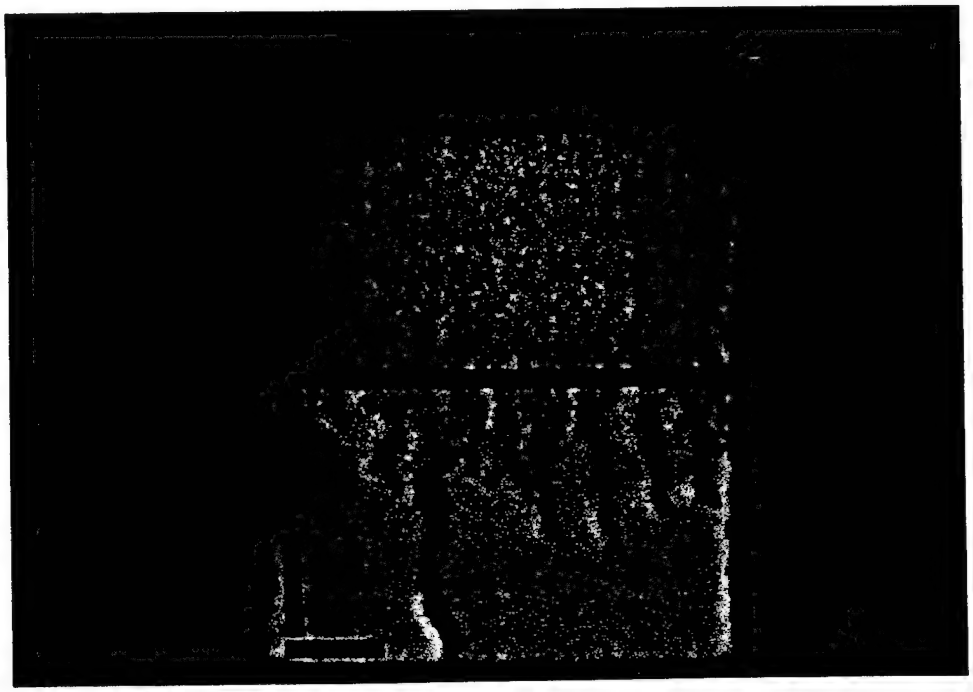

(b)

FIG 1

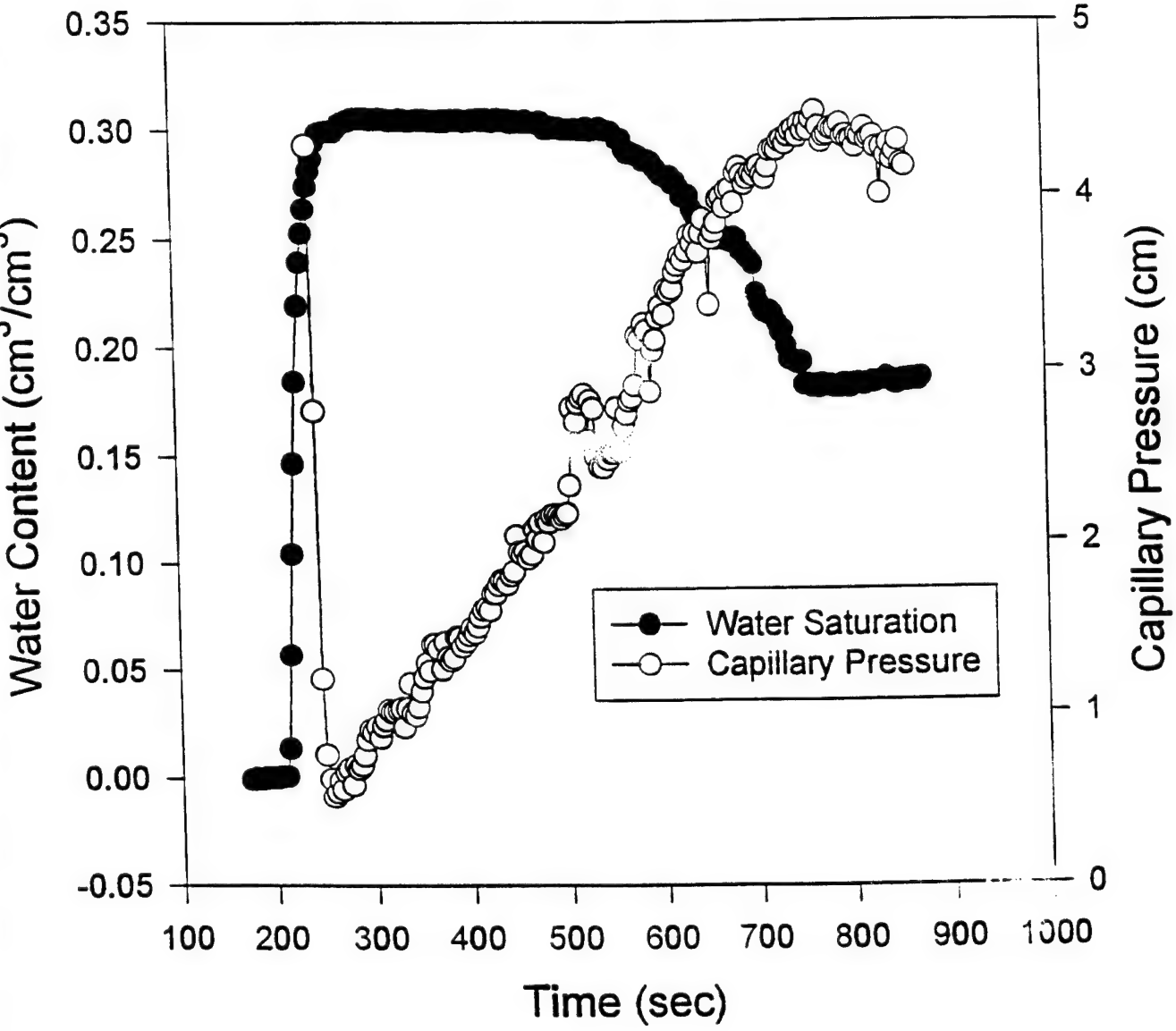
0.35
0.30
0.25
0.20
0.15
0.10
0.05
0.00
-0.05
Water Content (cm3/cm3)
5
4
3
2
1
0
Capillary Pressure (cm)
100
200
300
400
500
600
700
800
900
1000
Time (sec)
Water Saturation
Capillary Pressure

F162

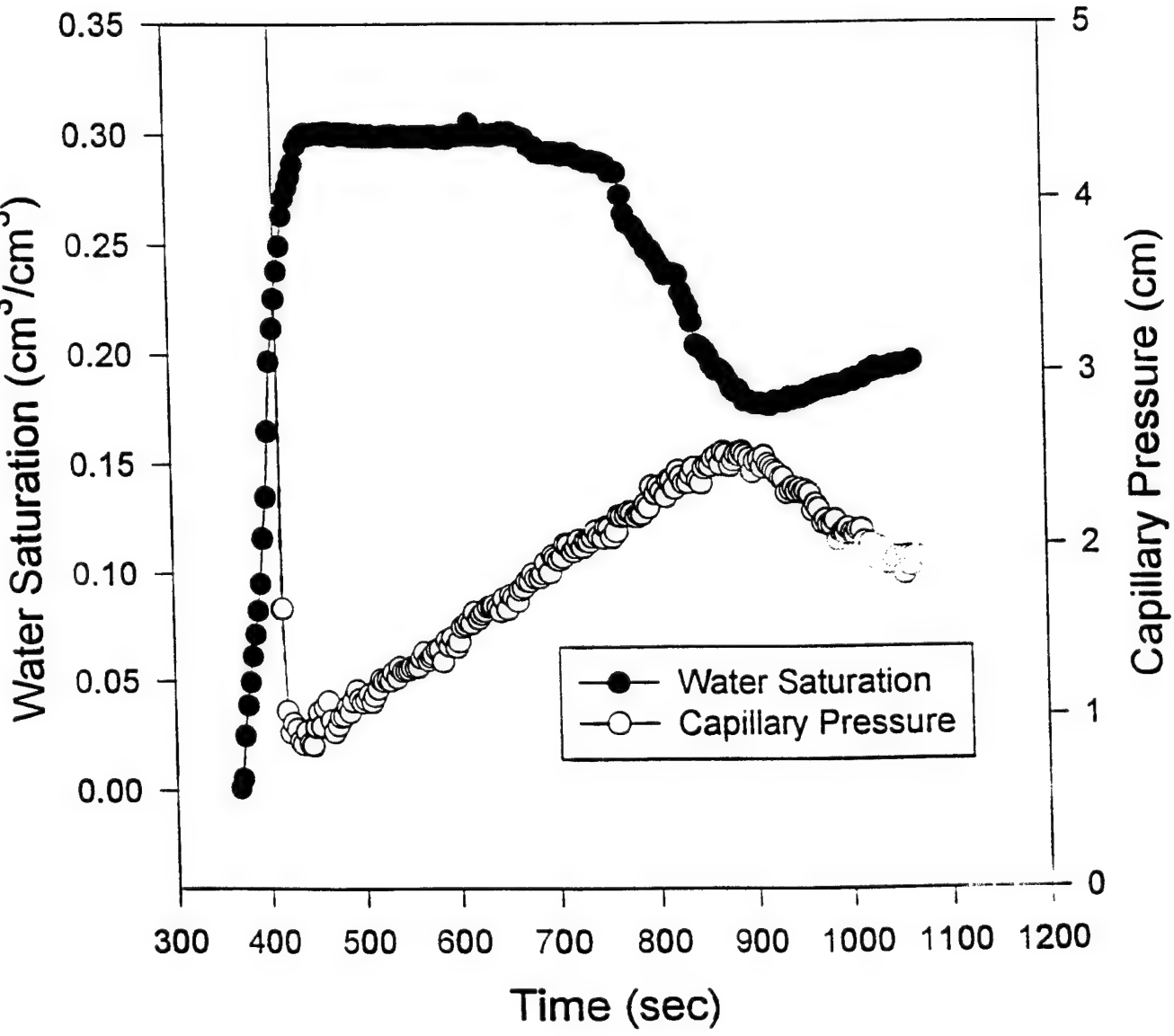
0.35
0.30
0.25
0.20
0.15
0.10
0.05
0.00
Water Saturation (cm3/cm3)
5
4
3
2
1
0
Capillary Pressure (cm)
300
400
500
600
700
800
900
1000
1100
1200
Time (sec)
Water Saturation
Capillary Pressure

FIG 3

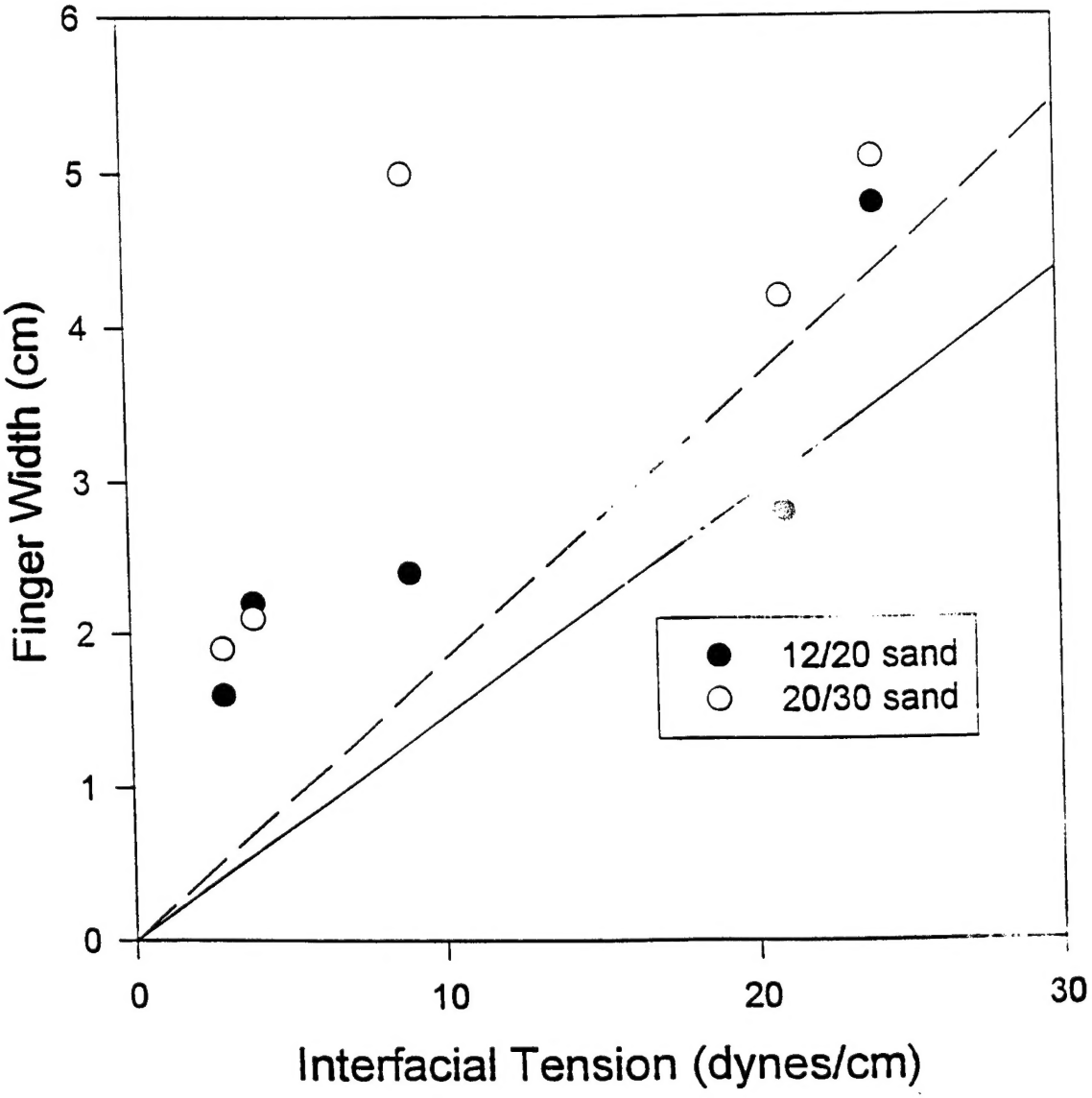
Finger Width (cm)
6
5
4
3
2
1
0
0
10
20
30
Interfacial Tension (dynes/cm)
12/20 sand
20/30 sand

FIGURE 4

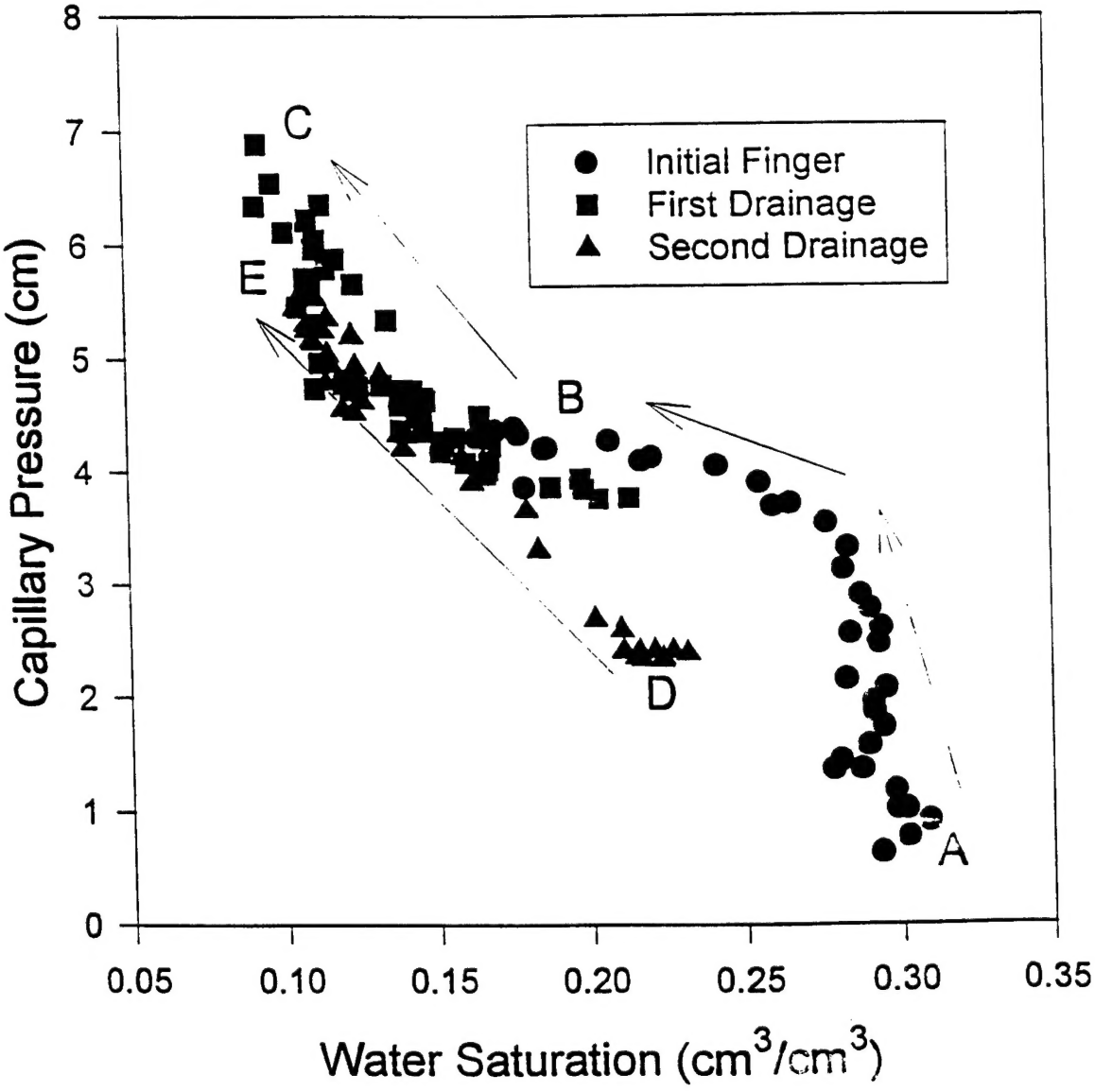
Capillary Pressure (cm)
Water Saturation (cm3/cm3)
Initial Finger
First Drainage
Second Drainage
A
B
C
D
E
0
1
2
3
4
5
6
7
8
0.05
0.10
0.15
0.20
0.25
0.30
0.35

FIGURE 5

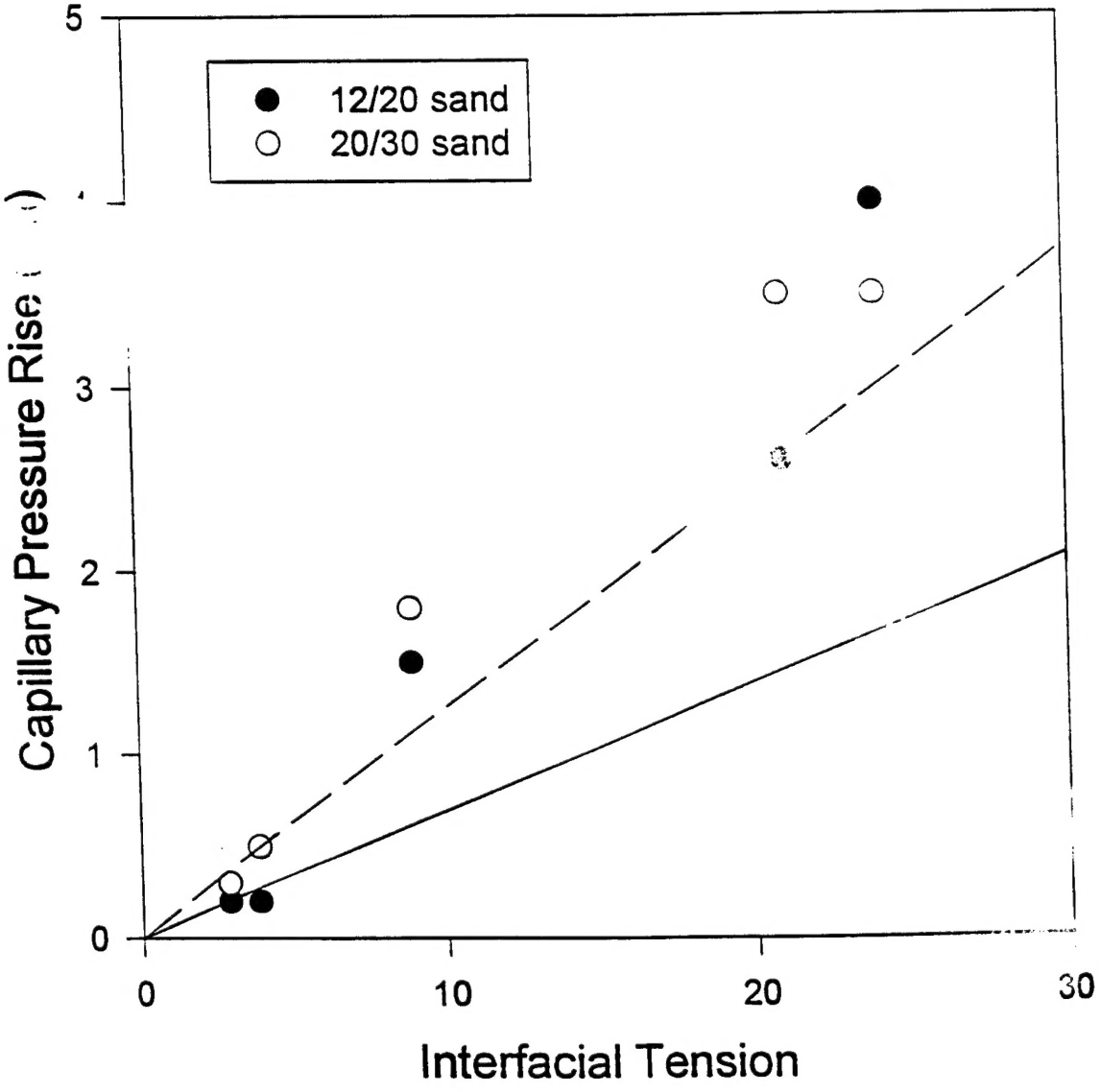
12/20 sand
20/30 sand
Capillary Pressure Rise
Interfacial Tension
0
1
2
3
5
0
10
20
30

Figure 6

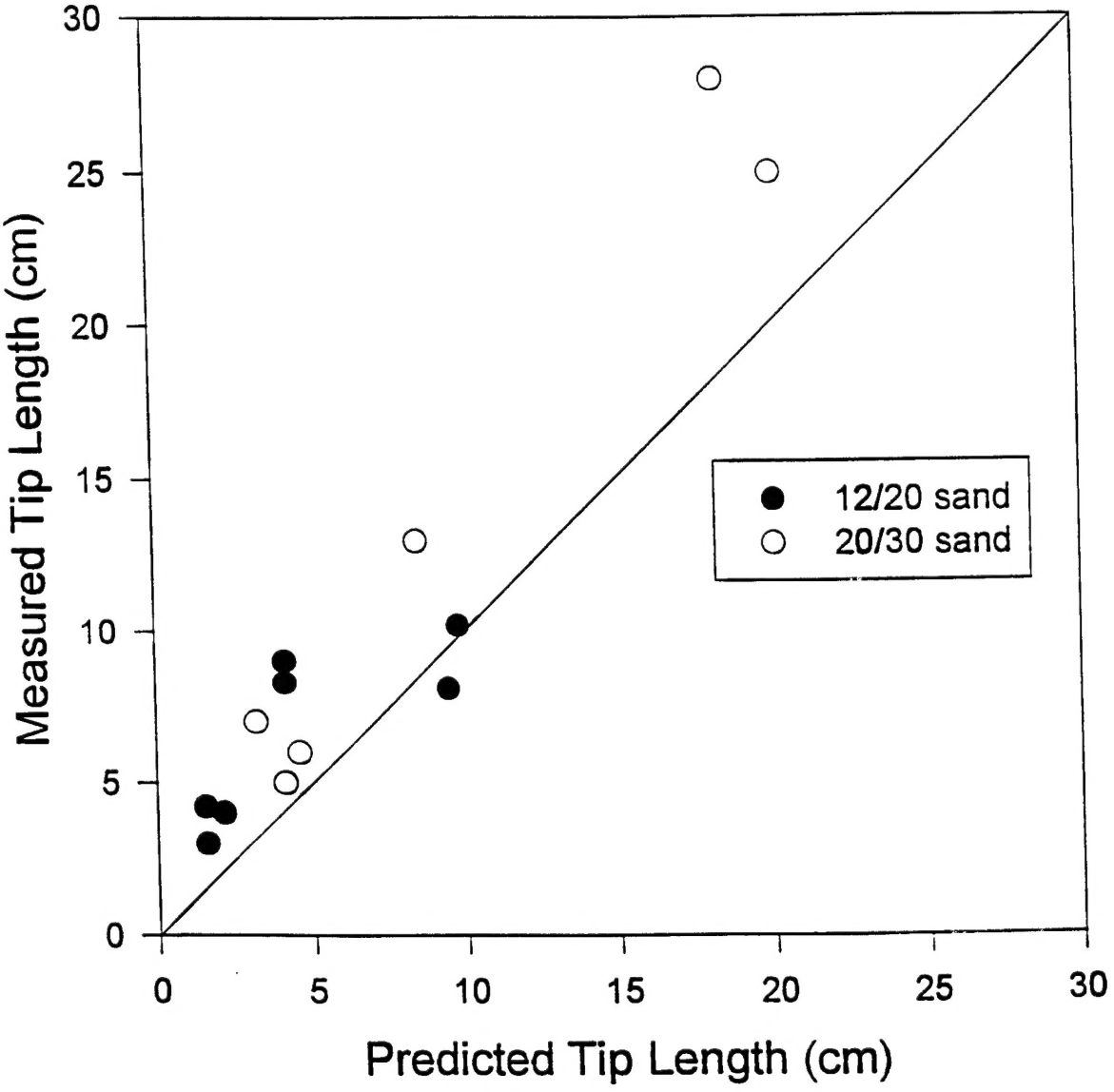
Measured Tip Length (cm)
Predicted Tip Length (cm)
0
5
10
15
20
25
30
12/20 sand
20/30 sand

FIGURE 7